Patterned Atomic Reaction at Surfaces

Iain Ross McNab and John Charles Polanyi*

Lash Miller Chemical Laboratories, 80 Saint George Street, Toronto, Ontario M5S 3H6, Canada

Received June 26, 2006

Contents

* To whom correspondence should be addressed. Phone: (416) 978 3580. Fax: (416) 978 7580. E-mail: jpolanyi@chem.utoronto.ca.

1. Introduction

1.1. Reaction Dynamics and Patterning

The field of molecular 'reaction dynamics' is now half a century old. It has its origins in the collision theory of chemical reactions according to which the essential step in a chemical reaction is the close approach of a colliding pair of reagent molecules in some preferred geometry with sufficient energy to exchange atomic partners. Since microscopic reversibility applies, this implies that newly formed reaction products separate in a preferred geometry with a preferred energy distribution. The advent of such techniques as crossed molecular beams made possible the isolation of single collisions in the gas phase and determination of the motions of the colliding species both immediately before and after a reactive encounter. This is the information required in order to define the dynamics.

The strength of molecular-beam chemistry was to isolate the 'elementary step'—the molecular encounter between the reagents that was responsible for the reaction. The weakness was that it averaged over all angles of collision and over all miss distances, the so-called 'impact parameters'. Reaction, particularly photoinduced reaction, at surfaces offered the possibility of a partial escape from these limitations. A photorecoiling reactant atom, A, coming from a photodissociating reagent in the adsorbed state could, in principle, approach a second adsorbed molecule, B−C, at a selected angle to the B−C axis and with its velocity vector aimed at a defined distance from the center-of-mass of B−C, i.e., with a selected impact parameter. Progress was made toward this goal of surface-aligned photochemistry (SAP) as a means to controlling the basic parameters of chemical reaction.[1−4]

More recently it has become evident that the powerful tool of STM has unprecedented potential to reveal the pattern of atomic motion in surface reactions and hence their molecular dynamics. This cannot be done (at present) in real time since

10.1021/cr0501745 CCC: $59.00
Published on Web 09/07/2006

Iain R. McNab obtained his B.Sc. degree in Chemical Physics from the University of Sussex and his D.Phil. degree from Oxford under the supervision of Professor Alan Carrington, F.R.S. He was a research fellow in chemistry at the University of Southampton and then a lecturer in physics at the University of Newcastle upon Tyne. He first worked with Professor Polanyi while on a sabbatical visit and moved to Canada permanently in 2004. His research interests are in nanoscience and spectroscopy.

John Polanyi, following receiving his Ph.D. degree from Manchester University, was a postdoctoral fellow at the National Research Council Laboratories in Ottawa and Princeton University. He is a professor of chemistry at the University of Toronto, with interest in the molecular motions involved in chemical reactions at surfaces. This led to his current work, with his research group, on patterned reaction products as viewed by scanning tunneling microscopy.

the reactive event typically takes the time of a molecular collision (10−100 fs) whereas the response time of STM is at least 10 orders-of-magnitude longer. Nonetheless, if STM can be used to locate the reagents and products immediately before and after the reactive event, it will be possible in simple systems, as recent experiments have shown, to infer the motions that intervene. This approaches more closely than ever before the ideal of "seeing a reactive event". Here we review progress toward this goal. The field is at present a young one.

This approach to the experimental characterization of reaction dynamics is an outgrowth of strides that have been made particularly through pioneering studies in the laboratories of Avouris, Wolkow, Hamers, and others in recent years using STM to characterize the geometries of intact aromatic organic molecules adsorbed on silicon (for reviews see refs 5-10). Since the field of organic structures at silicon surfaces has been well-reviewed, we do not review it here.

Characterization of molecular reaction dynamics by STM dates definitively from the time that a connection was established between reagent and product geometries. Elements of this are to be found in studies, described in the following, that attempt to link the size and shape of the reactants—the adsorbate and substrate in reactions with a surface— to the size and shape of the product seen as an STM imprint at the surface. As in scattering theory in the gas phase, the most telling data embody information on both reactants and products. In the present context this presumes, ideally, the existence of a precursor to reaction, sufficiently stable to be subjected to STM prior to reaction. Reaction is then induced by heat, light, or electrons. These last two modes of initiation resemble one another since illumination of a surface generally results in electronic excitation, the surface acting as an antenna for light; excited electrons then provide the intermediate agent to photoinduced reaction.

The characteristic imprint of the reaction products chemically bound to the surface is the 'pattern' referred to in the title of this review. By 'chemical reaction', in this review, we understand that the reaction product at the surface is no longer an intact molecule. The manner in which individual polyatomic molecules of varying size and shape can be used to chemically imprint differing patterns of reaction products at surfaces is discussed in section 3.3. This 'single-molecule' imprinting in which a 'parent' molecule fragments at the surface is especially revealing of the molecular reaction dynamics. Although many techniques, such as low-energy electron diffraction (LEED), are able to detect long-range surface patterns or reconstructions, only scanning probe microscopies are able to detect this local patterning at the nanometer scale. The studies mentioned in this review were, therefore, for the most part conducted using STM.[11]

One use of STM is to directly pattern a surface, atom by atom, by direct manipulations;[12] for a review, see ref 13. We do not consider such physical manipulations to obtain patterns in this review. It is also possible to induce atomic reactions using electrons from the STM tip;[14] we do consider such reactions since it is possible to induce them by wide-area irradiation rather than atom by atom. The current density of electrons from an STM tip, however, is on the order of 10^6 A cm^{-2}, which would be difficult to achieve with other sources. This allows multielectron reactive processes to be efficiently induced by the STM tip.

Where the chemically bound pattern is the desired outcome, as in the fabrication of stable extended nanostructures, the route to long-range order is through the 'imprinting' (i.e., chemical binding) of previously physisorbed patterned adsorbates. Surfaces can impose order on mobile adsorbates through preferential physisorption at restricted sites before reaction takes place. In such cases durable long-range order can result from subsequent chemical reaction. A second source of long-range chemical patterning is to be found in the ordered self-assembly of reagents due to weak forces—of which hydrogen bonding is the most common—acting between the adsorbate molecules. Such self-assembly, without subsequent chemical reaction at the surface, is an important field of study in its own right. Since numerous reviews exist (see, for example, refs 15−22), it is not reviewed here.

In order that a pattern of adsorbate shall result in a pattern of chemically bound (e.g., atomic) reaction products at the surface, the reaction dynamics must be such as to favor what has been termed localized atomic reaction, LAR.[23] The requirement for LAR is that the 'daughter' atom formed from the parent reagent and chemically bound to the surface be

minimally displaced laterally from the location of the parent adsorbate molecule giving rise to it. The topic of LAR will be the subject of further discussion in section 3.5, where we present evidence for a predisposition of chemical reaction to this type of dynamics. The rationale, given there in more detail, is that the activation barrier to atomic reaction is less for LAR, and hence the reaction rate is greater. Reaction at a closely neighboring site to the parent adsorbate molecule allows both the parent bond that is breaking and the daughter bond that is forming to coexist and therefore contribute additively to the stabilization of the reactive transition state.

Though LAR is a necessary condition for chemically bound pattern formation, it is not a sufficient condition. It could be that surface reaction results in a local imprint initially but that the newly formed chemical bond at the surface retains enough energy in the form of linear and angular momentum (vibration and rotation) that it diffuses to a neighboring surface site. This surface diffusion, repeated in stochastic sequence as the excess energy in the reaction product gradually leaks into the bulk, could destroy the patterned imprint. The weight of the evidence at present (following early findings that suggested otherwise[24−27]) is such as to suggest that the blurring of reaction-product patterns due to lateral diffusion is not, in general, a serious impediment to chemical patterning. This will depend, however, upon the case. In the following section we give a brief review of the factors governing surface diffusion that might cause blurring of patterns.

1.2. Surface Diffusion

When an adsorbate dissociates at a surface fragments are released and can react with the surface. As will be described below, such fragments can give rise to local reaction despite the fact that the fragments have kinetic energy when they are formed. It appears that energy dissipation is efficient at the surface.

Semiconductor surfaces have localized charge densities that give rise to dangling-bond surface states which give large potential-energy corrugations relative to the Fermi level. Metal surfaces, on the other hand, have more shallow potential corrugations dominated by delocalized states. We would therefore expect a priori that transport will occur more efficiently on metal surfaces.

Diffusion across a surface occurs by random jumps between nearest-neighbor sites. Such motion has been studied experimentally by Lauhon and Ho.[28] Long jumps that span multiple lattice spacings can also contribute to diffusion if the adsorbate−substrate interaction is sufficiently weak. The Besenbacher laboratory[29] recently demonstrated such long jumps experimentally in the surface diffusion of large molecules. They found root-mean-squared jump lengths as large as four or seven lattice spacings for decacyclene and hexa-*tert*-butyl-decacyclene moving across Cu(110).

2. Patterned Atomic Reaction at Metal Surfaces

Metal surfaces are flat and featureless compared to reconstructions of semiconductor surfaces. Tanaka et al.[30] reviewed the nanoscale reconstruction of these surfaces by adsorption and reaction. Many reconstructions are known to exist and are well understood; see, for example, the review by Besenbacher.[31] The imaging of small adsorbed molecules on metal surfaces under UHV conditions was not routinely achieved in the early days of STM; Chiang reviewed the early work until 1997.[32]

Chemisorption may occur directly or via a physisorbed precursor state. Chemisorption of molecules may give rise to whole molecules at the surface with concomitant bond formation and rupture or to one or more fragments adsorbed at the surface. Abstractive chemisorption, in the terminology used here, gives rise to one molecular fragment at the surface. Dissociative chemisorption gives rise to two or more fragments at the surface. An inverse of dissociation is formation of new chemical bonds between fragments at a surface. We give two recent examples of STM-tip-induced chemical reactions on metal surfaces. In the future comparative studies of the probabilities of reaction for different initial geometries can be expected to yield detailed dynamical information.

In STM we cannot always infer the chemical identity of species. For small moieties the identity may be determined spectroscopically. The simplest form of spectroscopy is to measure the local current−voltage (I/V) response, different for different species. More recently vibrational spectroscopy has been achieved using STM-inelastic electron tunneling spectroscopy (STM-IETS).

2.1. Abstractive and Dissociative Chemisorption

There has been interest in examining the reaction of diatomic molecules at metal surfaces to reveal the dynamics of fragmentation. In this section we consider some reactions that have been studied in sufficient detail to give information as to the local patterning.

2.1.1. Al(111)/O_2

An early prototype atomic reaction to be studied on a metal surface was the dissociation of O_2 on Al(111)[24,25] at 300 K. It was found that spontaneous dissociation with attachment of both O atoms to the surface occurred and that the resulting oxygen atoms were widely spaced by more than 80 Å at low coverages; in contrast, the equilibrium separation in molecular O_2 is 1.21 Å.[33] The experimental result of widely separated atoms was interpreted as evidence for "hot" atomic motion with at least part of the chemisorption energy being transformed into translational energy parallel to the surface. The lifetime of the "hot" adatoms was estimated to be greater than 1 ps.

After this work Engdahl and Wahnström[34,35] made a theoretical study of hot-atom motion. Using a molecular dynamics model of the dissociative absorption of oxygen on Al(111) they found that most of the atomic motion occurred during the first 0.2 ps after dissociation. During this first 0.2 ps atoms were found to move ballistically before the translational degrees of freedom equilibrated due to scattering on the corrugated atom−surface potential. Following this initial ballistic motion a random hopping motion occurred during which the remaining energy was lost. The principal conclusion was that hot-atom mobility was limited primarily by three-dimensional randomization of the initial energy due to scattering at the corrugated interaction potential rather than by dissipative friction. These authors found that using a reasonable value (3.5 eV) for the initial kinetic energy of the oxygen atom led to an average oxygen separation of 16 Å.

Strömquist et al.[36] made a theoretical study of ballistic dissociation and also abstraction in which one atom attaches to the surface and the other leaves. They found that both

pathways could result from chemisorption due to electron transfer from the surface to the molecule. They argued that the random distribution of single O atoms found by Brune et al.[24,25] could result from either ballistic motion of neutral O atoms along the surface in dissociative attachment or an abstraction reaction in which only one of the O atoms stayed on the surface.

Subsequently, Österlund et al.[37] measured the dissociative sticking probability (S_0) of O_2 on Al(111) as a function of incident translational and vibrational energy. They found very low sticking probability at low kinetic energy ($S_0 = 0.01$ at 30 meV), increasing to unit probability at high kinetic energy (above 0.6−2.0 eV). They proposed that only selected initial trajectories of favorably oriented oxygen molecules dissociate to give large O-atom separations. They further suggested that the dynamics were sensitive to collision energy.

This proved to be the case. Binetti et al.[38] and Komrowski et al.[39] found, at incident O_2 kinetic energies of 0.5 eV on Al(111), that pairs and single oxygen atoms could be seen on the surface, indicating two mechanisms of chemisorption of O_2 on Al(111): dissociative chemisorption for pairs and abstraction for singles. These mechanisms can be envisaged as follows.

dissociative chemisorption

$$O_2(g) + Al(111) \rightarrow 2O(ads)/Al(111) \quad (1)$$

abstraction

$$O_2(g) + Al(111) \rightarrow O(ads)/Al(111) + O(g) \quad (2)$$

It was found that abstraction (eq 2) accounted for 50% of dissociative events at 0.5 eV incident kinetic energy. As a result, isolated O atoms were observed in the STM image as originally seen.[24,25] The 80 Å separations measured originally[24,25] were, it now appeared, due to single O atoms formed by reaction 2 rather than pairs formed by reaction 1.

The earlier work of Brune et al.[24,25] used thermal oxygen (0.025 eV) and hence would have resulted in isolated O atoms, as Binetti et al.[38] pointed out. With increasing O_2 incident energy, as Komrowski et al.[39] showed, dissociative chemisorption to yield pairs of oxygen atoms increased in importance.

Dissociation of oxygen on Al(111) does not proceed from a physisorbed state, and hence, no STM data is available to link the final observed distribution of oxygen atoms with an initial state. However, the dynamics of the process have been the subject of numerous calculations. The most revealing was that of Ciacci and Payne[40] using first-principles molecular-dynamics simulations to study the dissociative absorption of oxygen molecules on Al(111). They found that the dissociative chemisorption (in the adiabatic limit) was caused by hybridization of the s* antibonding molecular orbital of molecular oxygen with the surface states of Al(111). The hybridization resulted in partial filling of the s* antibonding molecular orbital, and this caused dissociation to yield pairs of adsorbed oxygen atoms. This is in satisfying agreement with the arguments of Strömquist et al.[36]

2.1.2. Pt(111)/O_2

For O_2 adsorbed on Pt(111) at low temperature (150−160 K)[41] pairs of oxygen atoms were imaged that had clearly been produced spontaneously by dissociative adsorption. The O-atom pairs were typically separated by two lattice constants. The dynamics was referred to as transient ballistic motion. Figures 1 and 2 show the distribution of the pairs in the STM images and also graphically.

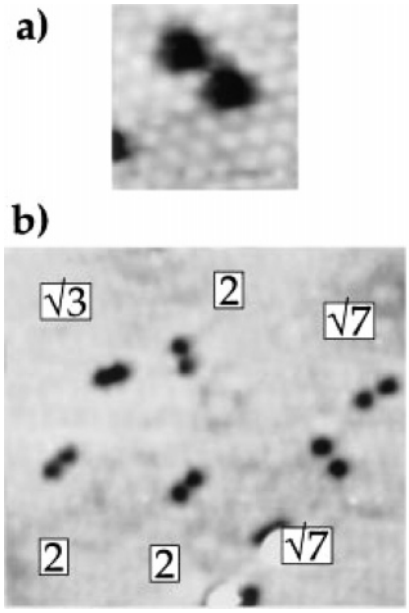

Figure 1. STM images of Pt(111), recorded after dissociative adsorption of O_2 at around 160 K; black dots are oxygen atoms: (a) 2 L O_2, 19 Å × 19 Å, 163 K, $V_s = -0.2$ V, $I_t = 28$ nA; (b) 1.2 L O_2, 110 Å × 92 Å, 154 K, +0.13 V, $I_t = 0.8$ nA; the distances between the O atoms in the pairs are indicated. Reprinted with permission from ref 41. Copyright 1996 American Physical Society.

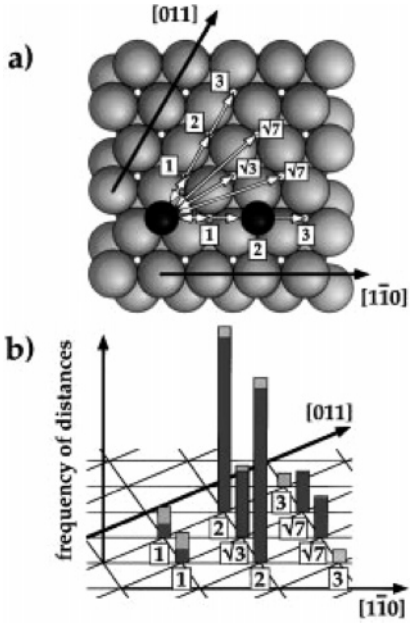

Figure 2. (a) Model of the Pt(111) surface with two oxygen atoms after dissociation of a molecule (platinum atoms gray, oxygen atoms smaller, dark spheres). (b) Histogram of frequencies of intrapair distances, based on 55 pairs. Average frequencies of 1, √3, 2, √7, and 3 lattice constant separations were 7.3%, 21.8%, 56.4%, 12.7%, and 1.8%. Gray tops of the bars indicate variations between two data sets at 160 and 163 K. Reprinted permission from ref 41. Copyright 1996 American Physical Society.

The induced dissociation of O_2 on Pt(111) at still lower temperatures (40−150 K) was studied by Stipe et al. in the Ho laboratory.[42] These authors used electrons from an STM tip to image and dissociate single oxygen molecules on a Pt(111) surface. They found that the dissociation proceeded

by multiple vibrational excitation caused by inelastic collisions of the electrons with the O_2 molecules. For this induced reaction the two fragment O atoms were once again spaced one to three lattice constants apart, a comparable separation to that found in the low-temperature thermal experiments above. In later work[43] (reviewed by Ho in 1997[44]) the adsorbed molecules were dissociated with UV radiation, inelastic tunneling electrons, and heating. In each case the O atoms were found to be within two lattice constants of the original molecule site, i.e., one to three lattice-constants apart. The similarity of the results no matter what the cause of molecular fission led the authors to conclude that the O atoms received the same amount of energy in each case. Since this appears unlikely, we suggest instead that the factors favoring localized atomic reaction (see below) together with efficient quenching of the excess energy are suffice to capture the atoms in a closely spaced configuration. The energy loss to the surface need only be a small fraction of the binding energy for the O atoms to be prevented from escaping far from their initial bonding sites.

2.2. Site Orientation and Separation in Dissociation

2.2.1. Ag(110)/O2

Detailed studies from the Ho laboratory were made of STM-tip-induced, thermal- and photodissociation of O_2 on Ag(110). Work on the Ag(110)/O_2 system until the year 2000 was summarized and extended by Hahn et al.[45] In recent work from that laboratory[46] on dissociation of single oxygen molecules at 13 K dissociation was induced exclusively by tunneling electrons from an STM tip. A pleasing asymmetry was observed: fragment O atoms were ejected in different directions depending upon the direction of the tunneling current. This showed that a molecular orbital located at the Fermi level was responsible for dissociation. With O_2 aligned along [001], injection of electrons into an O_2 orbital (believed to be the $1\pi_g^{\perp}$) gave rise to two adsorbed oxygen atoms separated along the [1−10] direction, while removal of electrons from the same O_2 orbital gave rise to two adsorbed oxygen atoms separated along the [001] direction. Figure 3 illustrates these processes, which we detail below. Transfer of a CO molecule to the STM tip enabled atomically resolved images of the metal surface to be obtained so that the registration of the molecules could be determined.

A positive voltage pulse applied to the sample (injection of electrons into the O_2 $1\pi_g^{\perp}$ orbital) caused O_2 (001) to rotate by 90°, changing the molecular axis to the [1−10] direction. Rotation was irreversible and occurred only with a positive sample voltage pulse. It was found that O_2(001) was rotated to O_2(1−10) before it dissociated. The barrier to rotation was +450 mV, while the threshold for dissociation was + 470 mV.

When the O_2(001) molecule was dissociated by negative voltage pulses (removal of electrons from the O_2 $1\pi_g^{\perp}$ orbital) differently located products were formed. One oxygen atom occupied the 4-fold hollow site (O_{ffh}), while the other bonded to the short-bridge site (O_{sb}). O_{ffh} remained in the position of the original molecule with O_{sb} moving away along the [001] direction for distances of more than 10 Å. The threshold voltage for dissociation was −390 mV.

The difference in the dissociation dynamics was thought to be due to the different alignment of the molecular axis before dissociation. The molecule could be regarded as dissociating by extending the oxygen−oxygen bond in the chemisorbed state. The O atom on these short bridge sites underwent thermal diffusive motion, moving up two lattice spacings within a few tens of minutes at 13 K. The oxygen atoms on these short-bridge sites always diffused to other short-bridge sites, which showed that the barrier to reach the more-stable 4-fold hollow site was greater than the barrier for diffusion from one short-bridge site to another. The higher mobility of the short-bridge O atoms explained the larger atomic separation that resulted from the negative voltage pulse. The average atomic separations found were 4.3 Å for positive voltage pulses and 11.7 Å for negative voltage pulses.

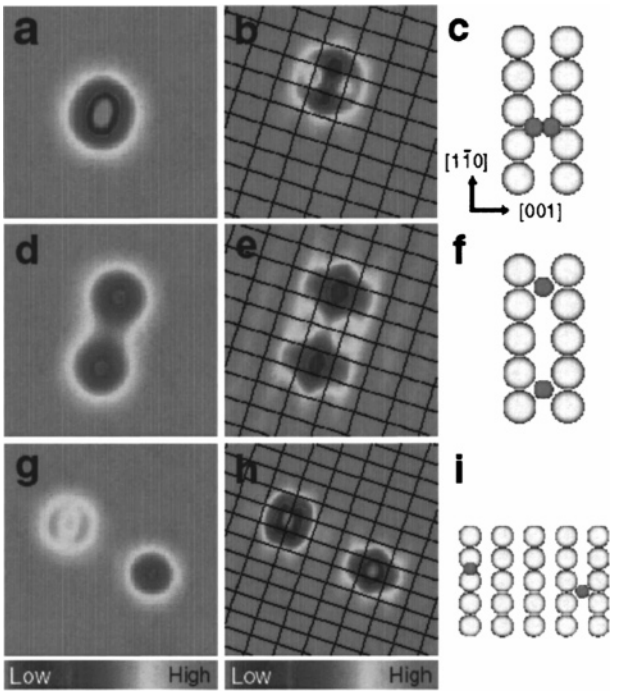

Figure 3. Dissociation of O_2 chemisorbed on Ag(110) at 13 K. (left) Topographical images obtained using a bare tip at a sample bias voltage of 70 mV and a tunneling current of 1 nA (a, d, and g). (center) Atomically resolved topographical images obtained using a CO-terminated tip; V_s = 70 mV and I_t = 1 nA (b, e, and h). Grid lines are drawn through the Ag surface atoms. Schematic diagrams of the adsorption sites are shown in the right column (c, f, and i). Small circles represent O atoms, and large circles represent Ag atoms. Sizes of the circles are scaled to the atomic covalent radii. (a−c) O_2 molecule chemisorbed on the 4-fold hollow site with its molecular axis aligned along the [001] direction. Scan area of images a and b is 25 Å × 25 Å. (d−f) O_2 molecule is dissociated along the [1−10] direction by a +480 mV voltage pulse applied to the sample with the feedback off. The dissociated O atoms are adsorbed on 4-fold hollow sites. Scan area of images d and e is 25 Å × 25 Å. (g−i) Two O atoms dissociated along the [001] direction by a −390 mV voltage pulse applied to the sample with the feedback off. One O atom is adsorbed on the 4-fold hollow site, and the other is bonded onto the short bridge site. Scan area of images g and h is 31 Å × 31 Å. Reprinted with permission from ref 46. Copyright 2005 American Institute of Physics.

As can be seen in Figure 3, in individual dissociation events the oxygen fragments were, as found previously in related studies, only a few lattice spacings apart. The O-atom fragments were formed either parallel or perpendicular to the original axis of the molecule.

More recently, Zambelli et al.[47] studied the thermal dissociation of O_2 at Ag(110) at 170 K. They found, for the first time, a different distribution of thermal O atoms from that which resulted from the current-induced dissociation.

At low temperature (110 K) oxygen molecules absorbed intact onto the surface and tended to form chains along the [1−10] direction. Thermal dissociation was studied by dosing the surface with oxygen at temperatures around 110 K and annealing at higher temperatures; STM images were taken after recooling to 110 K. A complex image was found that contained five features: undissociated molecular oxygen, pairs of oxygen atoms, a structure identified as Ag−O chains, and two unidentified structures. The oxygen pairs due to thermal dissociation were found to be perpendicular to the expected [1−10] direction that resulted from electron impact dissociation, lying instead along [001]. The separations found were once again modest, mostly two [001] lattice spacings.

Dissociation of molecular oxygen on Ag(110) was also initiated by light. Photodissociation of 0.03 monolayers of oxygen at 110 K was studied by the same authors.[47] Ultraviolet light from a 100 W high-pressure mercury arc lamp provided illumination for times of 100 or 300 s. For 100 s illumination chains of adsorbed molecular oxygen were visible together with some "black dots", which were shown to be an oxygen-containing species. After further irradiation, which resulted in complete removal of the molecular oxygen, only the "black dots" oxygen species remained; the authors speculated that the black dots were a subsurface oxygen species. Theoretical STM images of atomically and molecularly chemisorbed oxygen on silver have been constructed by Olsson et al.[48]

2.2.2. Cu(110)/O_2

The adsorption of O_2 on Cu(110) at 4 K was examined by Briner et al.[49] They found that weakly bound intact molecules coexisted with clusters, single atoms, and pairs of atoms. The pairs of oxygen atoms were found to be preferentially oriented along the [1−10] and [001] directions. The distribution was particularly strongly peaked in the [001] direction, although more pairs were oriented along the [1−10] direction. Obliquely oriented pairs were rare. The most probable separation was found to be two lattice constants (that is 5.12 Å[29]), which can be compared with the oxygen bond length of 1.2 Å.[33]

It appeared that it was easier for an oxygen molecule to dissociate if it lay flat on the surface with its axis oriented parallel or perpendicular to [1−10]. This was interpreted as an example of limited ballistic motion comparable to oxygen molecules on Pt(111).

2.2.3. Pd(111)/O_2

The dissociative adsorption of O_2 on Pd(111) at low coverage was studied by Rose et al.[50] in the range 25−210 K. Thermal dissociation of adsorbed molecules was found to occur near 120 K. Molecules that dissociated were either at the periphery of islands or adsorbed close to subsurface defects. For the isolated O_2 molecules (close to subsurface defects) dissociation led to pairs of O atoms at adjacent fcc and hcp hollow sites.

2.2.4. Pt(111)/Br_2

Harrison and co-workers examined the behavior of atomic bromine[51] and molecular bromine[52] on Pt(111). For the case of molecular bromine, STM was used to study the dissociative adsorption on Pt(111) at 25 K. At low coverage they observed Br atoms in correlated pairs with an average separation of 9.2 ± 1 Å (compared with the equilibrium molecular bond length of 2.28 Å[33]). At higher molecular bromine exposures Br atoms were found to make chainlike structures on the surface, which eventually became two-dimensional islands.

2.3. Tip-Induced Approach of Reagents

2.3.1. Ag(110)/CO + Fe

An inverse of the processes that we have so far considered, of great potential interest, is formation of a single bond at a surface rather than its rupture. This process was first observed by Lee and Ho[53] using an STM tip to manipulate the reagents. Fe atoms were evaporated and coadsorbed with CO molecules on the silver surface at 30 K. A single CO molecule was then transferred from the surface to the STM tip, moved through the vacuum, and deposited on an Fe atom, forming FeCO. Next, a second CO molecule was similarly transferred and observed to form $Fe(CO)_2$. The process is illustrated in Figure 4. The corresponding sequence of STM images to the schematics of Figure 4 are shown in Figure 5. The geometry of both FeCO and $Fe(CO)_2$, once formed, could be inferred from the images. FeCO was found to have the CO ligand at some undetermined angle to the surface, while $Fe(CO)_2$ had the two CO ligands at 180° from one another, not parallel to the surface.

2.3.2. Cu(111)/2($C_6H_5^{\bullet}$)

A further striking example of STM-induced reaction at a surface is due to Hla et al.,[54,55] illustrated in Figure 6. These

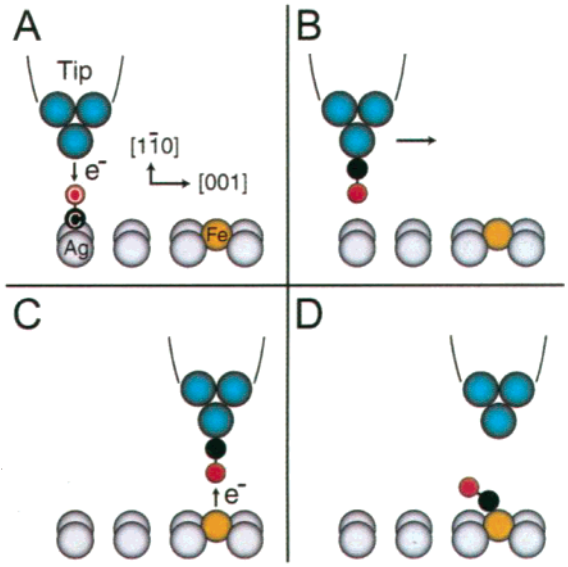

Figure 4. Schematic diagrams showing the different steps in the formation of a single bond with the STM. Binding sites were determined by imaging the adsorbate species with the CO molecule attached to the tip. Sizes of the circles are scaled to the atomic covalent radii. The polycrystalline tungsten tip was sputtered and annealed before use; physical contact was made with the silver surface to further condition the tip. (A) Tip is positioned over a single CO molecule to induce detachment of CO from silver and its subsequent bonding to the tip. Because CO forms a bond predominantly through the carbon, 180° rotation of the CO occurs in the transfer. (B) Tip with the attached single CO molecule is translated (indicated by the arrow) and positioned over an Fe atom. (C) Bias voltage and flow of electrons are reversed, inducing transfer of CO from the tip to the Fe. (C) A single Fe−CO bond is formed. The interaction of the electric field with the dipole moment of CO may also play a role in the transfer of A and C. Reprinted with permission from ref 53. Copyright 1999 AAAS.

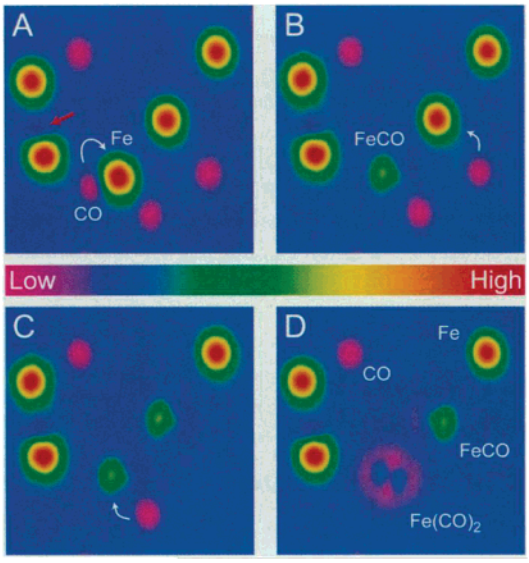

Figure 5. Sequence of STM topographical images recorded at $V_s = 70$ mV, $I_t = 0.1$ nA, and 13 K to show formation of the Fe−CO bond with the prescribed method (Figure 1). Size of each image is 63 Å × 63 Å. Fe atoms image as protrusions and CO molecules as depressions. White arrows indicate the pair of adsorbed species involved in each bond formation step. (A) Five Fe atoms and five CO molecules are adsorbed in this area of the Ag(110) surface. One CO is very close to an Fe atom (indicated by the red arrow). (B) CO molecule has been manipulated and bonded to an Fe atom to form Fe(CO). (C) Another Fe(CO) is formed by binding CO to a second Fe atom. (D) Additional CO has been bonded to Fe(CO) to form $Fe(CO)_2$. A 180° flip is observed for the remaining Fe-(CO). Reprinted with permission from ref 53. Copyright 1999 AAAS.

authors synthesized biphenyl at a step edge of Cu(111) from two molecules of iodobenzene. The molecules of iodobenzene were first dissociated by electron impact to yield two phenyl ($C_6H_5^{\bullet}$) radicals. The radicals were then pushed together with the STM tip, using the step edge as a guide. Finally, biphenyl, $C_{12}H_{10}$, was formed by electron impact on the two C_6H_5 radicals. This procedure was accomplished using both a bare tip[54] and an iodine-atom-functionalized tip.[55]

At the present stage of development of this highly promising approach it does not yet yield information as to the preferred pattern of reagents to yield reaction. A comparative study of the probability of reaction for different directions of approach to a molecule held aligned at a surface will be highly informative of the dynamics in the future.

2.4. Determination of Reaction Products by Inelastic Electron Tunneling Spectroscopy

2.4.1. Cu(100)/C_2H_2, C_5H_5N, C_6H_6

Induced reaction of acetylene (and its isotopomer C_2D_2) on the Cu(100) surface was examined by Stipe et al.[56] These authors found that C_2H_2 adsorbed molecularly in the 4-fold hollow site of the Cu(100) surface in four equivalent orientations. STM-inelastic electron-tunneling spectroscopy (STM-IETS) was used to distinguish the CH stretch mode from the CD stretch mode, thereby enabling spatial imaging to distinguish between the two isotopes.

STM-IETS is a method of obtaining vibrational spectroscopic information about molecules adsorbed on a solid surface with atomic resolution. The inelastic electron tunneling in STM-IETS is due to coupling and energy transfer between tunneling electrons and the vibrational modes of the molecule. This work[56] by the Ho laboratory demonstrated IETS combined with STM, thereby performing vibrational spectroscopy on single molecules at a surface.

In a further study Lauhon and Ho[57] showed that at 9 K irradiation of acetylene by electrons from the STM tip could be used to dissociate a single C−H or C−D bond, leaving a CCH or CCD fragment, and then further dissociation could be induced to leave CC at the surface. The CC end product was imaged on the same site as the parent acetylene. Rotation of the CCH and CCD fragments was studied in detail.

In this[57] and other work,[58] also in the Ho laboratory, both pyridine (C_5H_5N) and benzene (C_6H_6) were studied at 9 K and induced to react at the surface using tunneling electrons. The reagent pyridine was thought to bond to a single copper atom through the nitrogen atom and be perpendicular to the surface, whereas benzene adsorbed more weakly with its molecular plane parallel to the surface. Fragments from each parent molecule were imaged, and IETS were recorded. Both fragments displayed C−H stretches, but only the parent pyridine showed a C−H stretch mode. Detection of a C−H stretch mode upon dissociation of the benzene was attributed to a change in bonding geometry in the residue of the parent.

Dissociation of pyridine resulted in a fragment displaced from the parent molecule by 1.8 Å, one-half the lattice spacing in the [001] direction. Dissociation of benzene usually resulted in fragments modestly displaced from the parent molecules, but some dissociation events occurred in which the fragment was at the same site as the parent. The images and spectroscopic data were interpreted as being due to the processes $C_5H_5N \rightarrow C_5H_4N$ and $C_6H_6 \rightarrow C_6H_4$ induced by tunneling electrons, as shown in Figure 7; the H atom lost in each dehydrogenation was not observed.

Voltage pulses above 3.75 eV induced secondary dissociation of the residual pyridine and benzene fragments. These secondary dissociations did not consistently produce the same reaction products, different products often being seen in different experiments. The authors interpreted both fragments as evidence that the pi-resonant ring structure had broken, but the products were not identified.

2.4.2. Cu(110)/C_6H_6

Dehydrogenation of benzene (C_6H_6 and C_6D_6) on Cu(110) was induced using tunneling electrons by Komeda et al.[59] at a temperatures below 50 K. In accord with the results for benzene on Cu(100) reported above, dehydrogenation caused a change in bonding geometry at the surface from flat-lying to upright. The energy threshold for reaction was found to be 2.4 V, and reaction could only be induced with the sample positively biased; the reaction was shown to be induced by a single electron. A large isotope effect was found; the reaction rate per electron was 10^3 times lower for C_6D_6 than for C_6H_6. The fate of the lost H atom was not ascertained.

2.4.3. Ni(110)/C_2H_4

The dehydrogenation of ethylene and its deuterium isotopomers (C_2H_4, $C_2D_2H_2$, C_2D_4) to acetylene (C_2H_2, C_2HD, C_2D_2) on Ni(100) at 13 K was studied in further work by the Ho group.[60] Two different types of acetylene were found to exist on the surface: distinguishable both in the STM image (as small (S) and large (L) features) and by their shifted vibrational peaks. The most likely explanation is that acetylene binds to two different adsorption sites. Ethylene

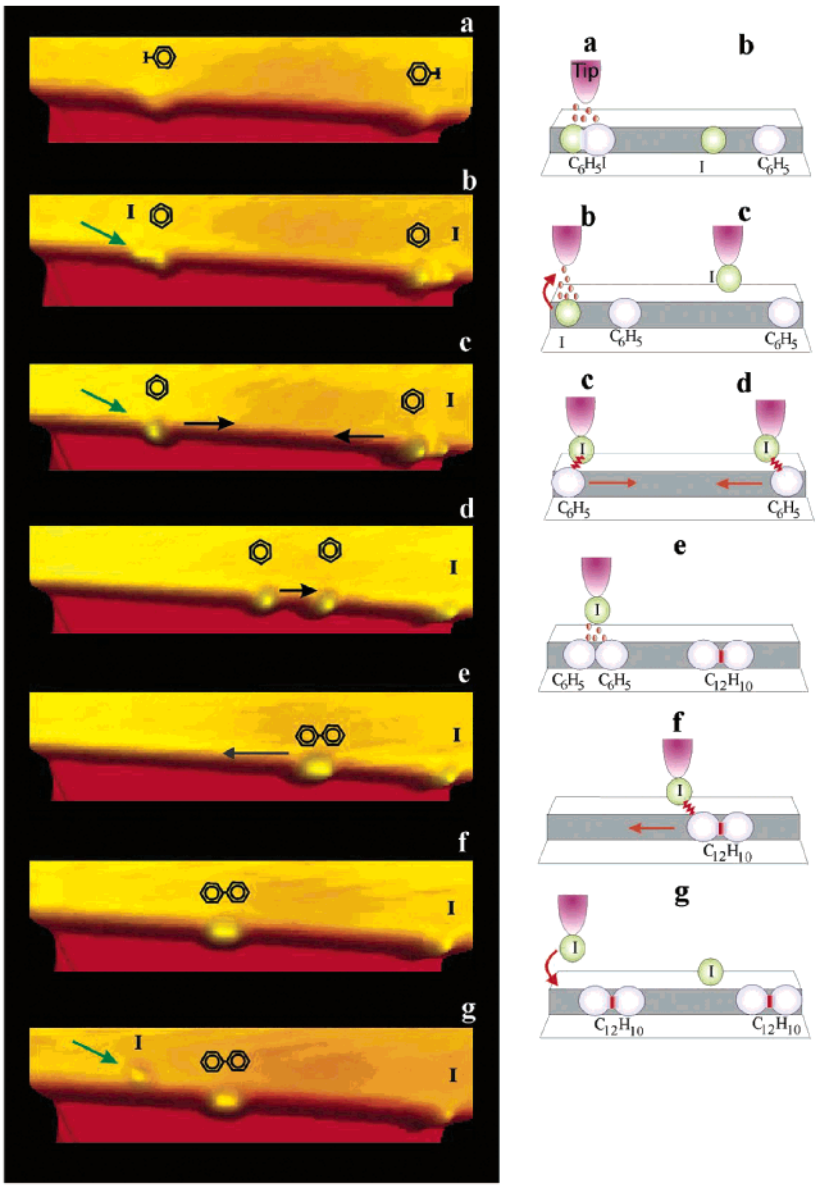

Figure 6. Formation of biphenyl using an iodine-functionalized tip. (a) Two iodobenzene molecules are adsorbed at a Cu(111) step. (b) After dissociation with tunneling electrons, two phenyl radicals (larger bumps) and two iodine atoms are adsorbed at the Cu step edge. (c) After the iodine at the far left (indicated by a green arrow) has been transferred to the tip apex using the vertical manipulation procedure, the image contrast improves. (d) Two phenyls are laterally moved toward each other with the tip. (e) When the two phenyls are in closest distance, a splash of electrons with 500 meV is supplied to excite them for biphenyl formation. (f) Then the synthesized biphenyl is pulled by the tip to the left side of the image to verify a successful chemical association. (g) Finally, the iodine from the tip apex is transferred back to the substrate (indicated by a green arrow). Reprinted with permission from ref 55. Copyright 2003 Annual Reviews.

was found to absorb on top of the Ni(110) rows, while acetylene preferentially adsorbed in the troughs.

At voltage pulses of 1.1−1.5 V, tunneling electrons induced dehydrogenation. The individual dehydrogenation products were identified by IETS. A strong primary isotope effect was observed in these dissociations. Remarkably, only the C−D stretch was observed after STM-induced dehydrogenation of *trans*-$C_2H_2D_2$, *cis*-$C_2H_2D_2$, and 1,1-$C_2H_2D_2$, showing a propensity to dissociate the C−H bond rather than the C−D bond. A small secondary isotope effect was also observed in dissociations. The threshold voltage for dehydrogenation differed with different isotopomers (see Table 1). Previous work on thermal decomposition of ethylene on Ni(110)[61] found product CCH. This was not found in the STM-induced dissociations. Once more, the fate of the H atoms was not ascertainable.

Further pulses of electrons from the STM tip induced dissociation of both remaining hydrogen atoms of the product acetylenes (L−C_2H_2, S−C_2H_2, L−C_2D_2, S−C_2D_2) leading to C_2 on the surface. The threshold voltages for dehydrogenation differed for the four acetylene species (see Table 1).

2.4.4. Pd(110)/C_4H_8

Dehydrogenation of *trans*-2-butene (C_4H_8) to 1,3-butadiene (C_4H_6) on Pd(110) at 4.7 K was induced by tunneling electrons by Kim et al.[62,63] The distinction between *trans*-2-butene and 1,3-butadiene could be made both in STM topographs[63] and by IETS.[62] The relative positions of parents and daughters was not reported.

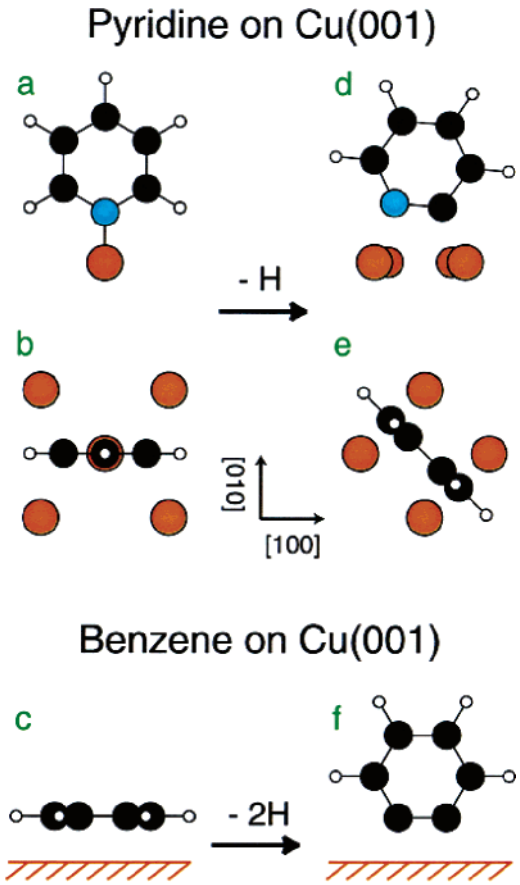

Figure 7. Proposed transformation of pyridine and benzene via electron-induced dissociation. (a, b and d, e) Side and plan elevations of the proposed dissociation reaction for C_5H_5N (C_5D_5N). (c−f) Side elevation of the proposed dissociation reaction for C_6H_6 (C_6D_6). Reprinted with permission from ref 58. Copyright 2000 American Chemical Society.

Table 1. Threshold Voltages (V) for STM-Induced Dehydrogenation of Ethylene to Acetylene and Acetylene to Carbon (C_2)[a]

ethylene C_2H_4	1.14 ± 0.07	*S*-acetylene	C_2H_2	1.35 ± 0.11
cis-$C_2H_2D_2$	1.23 ± 0.09		C_2D_2	2.18 ± 0.81
1,1-$C_2H_2D_2$	1.37 ± 0.09	*L*-acetylene	C_2H_2	1.14 ± 0.07
trans-$C_2H_2D_2$	1.46 ± 0.11		C_2D_2	4.52 ± 0.45
C_2D_4	1.47 ± 0.12			

[a] For each isotope threshold voltages were determined from 30−40 ethylene and 9−15 acetylene molecules.

3. Patterned Atomic Reaction at Semiconductor Surfaces

We now consider patterning by atomic reaction at semiconductor surfaces, in particular the surfaces of titanium dioxide and silicon, the only surfaces on which patterned atomic reactions have been well characterized. Many studies of reaction at other semiconductor surfaces have been made, but they have been too complicated to be interpreted as patterned atomic reaction and are not considered here.

3.1. Cannonballs in Reaction

3.1.1. TiO_2(110)-1×1/Cl_2

The case of Cl_2 on TiO_2(110)-1×1 is particularly interesting as an example of dissociative chemisorption that gives evidence of well-separated pairs of Cl atoms.[26] The surface after exposure to molecular chlorine is shown in Figure 8. The sticking probability was found to be unity. Abstractive chemisorption accounted for 10% of events leading to single Cl atoms at the surface, and dissociative chemisorption accounted for the remainder. Widely separated pairs of Cl atoms were found in the latter case, the average separation between pairs of Cl being 26 Å. There was a complete absence of nearest-neighbor and second-nearest-neighbor Cl atoms within a Ti row. An autocorrelation analysis of the separations is shown in Figure 9.

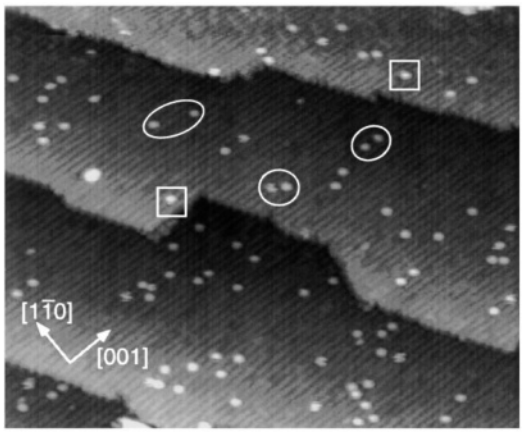

Figure 8. STM image of a TiO_2(110)-1×1 surface exposed to 0.07 L Cl_2 at room temperature (400 Å × 380 Å, V_s = +1.6 V, I_t = 1.6 nA). Adsorbed chlorine atoms appear as bright round spots on the bright rows parallel to the [001] direction (on 5-fold coordinated Ti atoms). Most Cl atoms are paired. Some of the Cl−Cl pairs and single chlorine adatoms are marked with circles and squares, respectively. Reprintedpermission from ref 26. Copyright 1998American Physical Society.

The proposed mechanism leading to the large observed Cl-atom pair separations is illustrated in Figure 10. The

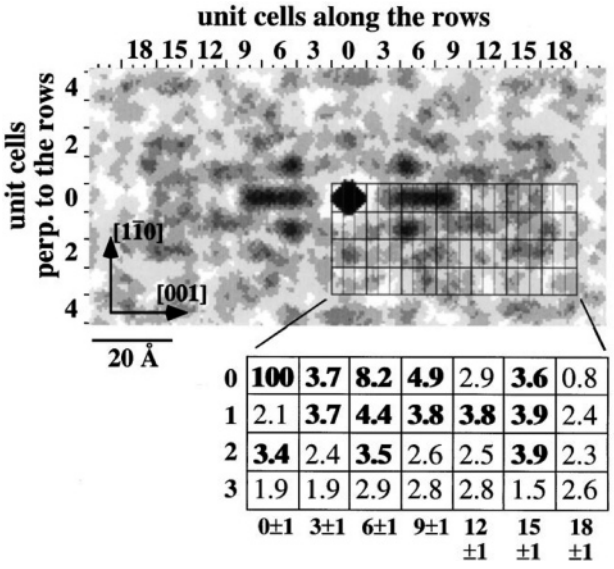

Figure 9. Autocorrelation of Cl−Cl distances in STM images with the same Cl coverage as shown in Figure 8. The table gives the probability (%) of finding a second Cl atom within the grid of surface unit cells overlaid on the plot. Probabilities are given for areas of three unit cells to smooth the statistical scatter and account for the limited accuracy of position determination along [001]. Probabilities that are significantly higher than the average value of 2% are printed in bold. Reprinted with permission from ref 26. Copyright 1998American Physical Society.

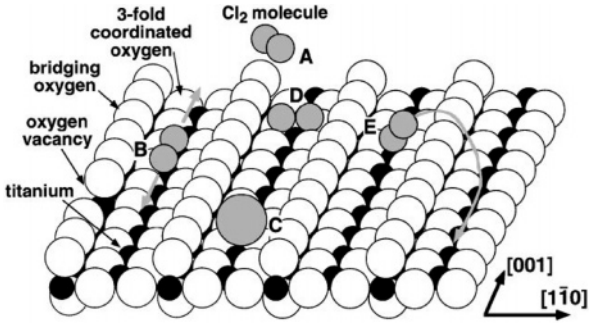

Figure 10. Ball model of the TiO_2(110)-1×1 surface. Five-fold-coordinated Ti atoms (black balls) are separated by rows of 3-fold-coordinated and bridge-bonded oxygen atoms (white balls). An oxygen vacancy is shown in the leftmost row of bridging oxygen atoms. Unit cell dimensions along [1−10] and [001] are 6.5 and 3 Å, respectively. See text for discussion of adsorption of chlorine (gray balls); "C" represents an absorbed Cl anion. Reprintedwith permission from ref 26. Copyright 1998American Physical Society.

dissociation event was estimated to be exothermic by at least 5 eV. The mechanisms thought to account for the majority of events are labeled B and E in Figure 10. Case B represents a flat-lying Cl_2 molecule oriented along the [100] direction. Assuming a linear bond extension during dissociation together with molecular alignment along the Ti rows explains the large average Cl−Cl distances along the [001] direction with a measured probability of 23% for finding a Cl−Cl pair on the same row. Case E represents a Cl_2 molecule adsorbed in an approximately upright configuration, tilted at azimuthal and polar angles. Again, assuming linear bond extension, the outer dissociating Cl atom can travel over the substrate, bridging oxygen rows, in a cannonball-like trajectory; such a motion can lead to a large average Cl−Cl distance perpendicular to the [001] troughs. The separating Cl atom is assumed to be negatively charged as dissociation is thought to occur by electron transfer to the antibonding orbital of Cl_2. The "cannonball" is therefore a Cl^- ion that is trapped by attraction to the surface due to its image potential.

3.2. Silicon Reconstructions

Although the reconstructions of the silicon surface are well known,[64] their nature is important to an understanding of the work that follows, and we now briefly summarize the properties of the two most commonly used reconstructions: Si(100)-2×1 and Si(111)-7×7.

3.2.1. Si(100)-2×1

Without reconstruction, the Si(100) surface is a square lattice in which each surface atom has two dangling bonds. The Si(100)-2×1 surface halves the number of dangling bonds by forming dimer pairs.[64] The resultant topographic STM images, taken at room temperature, consist of bright dimer rows separated by dark lines. Low-temperature STM images show that the dimers are not uniform but are buckled by about 18°; this nonuniformity is averaged out at room temperature due to dynamic motion that is fast on the time scale of the STM. Dimer rows on adjacent terraces run in perpendicular directions. Dimer rows that are adjacent to a terrace or close to a defect are pinned in one buckled configuration or another which appears in the filled state STM image as a zigzag chain with neighboring dimers being buckled in opposite directions (see Figure 11).

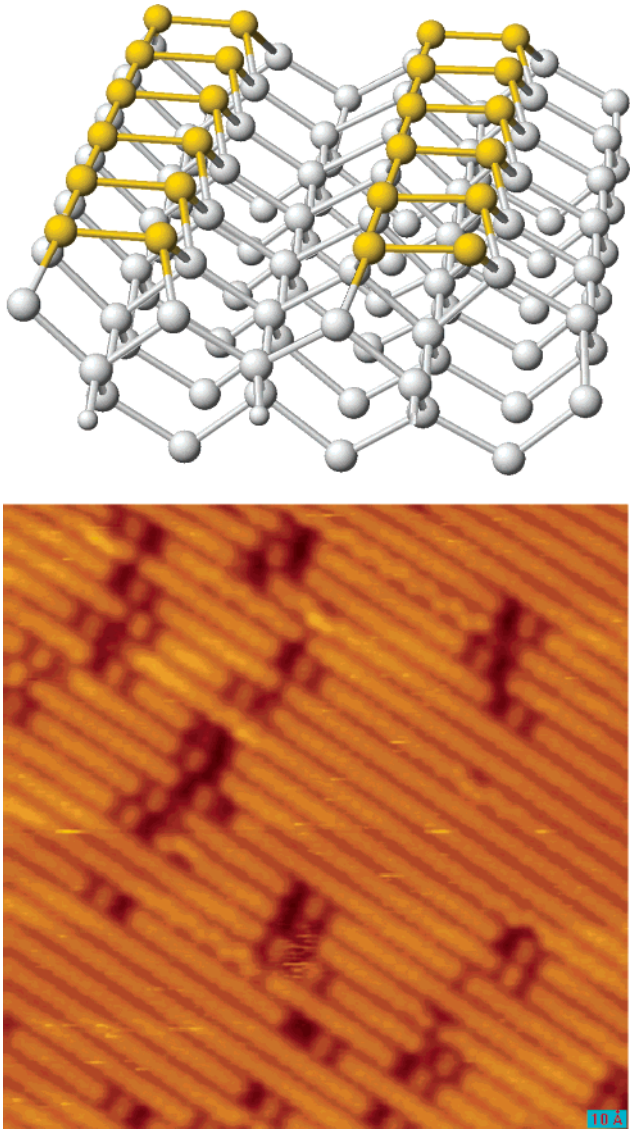

Figure 11. (Top) Si(100)-2×1 reconstructed silicon surface with five top layers of the silicon atoms. Dimers (shown in yellow) are formed from a strong σ bond and a weak π bond. (Bottom) STM image of the Si(100)-2×1 reconstruction (Obtained at room temperature; 163 Å × 163 Å; $V_s = -2$ V; $I_t = 0.3$ nA). Close to defects some examples of pinned buckled dimer rows can be seen. (Ball and stick model and STM image courtesy of Dr. K. R. Harikumar.)

3.2.2. Si(111)-7×7

In Figure 12 (top) we show a schematic plan and midsection of the accepted model of the Si(111)-7×7 reconstruction (adapted from ref 70): the dimer adatom stacking fault (DAS) model of Takayanagi et al.[65] The Si-(111)-7×7 unit cell is a rhombus with two triangular half unit cells, one of which is located above a stacking fault. The faulted (F) and unfaulted (U) half unit cells are bordered by nine dimer pairs, and the cross-linked boundaries between unit cells are therefore known as dimer rows.

Before reconstruction a 7×7 area of the native Si(111) surface has 49 dangling bonds, compared with 19 dangling bonds in each reconstructed unit cell. Both experiment[66−68] and calculation[69] show that the 19 remaining dangling bonds are of seven inequivalent (symmetrically distinct and therefore electronically distinct) types; one dangling bond of each type is present on the midsection. In Figure 12 the different

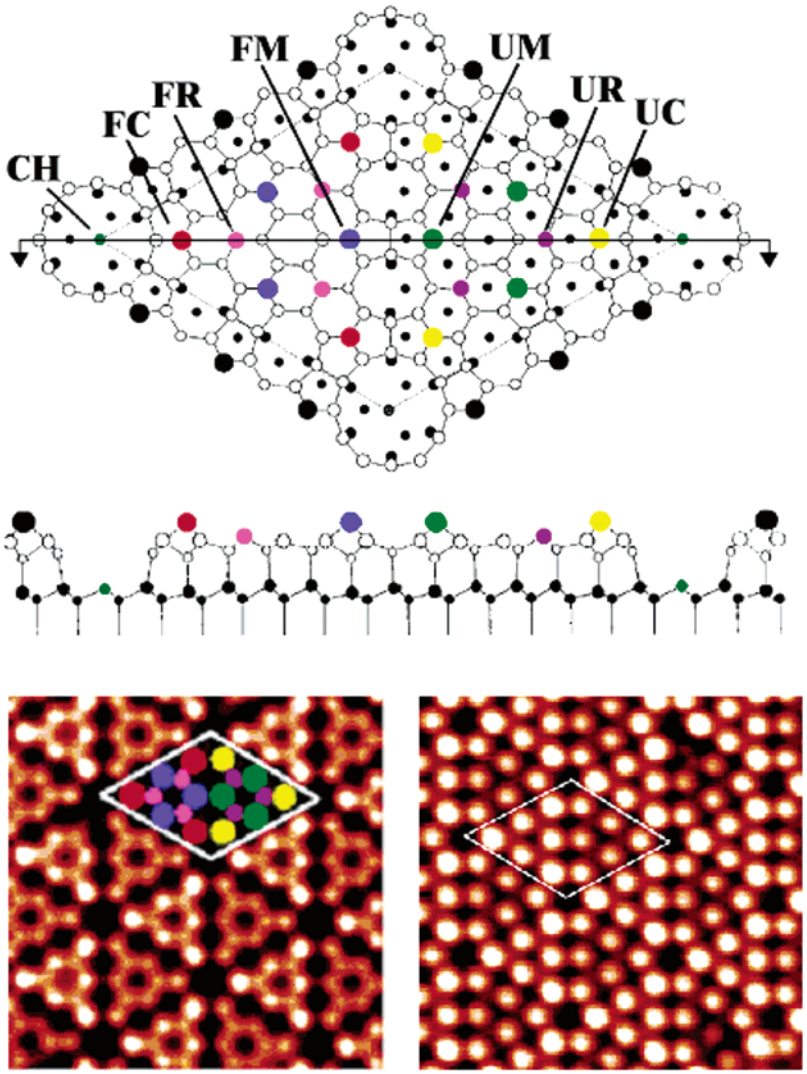

Figure 12. Si(111)-7×7 surface reconstruction. (Top and center) Dimer adatom stacking fault model of the reconstruction contains seven types of atoms that are inequivalent and have dangling bonds. Each of these types is present on the center section of the unit cell. They are, from left to right in the schematic section, corner hole (CH) adatom (dark green), faulted-half corner (FC) adatom (red), faulted-half rest (FR) atom (light purple), faulted-half middle (FM) adatom (blue), unfaulted-half middle (UM) adatom (light green), unfaulted-half rest (UR) atom (dark purple), unfaulted-half corner (UC) adatom (yellow). The same color coding has been superimposed on one unit cell of the STM image beneath. Adapted with permission from ref 70. Copyright 1994 Elsevier. (Bottom left) STM image of the Si(111)-7×7 reconstruction taken in negative bias ($V_s = -1.5$ V). This topographic image is unusual in showing both the adatoms and rest atoms, the faulted (bright) and unfaulted (less bright) halves of the unit cell are clearly distinguishable. Also clearly distinguished is the difference between faulted center (FC) and faulted middle (FM) adatoms and also between unfaulted center (UC) and unfaulted middle (UM) adatoms. Midway between the corner adatoms and the middle adatoms are the rest atoms (FR and UR). (Bottom right) More usual STM image of the Si(111)-7×7 surface taken in negative bias and clearly showing the adatoms in the two halves of the unit cell; the faulted half is bright and the unfaulted half dark. With care, here one can also notice the difference in intensity of four inequivalent types of adatoms: FC, FM, UM, UC. Reprintedwith permission from ref 71. Copyright 2004 American Physical Society.

types of dangling bonds have been color coded (see caption). The reactivity of each type of dangling bond to both nucleophilic and electrophilic reagents was estimated with density functional theory (DFT).[70] The middle-adatom electron density is found to be much less than that of the corner adatom due to charge transfer between the adatom and rest atom.[68]

Filled-state STM images (surface negatively biased with respect to the tip) of the Si(111)-7×7 surface are shown in Figure 12 (bottom left, bottom right). The bottom left STM image is the highest resolution image that has been published.[71] All dangling bonds (adatoms and rest atoms) are visible with the exception of the corner-hole adatoms (the corner hole adatoms can be imaged by STM using tips coated with bismuth[72]). One unit cell has been color coded in the above schematic to show the position of each dangling bond. A more usual STM image at slightly lower resolution is shown (bottom right). The dangling bonds on the rest atoms and in the corner hole are largely filled with a lone pair of electrons (containing about 1.5 to 2 electrons), but the dangling bonds on the adatoms are almost empty (containing about 0.5 electrons).

As will be seen below, the differing reactivities of parts of the Si(111)-7×7 unit cell often give rise to segregation of adsorbates with preferential adsorption on either the faulted (F) half unit cell or unfaulted (U) half unit cell. Also, different reagents preferentially react at adatoms or rest atoms. For metals deposited onto the Si(111)-7×7 surface, at temperatures that do not lead to mixed reconstructions, clusters are formed within the half unit cells. This has been demonstrated with many metals, for example, Pb,[73−77] Tl,[78] Ag,[79−81] Pd,[82] Ge,[83] Sn.[84,85] In,[84] Ga,[86] Al,[87] Mn,[81] Cu,[88] and

K,[89,90] but as no chemical reaction other than adsorption occurs in this process, we do not consider this surface-patterning further.

3.3. Types of Reaction and Energy Dependence

3.3.1. Si(111)-7×7/O_2

Oxidation of silicon is well studied, but the structure of the silicon oxide adsorbates is not known.[91] In STM images, after oxygen adsorption on Si(111)-7×7, both bright and dark adatom adsorption sites are seen. To elucidate the nature of these reacted oxygen adsorption sites, Mayne et al.[91] examined oxidation at 30 and 300 K and the effect of manipulating the adsorption sites using the STM tip at both fixed voltage and fixed current at 300 K. It was found that every manipulation of a bright site created a dark site, which was taken to indicate that the oxygen atoms were in the back bonds, in agreement with previous studies. Figure 13 shows two pairs of STM topographs showing such sites before and after manipulation; dark sites could be transformed into bright sites by electron irradiation. The manipulations indicated that there were different types of dark sites that coexisted on the surface.

These manipulations exhibited a local patterning of the surface, but neither the starting configurations nor the final configurations can yet be assigned with confidence. At room temperature it is thought that bright sites are Si adatoms with O atoms inserted into two of the back bonds while dark sites are of more than one type; one dark site has been assigned as being SiO_4 with three O atoms in back bonds and one attached to the dangling bond. At low temperature (30 K) dark sites have been assigned as Si adatoms with O atoms inserted into two of the back bonds (the same structure that appears bright at room temperature); the structure of the bright sites has yet to be determined.

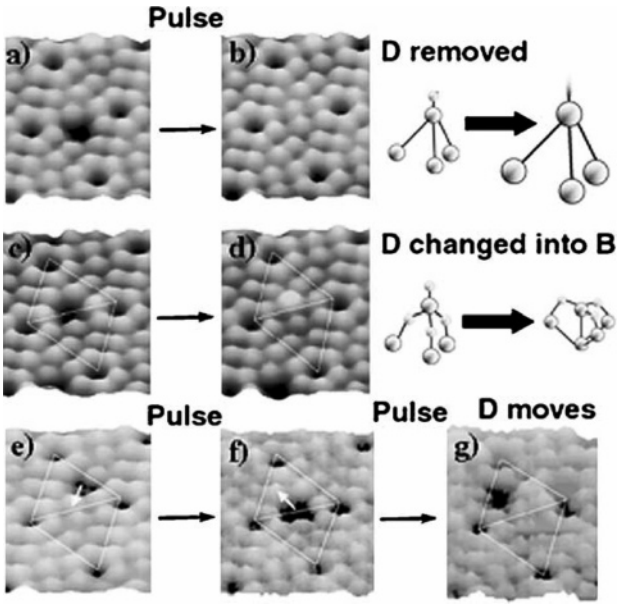

Figure 13. (a−d) Two pairs of STM topographs showing the dark sites before and after manipulation. D removed from a and b, D changed into B (c and d). (e−g) Apparent displacement of the dark site from adatom to adatom after each pulse. Each image is 40 Å × 50 Å in size. Proposed oxidation structures are shown on the right-hand side. Reprinted with permission from ref 91. Copyright 2003 Elsevier.

3.3.2. Si(111)-7×7/F_2, Cl_2, Br_2, ICl, IBr

Interaction of a range of halogen and interhalogen molecules with the Si(111)-7×7 surface was extensively studied in the Kummel laboratory using kinetic-energy-resolved molecular beam scattering and STM detection of the halogenation.

The reaction of incident Cl_2 molecules was studied as a function of collision energy by Yan et al.[92,93] At low incident energy (0.11 eV), precursor-mediated dissociative chemisorption was dominant with formation of giant two-dimensional islands of SiCl. The islands may be due to Cl_2 being mobile in a physisorbed state and migrating to edges of growing islands prior to dissociation with reaction to form SiCl. The lifetime of the freely moving physisorbed Cl_2 was estimated to be on the order of 800 ns using a simple 2D gas model.

At high incident energy (0.44 eV) both abstractive and dissociative chemisorption were seen. It was found that the ratio of the number of reacted middle adatoms to that of reacted corner adatoms was M/C = 2 ± 0.3 at low coverage. At this high translational energy only individual adsorption was observed, with the SiCl randomly located rather than being associated with islands.

In later work a competition between dissociative chemisorption and Cl-atom abstraction was observed[93] and found to be a function of the Cl_2 incident energy. The percentage of single sites formed by Cl abstraction, s_0, and pair sites of Cl atoms formed by dissociative chemisorption, p_0, was measured at three Cl_2 incident energies (where $s_0 + p_0 = 100\%$) as follows: $s_0(0.05\text{ eV}) = 54 \pm 1\%$, $s_0(0.11\text{ eV}) = 46 \pm 2\%$, and $s_0(0.44\text{ eV}) = 36 \pm 2\%$; this is shown graphically in Figure 14. Abstraction was favored at low energies, and dissociative chemisorption was favored at high energies. It was later found[94] that annealing the Cl-covered Si(111)-7×7 surface led to complete destruction of SiCl islands and pairs.

The same laboratory[95] studied dissociative chemisorption of fluorine molecules at the Si(111)-7×7 surface. They found that for fluorine molecules with low incident translational energy nearly all chemisorption produced isolated silicon fluoride. Single Si−F sites were formed through abstractive chemisorption in which one fluorine atom attached to the

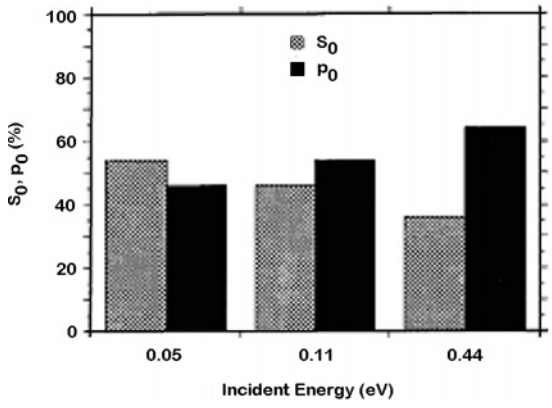

Figure 14. Percentage occurrence of singles ($s0$) and pairs ($p0$) as a function of increasing incident energy. $s0$ is denoted by the shaded bar. while $p0$ is denoted by the solid bar. $s0$ decreases with increasing incident energy, while $p0$ increases with incident energy: $s0(0.05\text{ eV}) = 54 \pm 1\%$, $s0(0.11\text{ eV}) = 46 \pm 2\%$, and $s0(0.44\text{ eV}) = 36 \pm 2\%$. $p0$ is given by $s0 + p0 = 1$. Reprinted with permission from ref 93. Copyright 1995 American Institute of Physics.

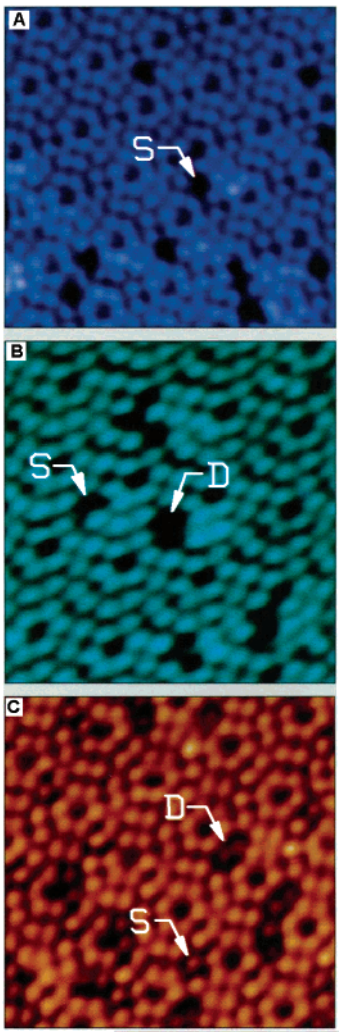

Figure 15. Constant-current, empty-state (sample positively biased with respect to the tip) STM images of Si(111)-7×7 after exposure to (A) 0.03 eV F_2 with a total coverage of 3.2% reacted adatoms, (B) 0.27 eV F_2 with a total coverage of 3.5% reacted adatoms, and (C) 0.5 eV Br_2 with a total coverage of 5.5% reacted adatoms. Imaging bias voltages were 0.8, 1.0, and 0.6 V, respectively. The Si−Br σ^* state is imaged at a relatively low bias: S, single site; D, dimer site. Single sites dominate for 0.03 eV F_2 (A), whereas dimers dominate adsorption for 0.5 eV Br_2 (C). Images were not corrected for thermal drift. Reprinted with permission from ref 95. Copyright 1995 AAAS.

surface while the other was ejected into the gas phase. In contrast, for fluorine molecules with higher incident translational energy, many more pairs of Si−F were formed through dissociative chemisorption, $F_2 + 2Si \rightarrow 2Si-F$, paralleling findings for O_2 on metals. For experimental reasons it was not possible to study F_2 with very high energy, but Br_2 molecules with a high incident translational energy of 0.5 eV were examined (Br_2 molecules with lower translational energies were not examined). It was found that at high incident energy Br_2 molecules gave largely dissociative chemisorption, with few single Si−Br. Figure 15 shows surfaces that have been reacted with F_2 and also with Br_2, showing single sites and dimer sites. These experiments showed that the competition between abstractive and dissociative chemisorption depends on the translational energy of the incident molecule in a qualitative fashion similar to O_2 on metals.

Adsorption of halogens at the Si(111)-7×7 surface was further studied by Jensen et al.[96] For abstractive chemisorption in which a single chemisorbed halogen atom was produced, the ratio of reaction at corner and middle adatoms showed that for F_2, Cl_2, and Br_2 middle adatom reaction was preferred.

Dissociative chemisorption (giving pairs of adsorbates on the surface) also showed site-specific reaction, and this was investigated in detail. There are five possible arrangements for pairs of adsorbates on the Si(111)-7×7 lattice (ignoring differences between faulted and unfaulted half unit cells); these are shown in Figure 16 (top). The distributions of different pairs of attachments were measured at low (Cl_2, 0.05 and 0.11 eV; Br_2, 0.2 eV) and high (Cl_2, 0.44 eV; Br_2, 0.5 eV) incident translational energies and found to differ markedly. Figure 16 (bottom) shows graphically the difference between the relative number of each type of adsorbate pair for dissociative chemisorption of Cl_2 and Br_2 at low and high translational energies (at high translational energy dissociative chemisorption is the dominant process). There is an extreme preference for the middle−middle pairwise adsorption site between two halves of the unit cell. This corresponds to the closest possible set of middle adatoms at a separation of 6.9 Å. This can be compared with the equilibrium bond distances for Cl_2 and Br_2 of 1.98 and 2.28 Å, respectively.[33]

In summary, abstractive chemisorption from halogen molecules on the Si(111)-7×7 surface showed a strong preference for attachment to middle adatoms, whereas dissociative chemisorption, at all energies, showed a strong preference for pairs of halogens sited at adjacent middle adatoms (less strongly for adjacent corner adatoms). The pairs of sites for dissociative chemisorption are separated by 6.9 Å, the smallest adatom separation on this surface.

Liu et al.,[97] in the Kummel laboratory, also examined ICl adsorption on Si(111)-7×7. They found that the dominant pathway of abstractive chemisorption was formation of silicon iodide by abstraction of I atoms with concurrent ejection of Cl atoms into the gas phase, represented as

$$ICl(g) + Si(111)\text{-}7\times7 \rightarrow I(ads)/Si(111)\text{-}7\times7 + Cl(g) \quad (3)$$

Surprisingly, this dominant channel (82%) is the least exothermic. The ratio of iodine to chlorine absorption at the surface was measured using both Auger electron spectroscopy and temperature-programmed desorption and found to be approximately 2.5 to 1. The preference of the surface for iodine abstraction was understood as being due to steering of the ICl into an iodine-toward-silicon orientation as it approached the surface due to the interaction between the partially filled silicon dangling bonds and the asymmetric highest-occupied molecular orbitals (HOMOs) of ICl in which the HOMOs are preferentially concentrated at the iodine atom. In the gas phase this effect has been termed rotational steering.

In a subsequent study IBr[98] adsorption was dominated by abstraction (90% at 0.15 eV incident energy, 77% at 0.82 eV incident energy, as for ICl). A preference for abstraction to occur at middle adatoms was found. In contrast to the work on ICl, no atomic selectivity for iodine or bromine was observed. This is attributed to the fact that the HOMOs of IBr distribute almost evenly on the I and Br atoms.

3.3.3. Si(100)-2×1/Cl₂

The dissociative chemisorption of molecular chlorine on Si(100)-2×1 has been the subject of detailed study at 300

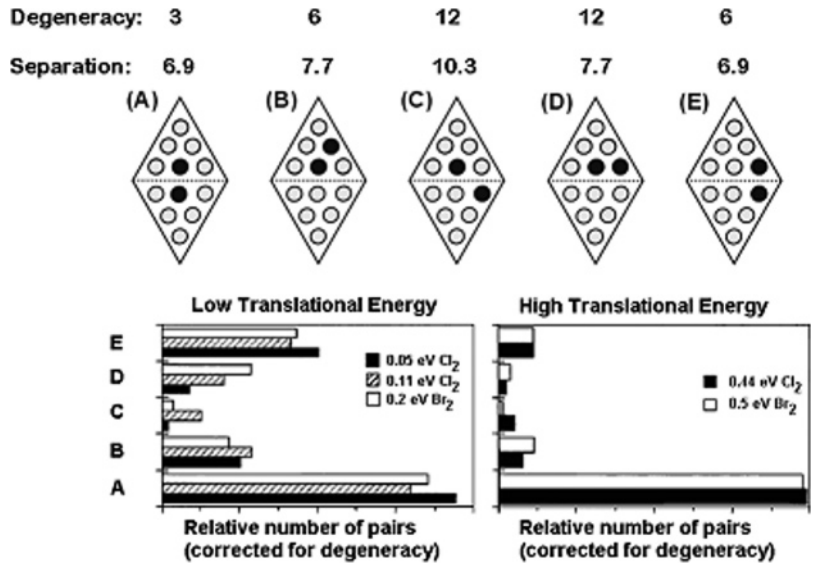

Figure 16. (Top) Five possible arrangements of pairs of adsorbates, due to chemisorption, on nearest-neighboring adatom pairs of the Si(111)-7×7 unit cell. In this analysis faulted and unfaulted half unit cells were treated as indistinguishable; separations are given in Ångstroms. (A) M−M, between two-half unit cells; (B) MM, within one-half unit cell; (C) M−C, between two-half unit cells; (D) M−C, within one-half unit cell; (E) C−C, between two-half unit cells. (Bottom) Relative number of each type of adatom pair (A−E as defined) is plotted for Cl_2 and Br_2 chemisorption at low and high translational energy. Data have been normalized for the degeneracy of each type of pair. (Adapted with permission from ref 96. Copyright 1996American Physical Society.

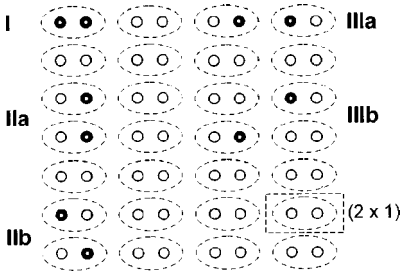

Figure 17. Schematic of the five geometrically distinguishable configurations of the neighboring pairs of Cl atoms on the Si(100)−2×1 surface. Si dimers and 2×1 unit cell are outlined by dashed lines. Reprintedwith permission from ref 99. Copyright 1998 American Physical Society.

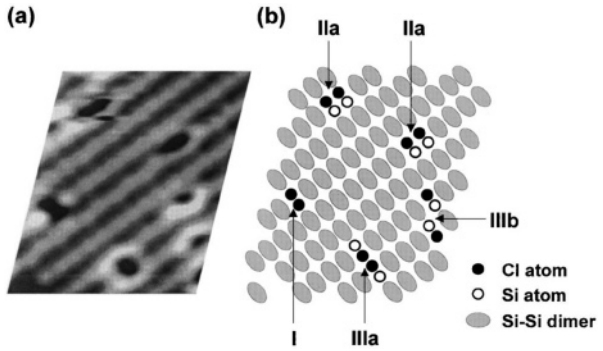

Figure 18. Image of the 46 Å × 55 Å region of the Si(100) surface at initial stages of Cl_2 adsorption showing the different Cl adsorption sites. (a) Filled-state STM image; $V_s = -1.5$ V, $I_t = 0.05$ nA. (b) Schematic identification of the observed features. Reprintedwith permission from ref 99. Copyright 1998American Physical Society.

K[99] in the Yates laboratory. The result was found to be markedly different from the adsorption on Si(111)-7×7. Five geometrically distinguishable configurations of neighboring pairs of Cl atoms were found; these are shown in Figure 17. In this work only pairs of Cl atoms were found, indicating that no abstractive chemisorption occurred. It was found that pairs of Cl atoms were always adsorbed on either single dimer pairs or adjacent dimer pairs (as shown in Figure 17), either within single rows or between adjacent rows. Analysis of the number of different types of adsorbate sites as a function of Cl coverage showed that the least-probable dimer configuration corresponded to the most favored thermodynamically, showing that the site-selection process was controlled by dynamic rather than thermodynamic factors. The observed selectivity, Figure 18, which involved preferential reaction at sites IIIa and IIIb of Figure 17, was consistent with Cl_2 dissociative chemisorption occurring via a mobile precursor. Localization of the halogenation to adjacent sites was marked.

3.3.4. Si(111)-7×7, Si(100)-2×1/(H_2S, D_2S)

The spontaneous thermal dissociation, at 200 K, of both H_2S and D_2S at the Si(111)-7×7 surface (50−300 K) was studied by Rezaei et al.[27] as was the dissociation of D_2S at Si(100)-2×1 (80−300 K).[100] In both cases it was found that absorption of H_2S (D_2S) took place dissociatively at low coverage, giving rise to HS (DS) at the surface. Particular interest attaches to the pattern of secondary reaction of the HS (DS) induced by tip electrons, studied in both cases.

For Si(111)-7×7, HS (or DS) adsorbed on the middle adatoms initially, but as coverage became higher, the corner adatoms also became populated. The characteristics of the adsorption were studied in detail[101] and found to be a function of both coverage and temperature.

Further reaction of SH (DH) at the Si(111)-7×7 surface was only examined for SH (DS) adsorbed onto middle adatoms. As shown in Figure 19, SH (darkened adatom) could be dissociated by the STM tip at low temperatures (200 K) without affecting a neighboring SH adsorbate. As seen in Figure 19, dissociation of SH gave rise to S (bright) bonded to the original adatom and H (dark) bonded to an adjacent adatom. The hydrogen (deuterium) atom bonded to a silicon atom (55 ± 8%) or desorbed. H and D on average moved one or two adatom sites away from the original molecule. It was also possible that H (D) adsorbed at sites that could not be imaged by STM, such as the dangling bonds

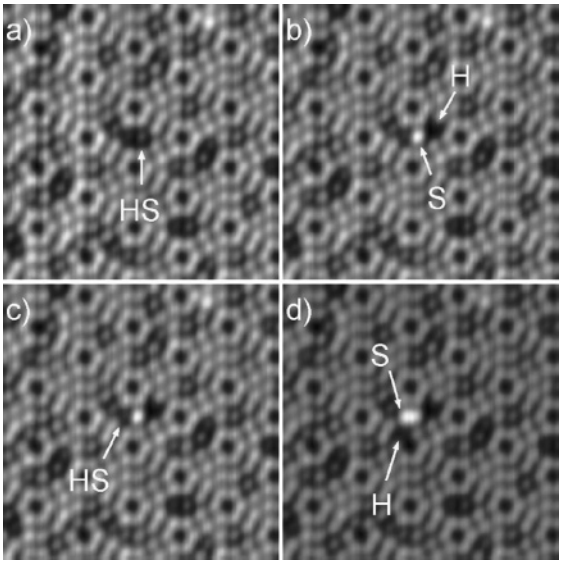

Figure 19. STM-induced single-molecule dissociation at 200 K. (a) Two HS molecules adjacent to one another. The tip is positioned over the right-hand side HS molecule as indicated by the arrow. (b) Image taken after a 2.5 V, 0.7 nA, 100 ms pulse showing that the right-hand side HS molecule is dissociated into H and S, without affecting the neighboring (left-hand side) HS. (c) Tip is moved over the second (left-hand side) HS molecule as indicated by the arrow. (d) After another 2.5 V, 0.7 nA, 100 ms pulse, the second HS molecule is dissociated. Images were scanned at $V_s = +1$ V, $I_t = 0.1$ nA. Reprinted with permission from ref 27. Copyright 1998 American Institute of Physics.

in the second layer, and that the H (D) that appeared to desorb had in fact reacted here. The sulfur atom was always found at the same position as the original SH molecule.

At 297 K and above dissociation occurred thermally (DS was used for all thermal measurements). By measuring the rate of dissociation as a function of temperature over the range 297−312 K, an Arrhenius plot was obtained and the dissociation barrier determined as 0.73 ± 0.15 eV with a preexponential factor of $10^{11.9\pm2.4}$ s^{-1}. For the thermal dissociation events it was found that the deuterium atoms could move over large distances, namely, 100 Å or more. This, if confirmed, is a rare example of delocalized reaction at a highly reactive surface. Surprisingly, the delocalized reaction appears to involve the DS with lower internal energy, i.e., thermal rather than electron-induced reaction.

For Si(100)-2×1 D_2S adsorption and dissociation was studied.[100] As before, D_2S only underwent partial dissociation on adsorption below 200 K to give SD + S. SD could subsequently be dissociated either by the action of scanning (at low temperatures) or thermally (with an appreciable rate above 200 K). On Si(100) the D atoms were always found adjacent to the adsorbed sulfur, in contrast to the 100 Å separation found on Si(111)-7×7. Adsorption at room temperature resulted in complete dissociation of the D_2S to atoms. The adsorption and dissociation behavior is shown in Figure 20.

3.3.5. Si(111)-7×7/H_2O

The first STM study of the room temperature thermal reaction of water with the silicon surface was that of Avouris and Lyo.[102] They found a 2 to 1 preference for middle−adatom reaction to form either H−Si or HO−Si, which could not be distinguished. These workers also pioneered the use of the electric field at the STM tip to induce localized reaction in this same system.

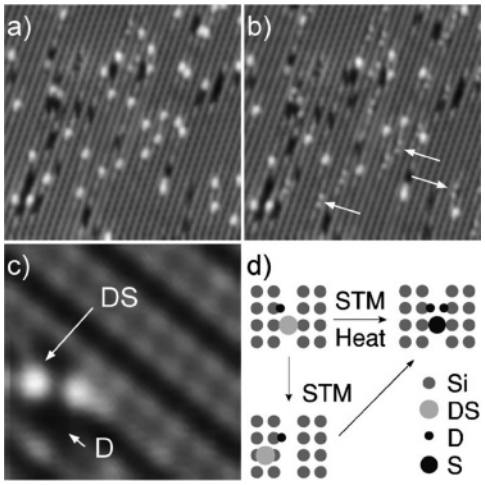

Figure 20. (a) D_2S on Si(100) at 130 K. (b) Same area as a but after a 2 V scan (both images obtained with $V_s = +1$ V, $I_t = 0.1$ nA). Some of the adsorbates, three of which are indicated by arrows, appear to be split into two smaller bright dots. (c) High-resolution close-up of the split adsorbate. DS molecule has moved onto the dimer bond. The other bright spot is a Si dangling bond that results from D adsorption onto the neighboring site. Image was scanned at $V_s = +2.45$ V, $I_t = 1$ nA. (d) Schematic model of the adsorption of D_2S on Si(100). The initial adsorption is partially dissociative; DS can be dissociated with STM or heat. STM can be used to move the DS onto the dimer bond. The sulfur atom does not stay on the dimer bond if the moved DS is dissociated. Reprinted with permission from ref 100. Copyright 1999 American Institute of Physics.

More recently Lo et al.[103] investigated adsorption and reaction at room temperature and high temperatures (up to 340 °C) at low, 0.02 L, exposures of H_2O. Remarkably, these authors were able to distinguish H−Si(rest atom) and HO−Si(adatom) in their images on rest atoms and adatoms, respectively. At room temperature, dissociative chemisorption was observed at an adatom and rest atom pair. No further dissociation occurred, and the sites were immobile.

In work at high temperature (340 °C) they were able to time-resolve diffusion of H and O and thermal dissociation of the OH product. A sequence of images obtained at 340 °C is shown in Figure 21. Dissociation of a single OH to give initially adjacent H−Si(rest atom) and O−Si is pictured. The nature of the O-atom site was thought to be insertion into a silicon adatom back bond. On the basis of these STM images it was concluded, surprisingly, that dissociation of OH was reversible to reform the hydroxyl radical within a half unit cell.

3.4. Site-Selective Reactivity on Si

3.4.1. Si(100)-2×1 and Si(111)-7×7/NH_3

The study by STM of the adsorption of ammonia on Si(100)-2×1 was the seminal work that showed the utility of STM as a probe for studying surface chemical reactions at the atomic level.[104−106] It was found that dissociative adsorption of NH_3 to yield H at the surface preserved the 2×1 local symmetry, but changes in the images allowed reacted and unreacted Si(001) dimers to be distinguished. The reaction with NH_3 was self-limiting, terminating with formation of a passivated hydrogen-covered H−Si(100)-2×1 monohydride surface layer. The fate of the nitrogen fragments could not be detected in the STM images, but it was thought from previous (non-STM) work[107] (using analytical techniques of

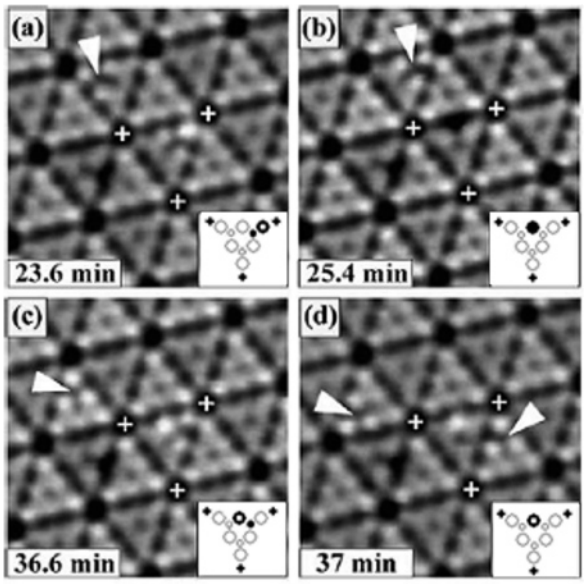

Figure 21. (a) OH radical dissociates into an O atom, which appears bright at the upper-right-hand corner of the enclosed half cell, and an H atom adsorbed at a rest atom site near that corner. The rest-atom site appears dark, and the Si adatoms neighboring the H atom appear brighter than normal. The O and H atoms can combine again to form an OH radical (b) or dissociate again (c). (d) After the H atom hops right to a faulted half (indicated also with a white arrow), only the O-induced bright species is left in the original half cell. At this point, the water molecule decomposes completely into two H atoms and one O atom, and all these species are mobile on the surface. For the atomic models illustrated in the inset, the O-induced adatom site is indicated with a dashed circle. The time indicated at each image refers to the time at which the image in Figure 1b of ref 103 was taken. Reprinted with permission from ref 103. Copyright 2003 Elsevier.

X-ray photoelectron spectroscopy, thermal desorption spectroscopy, electron-stimulated Auger spectroscopy, and electron energy-loss spectroscopy) that in this reaction the nitrogen-containing residue occupied subsurface sites.

Absorption of ammonia on Si(111)-7×7[67,68] was the first STM study of chemical reactivity at the Si(111)-7×7 surface reconstruction. Reacted silicon rest atoms and adatoms, H−Si and NH_2−Si, were both imaged with different images for differently reacted adatoms, but the images could not be unambiguously assigned. Using both STM imaging and spectroscopy[67,68] Wolkow and Avouris established the difference between the chemical reactivity of the rest atom, middle adatom, and corner adatom sites for reaction with H or NH_2 from NH_3; reactivity decreased in the stated order. Geometric factors contributed to the reaction propensities; there are two adjacent middle adatoms to each rest atom and only one adjacent corner adatom to each rest atom, so middle adatoms are at least twice as likely to see a free radical in the initial stages of rest-atom reaction. That a preference much greater than two was seen indicated that both geometric and electronic structure was important. These results continue to generate interest, as evidenced by the recent theoretical work of Kang.[108]

3.4.2. Si(100)-2×1/Si_2H_6

The surface chemistry of silanes was extensively reviewed by Rauscher in 2001.[109] The Hamers' laboratory, in a study of the thermal decomposition of disilane on Si(100),[110] showed that it dissociated to produce SiH_3 and SiH_2 fragments. The SiH_3 group thereupon dissociated into SiH_2 and H on a time scale of minutes. The H fragment was found to migrate several unit cells away from the original SiH_3 group (see Figure 22).

3.4.3. Si(111)-7×7/SiH_4, SiH_2Cl_2

STM was used by Memmert et al.[111] to investigate the room-temperature dissociative chemisorption of silane (SiH_4) on Si(111)-7×7. The H-atom reaction product was found to be formed largely at corner holes, with one H−Si formed per corner hole. The original suggestion was made by these authors that the reaction might involve insertion of the SiH_3 radical into the corner hole with concurrent reaction of H at the corner adatom. A parallel theoretical study of H-atom binding at the same surface performed by Lim et al.[112] identified the corner hole Si atoms as the most strongly bound to atomic H, linking this to its reactivity.

Subsequently, Komura et al.[113] arrived at a similar conclusion with regard to the site-selective reaction of Cl at corner adatoms in the room-temperature reaction of SiH_2Cl_2 at Si(111)-7×7. Once again a single atom—Cl in this instance—was found to react adjacent to each corner hole, and it was proposed that the radical, SiH_2Cl, had 'disappeared' from the view of the STM by entering the corner hole, where it reacted with the dangling bond at the corner hole adatom.

Positive evidence for this interesting mechanism of dissociative chemisorption is presently lacking, but in an imaginative experimental study reaction of the corner hole adatom with atomic H has been shown using specially prepared STM tips.[72]

3.4.4. Si(111)-7×7/HBO

Reaction of Si(111)-7×7 with HBO was examined by Miyake and co-workers.[114−116] At room temperature HBO molecules adsorbed intact at the surface; thermal reaction

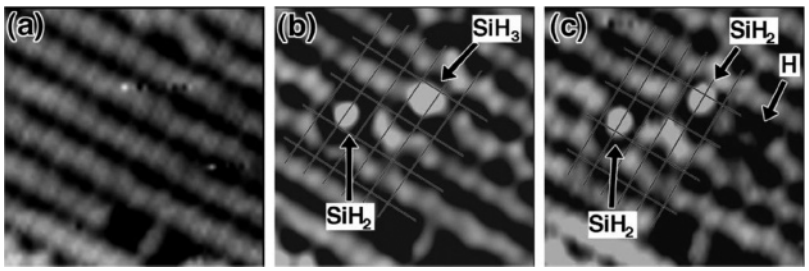

Figure 22. Sequential images of Si(100) surface showing adsorption of SiH_2 and SiH_3 and the dissociation reaction $SiH_3(ads) \rightarrow SiH_2(ads) + H(ads)$. (a) Clean Si(100) surface before exposure to Si_2H_6. (b) Same area as a after exposure to 0.1 L S_2H_6 at 300 K, showing an adsorbed SiH_2 group (upper) and a SiH_3 group (lower). (c) Same region as a and b, acquired 8 min after b, showing the shift in bonding location as the SiH_3 group dissociates to SiH_2 and the appearance of an atomic-sized depression due to H-atom adsorption. Dimensions: 47 Å × 47 Å, with $V_s = -2.2$ V, $I_t = 0.5$ nA. Reprinted with permission from ref 110. Copyright 1994 Elsevier.

could be induced at 300 °C. Reaction products were identified as O−Si and B−Si, the fate of H being undetermined. Reactive decomposition was the main channel. Even up to temperatures of 600 °C desorption from the surface was negligible, O−Si and B−Si being preferentially produced at corner and middle adatom sites, respectively. No analysis was made of pair separations, but it was suggested that B atoms would be expected to remain on the adatom site of the initial adsorption.

3.4.5. Si(111)-7×7/$B_{10}H_{14}$

STM was used at an early date, 1996, by Dujardin et al.[14] to selectively dissociate a molecule using localized charge transfer. These authors dosed decaborane ($B_{10}H_{14}$) at low surface coverages (0.01 L or so). The decaborane adsorbed preferentially close to surface defects, indicating an initially mobile precursor state. At higher doses, a propensity to adsorb at middle adatoms was noted. Two distinct adsorption geometries were found, which appeared as different sized bright spots in the STM images. Dissociation of the decaborane was induced by scanning at high positive bias voltage (greater than 4 V). Dissociation, thought to be due to impacting electrons, was directly observed, giving rise to a number of features in the images, close to the parent site, that at that date could not be specifically identified.

3.5. Localized Atomic Reaction (LAR)

As noted in the Introduction, extensive and revealing studies have been made of the mode of attachment of the intact aromatic organics to silicon surfaces by the opening of double bonds.[6,7] Our concern in this review has been with reactions involving adsorbate bond breaking. An early example is the study of the dissociative chemisorption of methyl chloride at room temperature on Si(100) made by the Hamers' group.[117] This was also the subject of a recent reexamination that substantiated the earlier findings.[118]

The methyl and chlorine fragments in the Hamers work were resolved, the signature of chlorine on the surface being known from previous studies by Boland.[119] Due to the varied types of chlorine−silicon bonding, it was not possible to determine the initial location of the Cl atoms following methyl chloride surface reaction. Instead, a statistical analysis was made of the relative yield of CH_3−Si and Cl−Si, suggesting that methyl chloride reacted in two ways with comparable probability: end-on abstraction reaction with attachment of Cl to a Si atom or sideways dissociative attachment to yield concurrently CH_3−Si and Cl−Si.

More recently it has proved possible to localize the initial reaction site of halogen atoms, X, coming from organic halides, RX, at Si(111) using STM. The distance by which the product X was separated from its parent RX,[23,120,121] or in the case of dihalides of various geometries, the internuclear separation between pairs of halogen atoms X and X′ originating from a single parent molecule, RXX′,[23,122−126] has been studied for several cases. The tendency for a halogen atom to imprint at a silicon adatom adjacent to its position in the parent molecule has been termed localized atomic reaction in this work.

The term localized atomic reaction was introduced some years ago to describe the observed tendency for energized molecules in the adsorbed state to react chemically in the vicinity of the parent adsorbate molecule.[127] The expectation that this might be the case was based on prior observations of what was termed localized atomic scattering, LAS, in which photodissociated adsorbates emitted fragments that gave evidence of scattering preferentially off adjacent atomic sites (ref 128 and references therein).

Where reaction with the surface is concerned, the propensity for LAR, as noted in ref 127, can be expected to be greater than that for localized scattering since chemical reaction commonly involves concurrent bond formation at the surface along with bond breaking (LAS only involves the latter). This is significant since it means that the reactive transition state (intermediate between the reagent and the product of chemical reaction) is being stabilized by the simultaneous existence of the old and new chemical bonds which together lower the barrier to reaction and favor localized reaction. This implies localized atomic reaction (LAR), as set out below.

If the favored reaction path, having the lowest energy barrier, involves what may be termed 'concerted' reaction, with old and new bonds coexistent in the intermediate configuration, it would follow that the reaction product must be formed within bonding distance of the parent molecule, i.e., by LAR.[127] (The qualifier 'atomic' in the acronym LAR refers to a reaction product consisting of an atom at the surface; this is not a necessary restriction but one imposed by the current state of experimental knowledge.)

At its most rudimentary, in LAR if AB(ad)/S_1 is the parent molecule adsorbed (physically or chemically) at surface site S_1 and the surface reaction is such as to transfer atom B to site S_2, the activated ('transition') state in the transfer reaction will be stabilized if there concurrently exist two partial chemical bonds indicated by dots in (A···B ···S_2)‡, partway between reagent A−B and product B−S_2. Since AB is located over site S_1 as AB(ad)/S_1, the coexistence of the bond being ruptured (A···B) and that being formed (B···S_2) requires that site S_1 and S_2 be adjacent, i.e., that the reaction be 'localized'. It should be noted that localized reaction due to this cause can occur even in cases where S_1 and S_2 are quite widely separated since A−B can displace B toward S_2, especially if A is polyatomic (see examples cited below).

3.5.1. Si(111)-7×7/C_6H_5Cl

Evidence for LAR is presented in Figure 23[127] for electron-induced chlorination of Si(111)-7×7 by chlorobenzene (ClPh), present at approximately 40% coverage. Parts a and

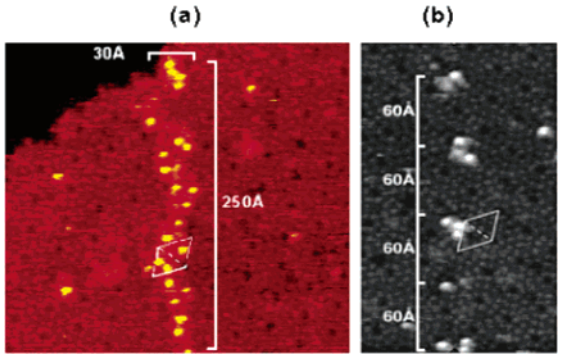

Figure 23. Localized atomic reaction (LAR). STM images of the Si(111)-7×7 surface showing localized chlorination of Si(111)-7×7 by electron impact at adsorbed chlorobenzene. Image was taken after application of a series of +4 V pulses to the surface while the tip was moved (left) continuously (colored) and (right) at 60 Å intervals (black and white) to successive positions along a line in the *y* direction. A 7×7 unit cell with sides 26.9 Å in length is outlined in white. Reprinted with permission from ref 127. Copyright 1999 American Institute of Physics.

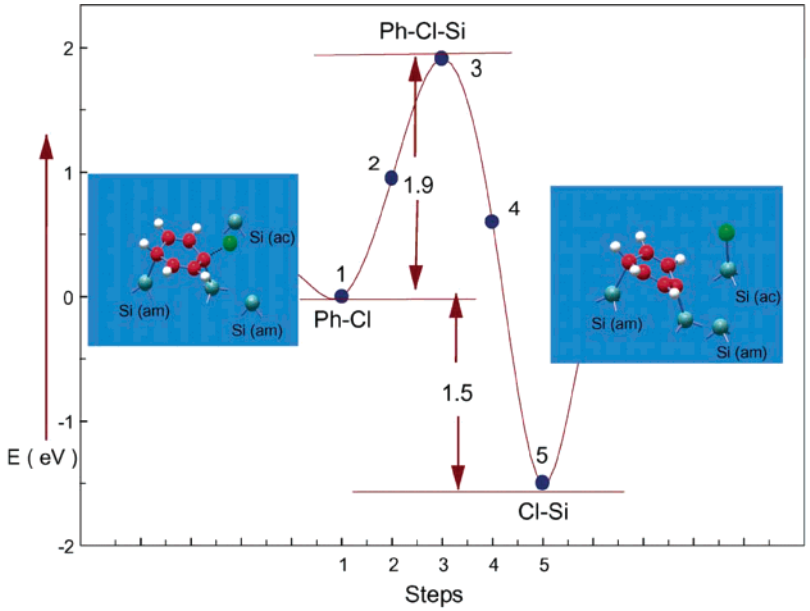

Figure 24. Dynamics of the chlorination reaction of an adsorbed chlorobenzene molecule on the ground potential-energy surface. The initial configuration shown at the left consists of a chlorobenzene molecule in the strained geometry, S, di-σ-bonded to a middle Si adatom (am), and a Si rest atom. The final configuration shown at the right consists of a Cl atom bonded to the adjacent corner adatom (ac) and a C_6H_5 free-radical at the surface, still in the S configuration. The computed activation energy is 1.9 eV, and the stabilization energy is 1.5 eV. Reprinted with permission from ref 120. Copyright 2003 Elsevier.

b of Figure 23 were traced at a surface voltage of $V_s = 3$ eV, at which voltage Cl atoms covalently bound to the Si adatoms appear as bright spots. The continuous line of Cl atoms seen in Figure 23a was formed from a continuous sequence of 4 eV pulses applied along the same line (this is in fact one-quarter of the length of the line recorded in the cited work). It is evident that the halogen atoms are localized to sites adjacent to the electron impact of ClPh.

A still more striking demonstration of localization was obtained by intermittently pulsing the tip at 60 Å intervals (again to a voltage of $V_s = 4$ eV at the surface), Figure 23b. The localized electron-induced reaction of ClPh to give Cl bound to the surface then yielded approximately three Cl atoms per pulse, localized along coordinates x and y to approximately three adjacent Si adatoms beneath the tip. Though LAR was clearly evident, the precise extent of localization was not fully determined at that time. Halogenation could, however, be seen to take place predominantly at an adatom adjacent to the parent ClPh molecule. Similar behavior has been reported for the thermal LAR of dibromobenzenes to yield separations from parent molecule to daughter Br (i.e., Br···Si) peaking at the nearest-neighbor separation of 7.7 Å.[129]

The rationale for LAR given above[127] has been confirmed in an ab initio computation, performed with DFT.[127] Chlorobenzene adsorbed on a model of the silicon, Si(111)-7×7, substrate (comprising 64 Si atoms in 5 layers) is shown in Figure 24. The molecule is σ bound to the surface at a middle and rest adatom.[130,131] The binding energy was calculated to be 0.47 eV for this strained configuration. The minimum-energy path en route to chlorination at the corner adatom (the atom marked ac) obtained by successive extension of the C−Cl bond with energy minimization at each step is shown in Figure 24. In view of the high dimensionality of the system, the calculated barrier height of 1.9 eV (see Figure 24) is best regarded as an upper limit; lower-energy pathways may exist.

This barrier is nonetheless informative since it is substantially less than that for complete severance of the C−Cl bond (3.4 eV). This stabilization of the transition-state configuration by approximately 1.5 eV was attributed to concurrent attraction of the Cl atom being transferred from its prior site C (carbon) to the subsequent corner Si atom, the Cl being bound at the same time to both its previous site and its subsequent binding site. Computation confirmed that, even for these widely spaced atoms, the reaction was concerted. Concerted reaction, as pointed out, could only occur with a neighboring atom; hence, LAR is to be expected.

The extent of 'localization' of reaction can be expected to depend on such factors as the nature of the reagents and products, i.e., the exoergicity, as well as the amount of reagent energy in excess of the barrier height to reaction. As will be reported in this review, substantial localization of reaction has been found for atomic transfer to the surface even in cases where photoinduced reaction with excess energy might be expected to drive the reaction products apart. This suggests that energy dissipation can be efficient in reactive systems. Since reaction may be triggered by charge transfer from the STM tip or the substrate, energy dissipation may be by subsequent charge transfer back to the surface as discussed below for Si(111)-7×7/CH_3Br.[121]

The work of Palmer, Sloan, and Xirouchaki[132,133] constitutes a study of the extent of localization of the chlorobenzene reaction. These authors performed an STM study of the electron-induced reaction of chlorobenzene with Si(111)-7×7 at room temperature. Reaction was found to occur only when electrons tunneled into the empty states of the adsorbed ClPh, i.e., with a positively charged surface.

A systematic study was made of the distance traveled by the Cl atom away from its parent ClPh molecule prior to covalent attachment at the surface (see Figure 25). Under typical conditions of $V_s = 4$ eV at the surface and 100 pA tunneling current, the Cl attached itself at the nearest-neighbor dangling bond. At five times this tunneling current,

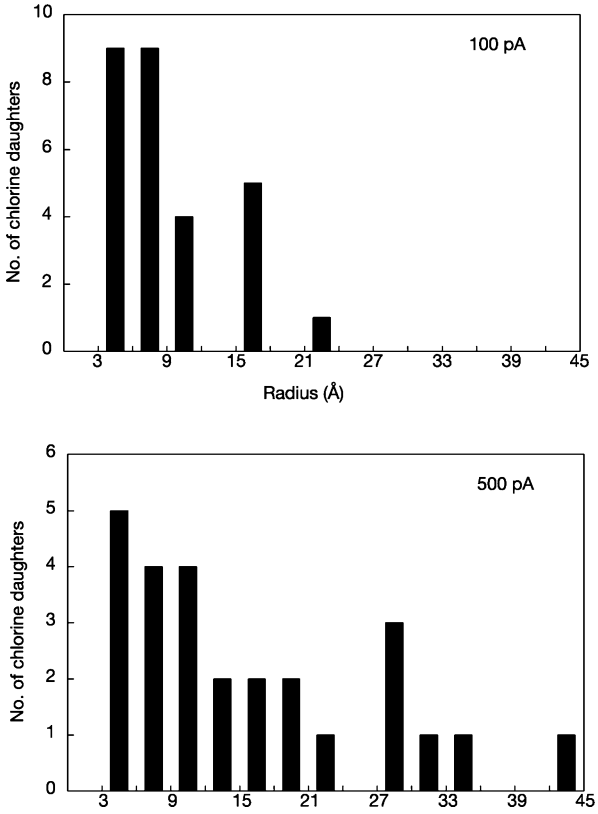

Figure 25. Radial distributions of daughter chlorine atoms formed by electron attachment to chlorobenzene adsorbed on Si(111)-7×7. Number of daughter chlorine atoms as a function of radial distance (3 Å wide bins) from their parent chlorobenzene molecules, generated by tunneling currents of 100 pA (top) and 500 pA (bottom). Adapted with permission from *Nature* (http://www.nature.com), ref 133. Copyright 2005 Nature Publishing Group.

higher mobility Cl atoms were also observed. The distance traveled by Cl from ClPh would be expected to depend on the azimuthal direction of the C−Cl bond, peaking in the region of the most probable separation, in the region of 7.5 Å, as observed for their lower tunneling current.

Though the link suggested here between alignment and distance traveled was not investigated, a remarkable aspect of this study was the direct observation of the alignment of individual di-σ-bound ClPh parent molecules and its correlation with the angular distribution of the Cl atoms measured relative to the σ-bond to σ-bond axis (see Figure 26). At the lower tunneling current of 100 pA the Cl-atom distribution was found to be strongly peaked 40−50° away from the σ-bond axis. This suggested a simple view of the reaction in which the original C−Cl bond, located at 60° to the σ bonds, extended approximately linearly and attached its Cl atom at the first dangling bond that it encountered. The same zero-order model had previously been offered to explain the differing patterns of reaction of halogen atoms at Si(111) observed for contrasting pairs of isomers of dichlorobenzene[23] or of dibromobenzene.[122,124,129,134]

Sloan and Palmer[133] reported a lesser degree of Cl-atom anisotropy in their experiments at 500 pA tunneling current (Figure 26g). It may be that longer Cl-atom travel distances correlated with wider angular scattering, in the course of energetically induced diffusion (though this was not investigated). Despite the fact that one tunneling electron at 4 eV should have more than enough energy to overcome the barrier to surface reaction (computed to be less than 2 eV[120])

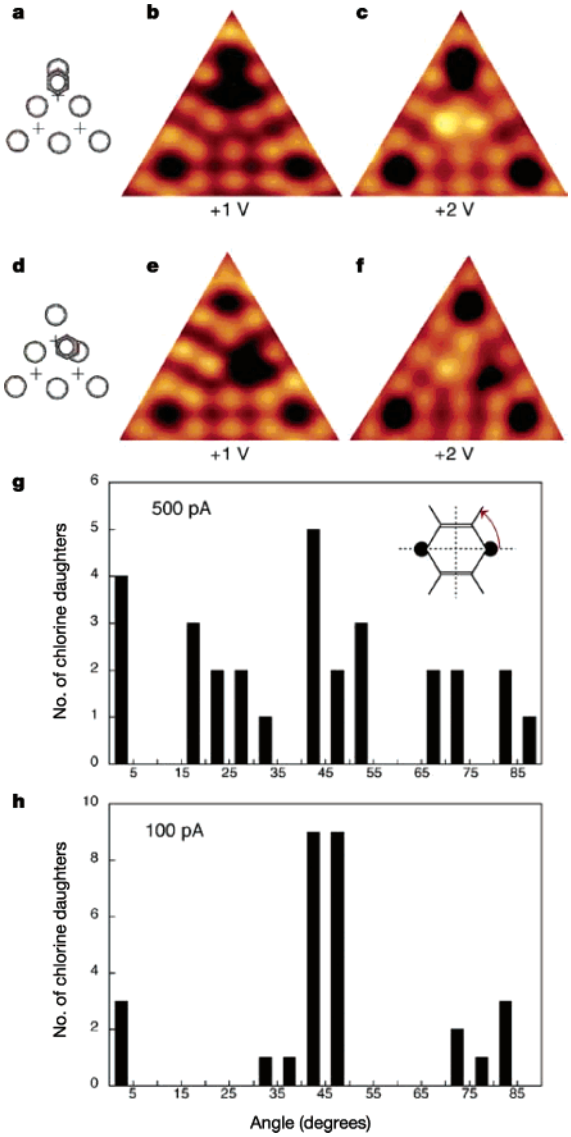

Figure 26. Angle-resolved dissociation. (a−f) STM images and schematic diagrams (circles represent adatoms, crosses represent rest atoms, and hexagons represent chlorobenzene molecules) showing the imaging characteristics of a single adsorbed chlorobenzene molecule as a function of sample bias (50 pA, bias voltages as marked). (a−c) Chlorobenzene bonded to a corner adatom. (d−f) Chlorobenzene bonded to a center adatom. Note the bright feature that appeared over the bonding rest atom in the case of a corner-bonded chlorobenzene molecule. This signature allowed the identification of the bonding rest atom when a chlorobenzene molecule was attached to a center adatom. (g, inset) Diagram of chlorobenzene adsorbate (filled circles represent the bonding silicon atoms) showing planes of symmetry (dashed lines) and angular coordinate system (red arrow). (g and h) Angular distribution of daughter chlorine atoms, relative to the adatom/rest-atom axis of each corresponding parent chlorobenzene molecule (inset) generated by tunneling currents of 500 pA (g) and 100 pA (h). Reprinted with permission from *Nature* (http://www.nature.com), ref 133. Copyright 2005 Nature Publishing Group.

Sloan and Palmer found that dissociation was a two-electron process. The mechanism of dissociation was attributed to initial vibrational excitation of the adsorbed ClPh reagent followed by formation of a short-lived $ClPh^-$ negative ion which subsequently reacted with the surface.

Some excess energy in the nascent Cl-atom product would be expected. The amount of excess energy will depend on factors that remain to be explored: (a) the total internal

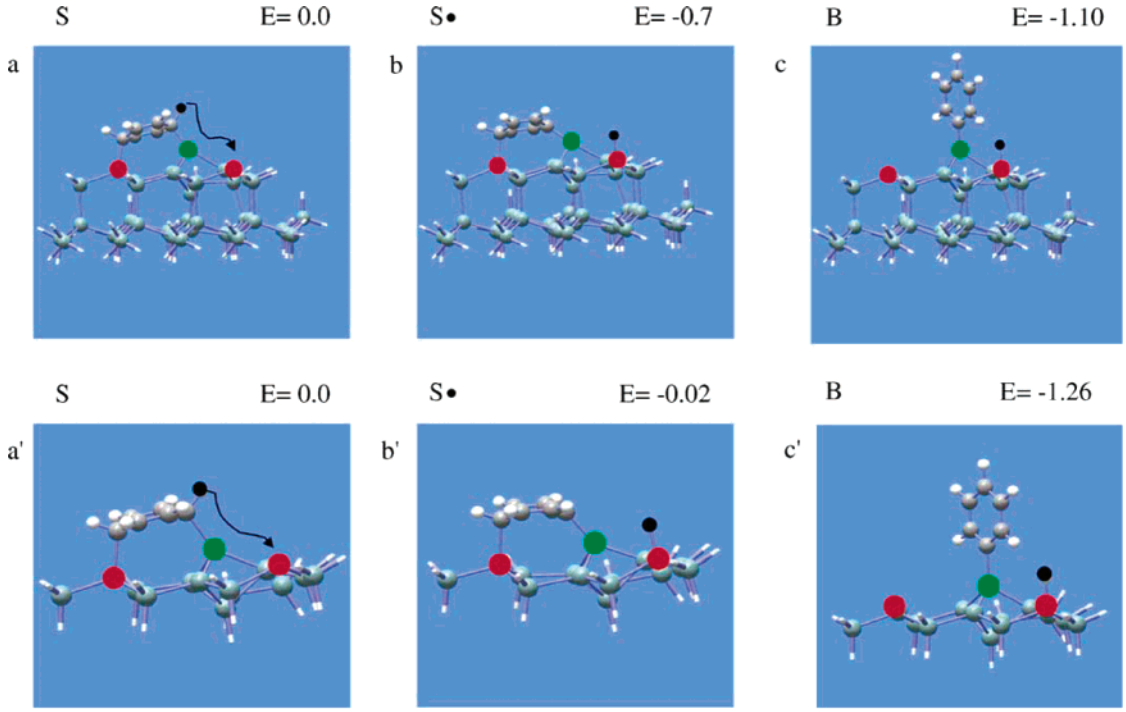

Figure 27. Minimum energy structures for reaction of benzene to hydrogenate on Si(111)-7×7 using the 2R1A model with five layers (top row) or three layers (bottom row). The top row was calculated by AM1 and the bottom row by DFT. Color coding is Si, gray; C, light gray; H, white; Si-adatom, green; Si-restatom, red; transferred H-atom, black. Reprinted with permission from ref 138. Copyright 2003 Elsevier.

energy in the reactive anion $ClPh^-$, (b) the energy released by the reaction including any concurrent reorganization of the organic residue on the surface as Cl^- departs, and (c) the total available energy partitioning between the organic residue, the recoiling Cl^-, and the electron transferred to the silicon.

The state of the organic residue, R−Si, at the surface following Cl-atom transfer to the silicon is not well known. Generally the residue appeared dark in images taken at $V_s \approx 1-2$ eV. If the doubly σ-bound hexadiene organic residue were to be left as a free radical, i.e., with a dangling bond at the location of the severed C−Cl, a brighter image would be expected for the organic residue than for the parent ClPh rather than the dark feature customarily observed.

It is possible that the di-σ-bound radical assumes a new bonding state at the surface following C−Cl rupture.[23] The di-σ-bound state constitutes a strained configuration with (experimentally) only ~1 eV binding to the surface.[135−137] Electron or photon (193 or 532 nm) irradiation of either di-σ-bound benzene or chlorobenzene at Si(111)-7×7 gave rise to a more strongly bound state.[120] This was postulated to be (counter-intuitively) due to conversion of the strained di-σ-bound state (S) to a more strongly bound state (B) consisting of a phenyl ring perpendicular to the surface.[120,138] This was computed, using AM1 (Austin model 1) and DFT, to have almost quadruple the total binding energy to the surface, i.e., 3.6 eV rather than 1 eV, due to stabilization of the ring which has ceased to be cyclohexadiene becoming instead fully aromatic. The dynamics of this conversion process is illustrated for the case of H-atom transfer to the surface from benzene in Figure 27 and for the case of Cl-atom transfer in Figure 28a−c.

Figure 28[138] gives stabilization energies for the possible stages of reaction of benzene calculated by AMI and DFT. Note that the mechanism requires that both of the strained σ bonds that formerly bound the hexadiene adduct (formed from benzene) to the surface break and a new σ bond be formed at the site of the atom that was lost to the surface.

3.5.2. Si(100)-2×1/ClC_6H_5, $Cl_2C_6H_5$

An experimental[139] and theoretical[140] study of electron-induced attachment of chlorinated benzenes at Si(100)-2×1 by STM showed a propensity for chlorobenzene and 1,2-dichlorobenzene to undergo a reaction akin to the S → B transformation described above but with severance of a C−Cl bond to give Cl−Si concurrently with formation of an adjacent vertical benzene ring, both fragments, R−Si and Cl−Si, being attached to a single dimer pair. The resulting 'displaced' configuration D, with a strongly singly σ-bound organic residue, R−Si, is shown in Figure 28 for (a) the chlorobenzene reagent in and (b) the 1,2-dichlorobenzene; Figure 28c shows the row-linking structure, L, that was identified as the most probable outcome of irradiation of 1,4-dichlorobenzene. In this case two C−Cl bonds of the parent molecule broke with the result that the organic residue was di-σ-bound as a fully aromatic ring. Calculation by HF-DFT gave the expected binding energy, $D_e \approx 3.5$ eV, for the singly C−Si-bonded D structure but much stronger binding, $D_e \approx 5.1$ eV, for the row-linking doubly C−Si-bonded L structure. Confirmation of the interpretation of the experimental STM images as being row-linking (L type) came from a DFT simulation (using the Vienna ab initio simulation package, VASP) of the observed height profile shown in Figure 29.

3.5.3. H–Si(100)-2×1/Styrene, Ferrocene, Alkane, Allyl Mercaptan

The examples cited above all involved atom transfer from an adsorbate to a silicon substrate, observed with atomic resolution by STM. There is, in addition, an important category of reaction in which the atomic transfer is from the surface to the adsorbate. The adsorbate was initially styrene.[141,142] The styrene was seen, by STM, to react with

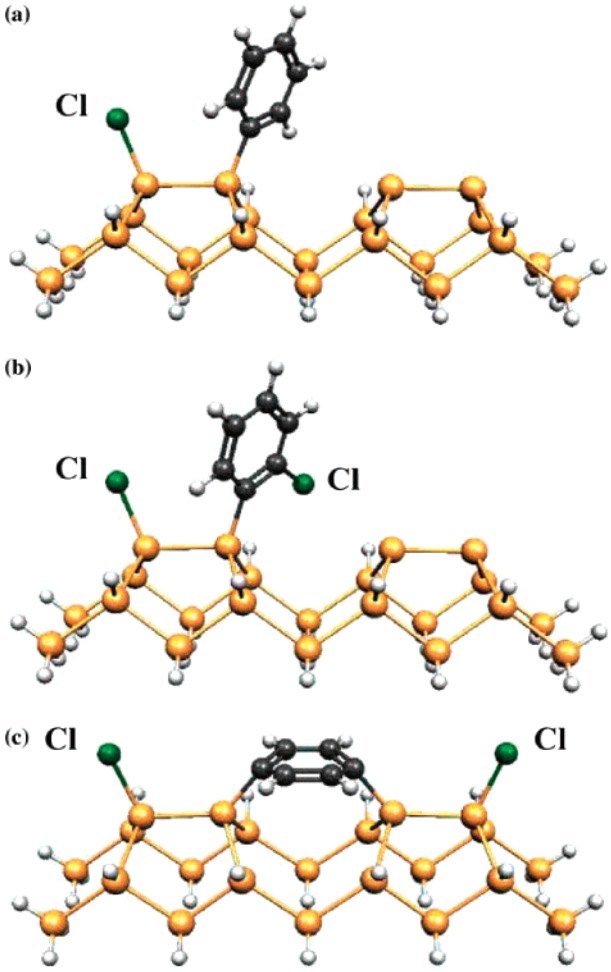

Figure 28. Calculated geometries of the displaced, D, and row-linking, L, configurations of chlorinated benzenes to chlorinate the Si(100)-2×1 surface. (a) Displaced configuration of chlorobenzene and (b) that of 1,2-dichlorobenzene. (c) Row-linking configuration of 1,4-dichlorobenzene. Si atoms of the dimers are shown in brown, Cl atoms in green, H atoms in white, and C atoms in black. (a and b) A single chlorine atom has been transferred to the surface; (c) two chlorine atoms have been transferred. Reprinted with permission from ref 139. Copyright 2003 Elsevier.

a dangling bond at a less than fully covered H−Si(100)-2×1 surface (H denotes hydrogenation of the surface). The double bond attached to the benzene ring of styrene opened spontaneously at room temperature, concurrently attaching to the dangling bond and abstracting a neighboring H from H−Si. As in the examples cited above, atom transfer involves an Si atom directly adjacent to the parent molecule. The parent molecule in this case is the recipient of atom donation rather than the donor as it was in the previously cited work.

The result of the H-atom abstraction from the adjacent H−Si, when repeated many times, was a line of styrene molecules extending along tens of adjacent Si in a dimer row (terminating, typically, at a surface defect). The styrene molecules were 3.84 Å apart, sufficiently close that they act as a 'molecular wire' for hole transport.[142] The current along such a wire has been shown by the same laboratory to be markedly affected by a point charge at an adjacent dangling bond,[143] offering the possibility of a future molecular transistor.

In addition to alkane molecules, CH_2═CH−R, with R = Ph (the case of styrene), ferrocene, and hydrocarbon chain, C_nH_{2n+1} ($n \geq 6$), have been shown to abstract an H atom

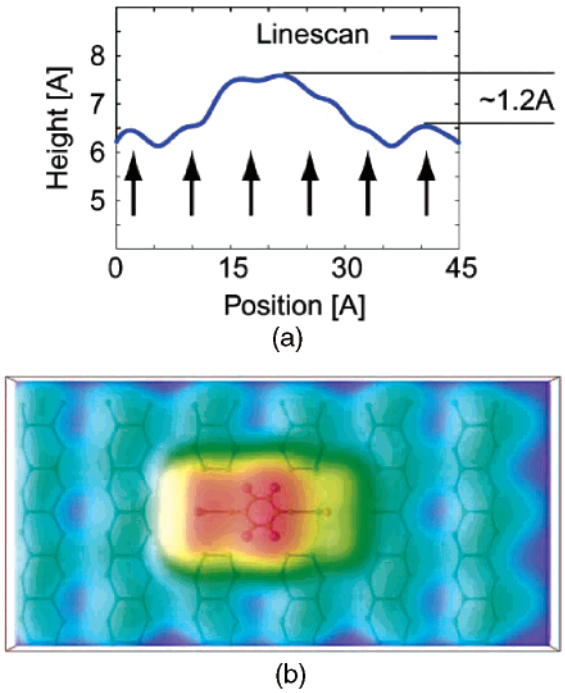

Figure 29. Simulated STM image of a 1,4-dichlorobenzene molecule in a row-linking configuration, L, on Si(100)-2×1. (a) Simulated STM scan line across the molecule. Maximum height of the molecule above the dimers in the simulation is 1.2 Å. This compares favorably with the 1.8 Å height measured in the STM images. A chlorobenzene molecule has been drawn to scale in the simulated image in b. Cl atoms are indistinguishable from the aromatic ring in these simulations. Reprinted with permission from ref 139. Copyright 2003 Elsevier.

from an adjacent H−Si, 3.84 Å away, along a Si(100) dimer row. This chain reaction is illustrated in the top schematic of Figure 30. When, however, R = CH_2−SH (i.e., the adsorbate is allyl mercaptan) the dangling bond in Si−CH_2−CH•−CH_2−SH was thought to migrate with H transfer along the attached hydrocarbon chain to form a thiyl radical, i.e., Si−CH_2−CH_2−CH_2−S•. The three-carbon chain, it was surmised, brought the terminal S• to a point adjacent to an adjacent Si-dimer row on the hydrogenated H−Si(100)-2×1 surface, as illustrated in the second line of the figure.

This geometric explanation of the altered reaction dynamics was tentative, but the observation that styrene and its analogues propagated predominantly across dimer rows of H−Si, at the larger separation of 5.1 Å, has been established.[144,145] The separation between H-atom abstraction sites on the surface agrees with the distance of the (presumed) sulfur radical from its C−Si anchor point (~5 Å). The markedly altered direction of chain propagation may, therefore, be predominantly dependent on the change in the geometry of the adsorbate molecule forming the links in the chain joining H-atom abstraction sites. The role of chemistry rather than geometry remains, however, to be explored.

3.5.4. Si(111)-7×7/C_2H_5OH, $(CH_3)_2CHOH$

The adsorption and reaction of methanol[146,147] and 2-propanol[148] on the Si(111)-7×7 surface was the subject of studies by the Tanaka group that has produced further examples of LAR. Methanol was found to react with the Si(111)-7×7 surface at room temperature, leading to darkened adatoms. By measuring site-dependent $I-V$ spectra at rest-atom positions adjacent to darkened silicon adatoms it was concluded that methanol reacted to form fragments

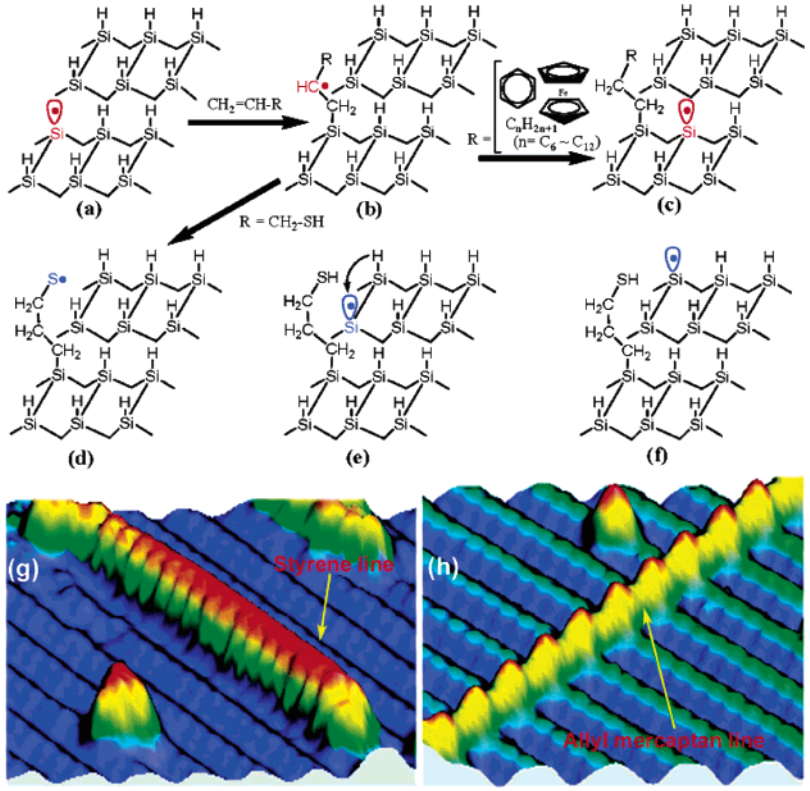

Figure 30. (a−f) Schematic of the mechanism of radical chain reactions along and across the dimer rows on the H-terminated Si(100)-2 × 1 surface. (g and h) STM images of molecular lines running along and across the dimer rows. (g) $V_s = -1.1$ V, $I_t = 0.2$ nA, scan area = 92 Å × 63 Å. (h) $V_s = -1.8$ V, $I_t = 0.2$ nA, scan area = 70 Å × 55 Å. Reprinted with permission from ref 145. Copyright 2005 American Chemical Society.

$CH_3O^•$ and $H^•$ attaching, respectively, to an adatom plus rest atom.

By measuring the number of darkened adatoms (CH_3O-Si) as a function of exposure to methanol, site-resolved kinetic information was obtained as shown in Figure 31. The methanol sticking probability was found to be independent of the coverage, showing the existence of a mobile precursor state to the dissociative chemisorption. At moderate doses of methanol, half unit cells were found to contain one, two, or three dark adatoms (CH_3O-Si). As the dose of methanol increased, the number of darkened adatoms changed as shown in Figure 31a.

A further analysis of the kinetics of the adsorption of methanol on Si(111)-7×7 was made in the same laboratory.[147] It was found that site selectivity between middle adatoms and corner adatoms changed with the occupation of adatoms in each particular half unit cell. For half unit cells with one, two, and three reacted adatoms, the middle/corner preference was 4, 2.6, and 1.8, respectively. This change in preference was understood as being due to decreasing probability of the dissociative chemisorption with increasing coverage.

Broadly similar results were found[148] for the dissociative chemisorption of 2-propanol on Si(111)-7×7. As before, dissociation led to an organic radical plus atomic H, attached, respectively, to an adatom and an adjacent rest atom. It was found that the coverage of $(CH_3)_2CHO-Si$ continuously increased in each half unit cell with adsorption becoming saturated when every half unit cell had three $(CH_3)_2CHO-Si$. As before, the site selectivity between middle and corner adatoms changed with the occupancy of adatoms in each particular half unit cell. For half unit cells with one, two, and three reacted adatoms, the middle/corner preference was now 4, 1.9, and 1.8, respectively.

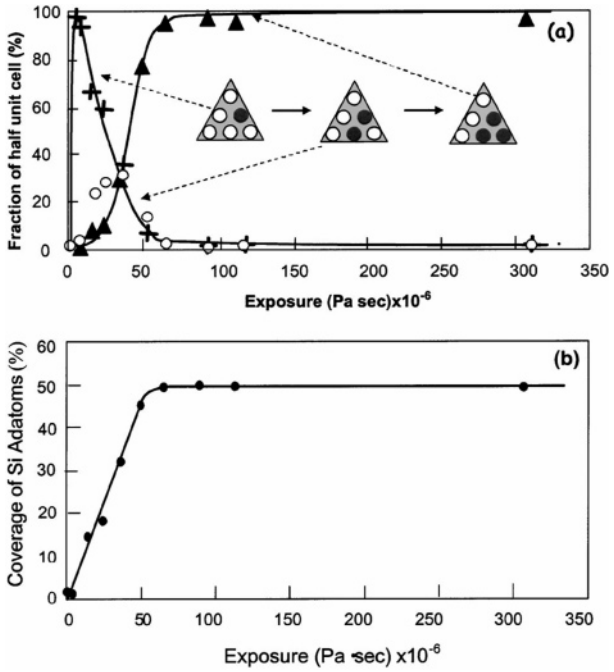

Figure 31. Site-resolved kinetics in adsorption of CH_3OH on the Si(111)-7×7 surface. (a) Fraction of the half unit cells having one, two, and three darkened adatoms changes consecutively with exposure (the graphics are not intended to imply particular positions of darkened adatoms). (b) Fraction of darkened adatoms linearly increases with exposure until saturation is reached at 50% adatom coverage. Reprinted with permission from ref 147. Copyright 2005 American Institute of Physics.

A significant difference between the adsorption of methanol and 2-propanol was that for methanol the dissociative chemisorption was independent of the coverage but for 2-propanol reaction probability depended on coverage at higher than 40%.

3.6. Molecular-Scale Imprinting (MSI)

3.6.1. Si(111)-7×7/CH_3Br

In this section we describe the highly localized photon- and electron-induced reaction, LAR, of CH_3Br(ad) at Si(111)-7×7. In such cases of highly localized reaction a loosely physisorbed self-assembled pattern can be imprinted to form an almost identical covalently bound pattern at the underlying surface. Considering the large downward shift that accompanies the abrupt change from physi- to chemisorption, this is a surprising observation. The phenomenon is expected to have practical value in molecular-scale imprinting (MSI), i.e., in rendering labile structures stable by means of strong attachment, without pattern change.

Alavi et al.[149] stressed the fragility of nanostructures formed—as they are most likely to be—by self-assembly in a physisorbed and hence mobile state. In almost any device, as they remark, there will be recurrent charge transfer, for example, in single-electron current flow. This will strongly and repeatedly alter the device−substrate interaction, tending to induce desorption (i.e., by repeated application of the well-known desorption-induced by electronic transitions, DIET). It will therefore be essential to find a means to attach the nanostructure to the surface without, however, destroying it. MSI represents a significant step in this direction.

From a chemist's standpoint the MSI 'printing' process constitutes an induced chemical reaction. Since self-assembly, which is a process of diffusion, takes a finite time, t_{sa}, it is advantageous to be able to select t_{sa} and only subsequently induce the imprinting reaction (physisorption → chemisorption) at a chosen instant, t_{imp}, by means of a brief pulse of energy delivered in the form of heat, light, or incident electrons.

The requirement that the pattern which constitutes the physisorbed nanostructure shall print, i.e., chemically react, with the underlying surface without alteration in pattern can be translated into the language of reaction dynamics; it is a requirement for fully localized reaction at the atomic level.

A priori one might suppose that the requirements for highly localized reaction would be stringent including (a) a reaction coordinate which is almost normal to the surface plane and (b) minimum possible translational energy along that reaction coordinate. Conditions a and b appear desirable so that the atom or group (the reacting moiety) approaching the surface has only a negligible momentum across the surface, thereby tending to suppress reaction at a distance from the original point of impact.

In fact, the example of the fully localized imprinting of a physisorbed nanostructure of the CH_3Br(ad) on Si(111)-7×7[121] is unlikely to have satisfied criterion a or b above; the transferred atom, Br, does not appear to approach entirely normal to the surface nor is it likely to have trivial translational energy. It would appear, therefore, that MSI does not make such stringent requirements on the molecular dynamics; the approach to the surface need not be strictly at 90° nor need the reaction be induced at its threshold energy. This is favorable to the prospects of generalizing MSI. It seems that a variety of physisorbed reagents will imprint as an identical, or closely related, pattern to the original.

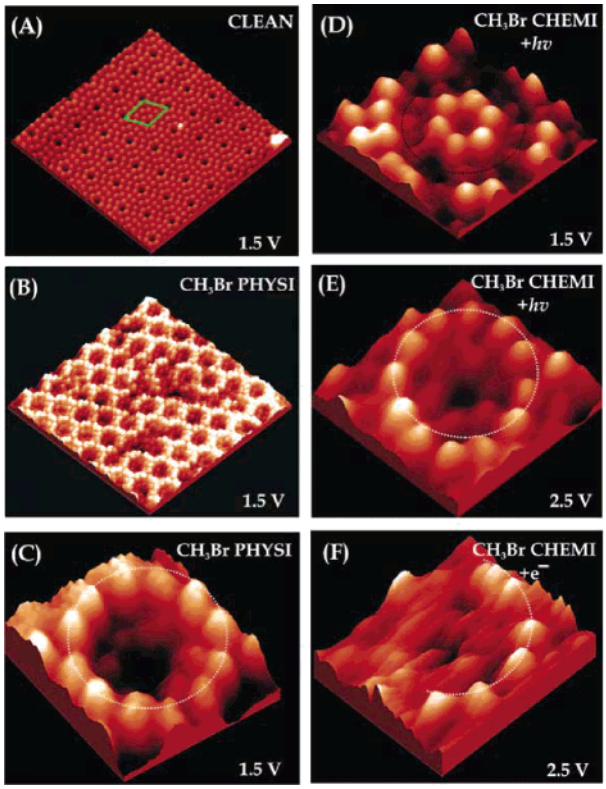

Figure 32. (A) STM image of the clean Si(111)-7×7 surface at 50 K. A 7×7 unit cell is indicated. $V_s = +1.5$ V, $I_t = 0.2$ nA, ≈200 Å × 200 Å. (B) STM image of physisorbed CH_3Br(ad) on the 50 K Si(111)-7×7 surface at a coverage of 0.41 monolayer. Physisorbed molecules appear as protrusions over the middle adatoms. $V_s = +1.5$ V, $I_t = 0.2$ nA, ≈ 200 Å × 200 Å. (C) Zoomed-in STM image of a single ring of physisorbed CH_3Br on Si(111)-7×7 surface (indicated by the dotted circle) as in B but ≈30 Å × 30 Å. (D) Chemisorbed Br on Si(111)-7×7 surface after photolysis of (three successive applications of) physisorbed CH_3Br(ad) at 50 K. Br (beneath dotted circle) now appears as depressions on the middle adatoms. $V_s = +1.5$ V, $I_t = 0.2$ nA, ≈30 Å × 30 Å. (E) STM image of chemisorbed Br imprints on the middle adatoms (indicated by a dotted circle) as in D but with $V_s = +2.5$ V. (F) STM image of chemisorbed Br on the middle adatoms (dotted in) obtained by scanning (a single application of) physisorbed CH_3Br(ad) at 2.5 V (scans from lower left to upper right); $V_s = +2.5$ V, $I_t = 0.2$ nA, ≈30 Å × 30 Å. Reprinted with permission from ref 121. Copyright 2004 Elsevier.

The published example[121] is that of a self-assembled pattern of methyl bromide, CH_3Br(ad), physisorbed at approximately 50 K surface temperature at the Si(111)-7×7 surface. Figure 32A shows an STM image of the clean surface at V_s=1.5 V, Figure 32B shows the circles of physisorbed CH_3Br(ad) found at 50 K, and Figure 32C shows a close-up of one of these circles comprising 12 well-separated CH_3Br(ad) molecules. This is the molecular type in the printing press, prior to imprinting. (Though not previously reported for CH_3Br(ad), such physisorbed patterns are well known for benzene at 78 K.[150] See also ref 151.)

Figure 32D shows the effect of 193 nm radiation on physisorbed CH_3Br(ad) at the unchanged surface voltage of V_s=1.5 V; the bright physisorbed circles of CH_3Br(ad) have disappeared, leaving dark circles of chemisorbed Br−Si which, in Figure 32E, 'light up' to give 12 bright Br−Si at V_s=2.5 V. This is the well-known voltage dependence of covalently bound Br−Si STM images.[126]

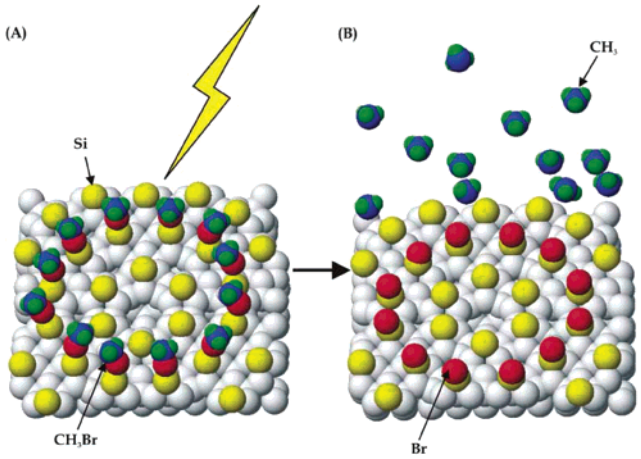

Figure 33. Schematic representation of (A) physisorption of CH_3-Br on Si(111)-7×7 surface with Br pointing down, and (B) chemisorbed Br on middle adatom positions after photolysis or electron impact at 50 K. Reprinted with permission from ref 121. Copyright 2004 Elsevier.

Definitive proof that the physisorbed CH_3Br(ad), only observable at the surface at ≤50 K, had been converted to a chemisorbed species was to be found in the fact that the circular patterns of Figure 32E following UV irradiation survived unaltered when heated to 200 °C for over 1 min. Undoubtedly chemisorption had occurred. There is no way that intact CH_3Br(ad) could itself become strongly chemisorbed at the surface as chemisorption requires formation of a bond. There is, however, abundant evidence that physisorbed methyl halides undergo photoreaction to halogenate reactive substrates.[152−158] What is new is the identification, by STM, of this photoreaction as being a highly localized event, i.e., Br−Si is found to form exclusively at the Si atoms directly beneath the parent CH_3Br(ad) molecules.

A number of authors have proposed and found evidence that the major cause of photoinduced surface reaction in physisorbed organic halides is charge transfer from the substrate to the adsorbate.[152−158] Not surprisingly, therefore, reaction of CH_3Br(ad) with Si(111)-7×7 could be induced by electrons of sufficient voltage coming from the STM tip, namely, 2.5V. Figure 32F shows that the reaction induced in this fashion is, as for photolysis, highly localized, giving rise to rings of chemisorbed Br−Si in place of the original rings of physisorbed CH_3Br(ad).

Figure 33 gives a schematic representation of the process of molecular-scale imprinting, MSI. A circle of 12 physisorbed CH_3Br(ad) are shown in Figure 33A. In Figure 33B, following irradiation by photons or electrons, the Br (red) atoms are shown reacting locally to brominate only the Si atoms beneath the CH_3Br(ad). The CH_3(g) radicals are thought to leave the surface since the characteristic black features indicative of methyl bound to silicon were not observed in the STM images following irradiation.

It remains to explain the highly localized nature of the observed reaction. Figure 34 (top) shows the physisorption geometry of CH_3Br(ad)/Si(111)-7×7 computed in the MP2 approximation (Møller−Plesset perturbation theory to second order). As expected, the most stable configuration is that with the Br end of CH_3Br pointing downward toward the Si surface. However, the C−Br bond is found in this calculation to be at an angle of approximately 60° to the surface normal. When, therefore, an electron is transferred to the CH_3Br^-

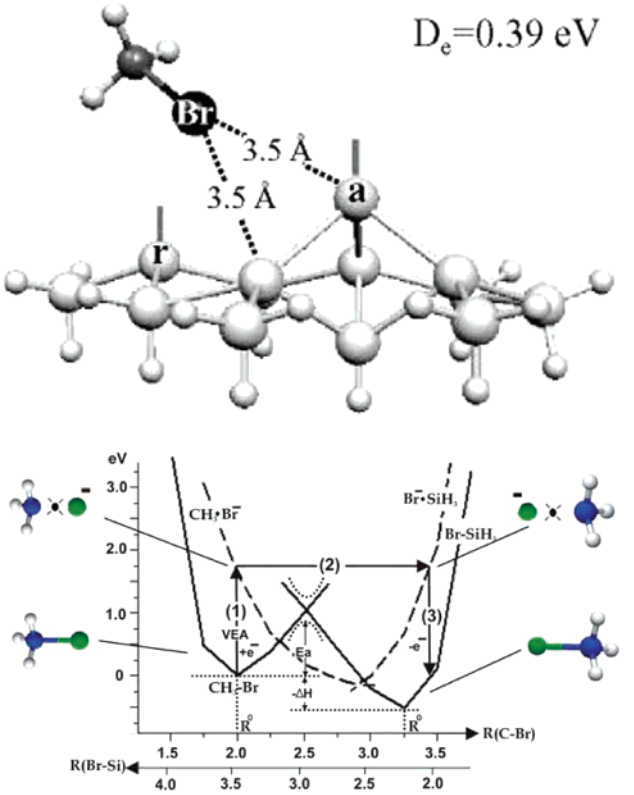

Figure 34. (Top) Simple DFT ab initio model of the charge-transfer (CT) reaction with collinear C−Br−Si: (1) CH_3Br(ad) + e^- gives $CH_3•Br^-$, (2) $CH_3•Br^-$ gives $Br^-•SiH_3$, and (3) $Br^-•SiH_3$ gives Br−SiH_3 + e^-. The dots indicate repulsion. Repulsion in step 2 was calculated separately for $CH_3•Br^-$ and $Br^-•SiH_3$. VEA = vertical electron affinity; E_a = activation energy; ΔH = heat of reaction. (Bottom) CH_3Br physisorption equilibrium geometry (C−Br 60° to surface normal). The cluster is $Si_{13}H_{18}$ distributed in three layers (a = adatom, r = rest atom). Reprinted with permission from ref 121. Copyright 2004 Elsevier.

antibonding orbital, causing the C−Br bond in CH_3Br^- to extend, the Br is expected to impact the surface at an angle to the surface plane (cf. condition a of the previous discussion). Since the photon energy at 193 nm is 6.3 eV, the photoelectron will bring several electronvolts of excess energy to the CH_3Br (cf. condition b; previous discussion). One might expect, therefore, that there would be substantial migration of Br across the surface with a resultant blurring of the Br−Si imprint as compared with the parent CH_3Br-(ad) pattern. This was not, however, observed.

From a fundamental standpoint observation of a highly localized reaction under conditions that seem to strongly favor delocalization is interesting. The proposed explanation[121] was that the Br^- from CH_3Br recoiling toward the surface, even though at a glancing angle of incidence, rode up a repulsive wall and spent ~10^{-13} s at the repulsive turning point before bouncing back. These hundred femtoseconds should be long enough to permit reverse charge transfer to take place from Br^- to the underlying silicon surface,[158] with the result that Br^- was trapped in the potential well of the first Si atom that it encountered, i.e., the reaction was highly localized.

The proposed mechanism for MSI[121] is illustrated in Figure 34 (bottom) as a three-stage process. The energies were calculated by DFT for the simple model of (1) charge transfer to the methyl bromide from the silicon surface, CH_3Br + e^- → CH_3Br^-, (2) transfer of Br^- from methyl bromide to

the surface, modeled as $CH_3Br^- + SiH_3 \rightarrow CH_3 + Br^-{}^{\bullet}SiH_3$, followed by (3) charge transfer of e^- in $\sim 10^{-13}$ s back to the silicon surface, $Br^-{}^{\bullet}SiH_3 \rightarrow Br-SiH_3 + e^-$. The three consecutive stages are indicated by the three arrows labeled 1, 2, and 3 in the figure. It is evident that the loss of energy to the surface in stage 3 transfers Br from the repulsive $Br^-{}^{\bullet}SiH_3$ state to the bound $Br-SiH_3$ state in which it is held captive by a strong covalent bond. Localized reaction, and hence MSI, has taken place.

3.7. Atomic Pairs from Dihalobenzenes

Mention was made in the previous section of the types of organic residue left at a silicon surface following C−X bond scission in monohalo- and dihalobenzenes. In the dihalo case the relative positioning of the two halogen atoms in the parent molecule has been shown to affect the resultant bonding of its organic residue to the surface.

In this section we are concerned with a more direct consequence of dihalobenzene reaction, namely, the interatomic separation and positioning of pairs of X−Si formed by reactions at a silicon surface. Dihalobenzenes leave single X−Si at silicon with 2−3 times the probability of pairs of halogen atoms. However, we shall principally be discussing here the reaction to form double halogen imprints (X−Si pairs) since this has clear implications for the reaction dynamics.

It can be assumed that the two bond-breaking events in the X_2−Ph parent required for X−Si pair formation take place sequentially since the energy required to expand both C−X bonds concurrently in the molecule to give 2X + Ph, in one step, exceeds that for sequential bond breaking.[122] The second bond to break is X−Ph•, where the dot indicates the free radical formed by the departure of the first X atom. This second bond can be weaker than the first. This would account for the fact that, even for modest percent reaction, pair formation was seen, i.e., the X−C bond scission took place twice in the same molecule as required for atomic 'pair' formation. The experimental proof that two adjacent imprints at the surface, i.e., two X−Si, constituted a pair was that the distribution of pair separations was independent of coverage, depending only on the nature of the molecules each of which gave rise to a pair of X−Si.

In what follows we discuss halogen-atom pair formation for several dihalobenzene parent molecules. The central question in each case will be whether the geometry of the parent molecule, which may have adjacent or nonadjacent halogen substituents, affects the pattern of halogenation at the surface and whether the observed pattern of halogenation correlates with the substituent geometry (i.e., the prior location of X−C) in the parent molecule.

We shall show in every case that there is, in fact, a correlation between the location of the two X−C bonds in the parent molecule and the subsequent mean location of the X−Si reaction products at the surface. Such reagent−product correlations are the subject of molecular reaction dynamics. STM observation reveals itself as a promising tool for uncovering the atomic and molecular motions in surface chemical reaction. Time-dependent STM on the femtosecond scale, required to follow the particles at the surface in the process of rearranging themselves, is at present impractical. However, we can adequately infer the motions, in the 2D world of surface science, from the initial and final molecular patterns revealed by STM.

3.7.1. Si(111)-7×7/$C_6H_4Cl_2$

Mono- and dichlorination of Si(111)-7×7 by dichlorobenzene has been induced by laser irradiation at 193 nm.[23] The reagents were the isomeric pair 1,2- and 1,4-dichlorobenzene (symbolized 1,2-diClPh and 1,4-diClPh). These parent molecules were individually dosed onto an Si(111)-7×7 surface. The distribution of nearest-neighbor distances between parent molecules (1,2- and 1,4-isomers) was shown to be identical; however, the pair distribution (interatomic separations) in the Cl−Si product of photoreaction in the two cases was visibly different (Figure 35, top). The cross-section for photodissociation was measured as $s_{ph} = 2.9 \times 10^{-21}$ cm^2 (2.9×10^{-3} Å^2) over a range of intensities for both single and pairs of Cl, showing that photodissociation was a single-photon process in both cases. The photoformation of single Cl (i.e., Cl−Si) relative to pairs of Cl was in the ratio 2:1; it appeared that the photolytic breaking of one C−Cl bond in dichlorobenzene was followed by thermal dissociation of the photoformed chlorophenyl radical in roughly a third of the photolytic events.

To compare the photoproduct Cl-atom imprint of 1,2-diClPh with that of 1,4-diClPh the distance between Cl−Si nearest neighbors was plotted as a histogram using these reagents in turn (Figure 35, bottom). Though the distribution

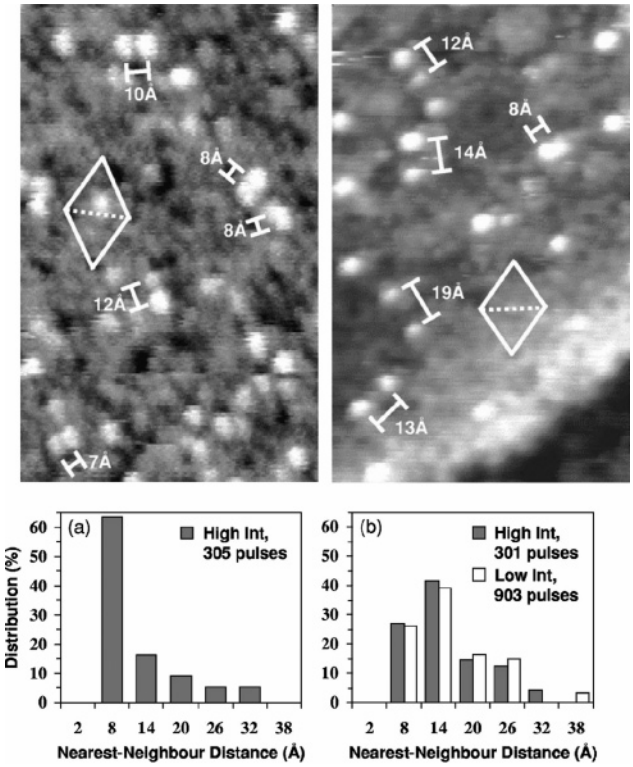

Figure 35. (Top) Sample STM images of the surfaces with adsorbed parent molecules showing the (bright) Cl−Si daughters after illumination with 193 nm photons: (a) 1,2-diClPh and (b) for 1,4-diClPh; $V_s = +3$ V. Separations within pairs of Cl−Si are indicated. A 7×7 unit cell with sides 26.9 Å in length is outlined in each image. (Bottom) Distributions of Cl atoms over the distance to the nearest-neighbor Cl atom (present as Cl−Si) for (a) 1,2-diClPh and (b) 1,4-diClPh. (a) Results at high intensity @180 mJ/(cm^2 pulse) are shown for 305 pulses. (b) Solid bars are for high intensity @180 mJ/(cm^2 pulse) and 301 pulses and the open bars for low intensity @60 mJ/(cm^2 pulse) and 903 pulses. The histogram bars in b form pairs at 8, 14, 20, and 26 Å. The total number of Cl−Si recorded in a is 55, and the total in b is 48 at high intensity and 61 at low intensity. Reprinted with permission from ref 23. Copyright 2000 American Institute of Physics.

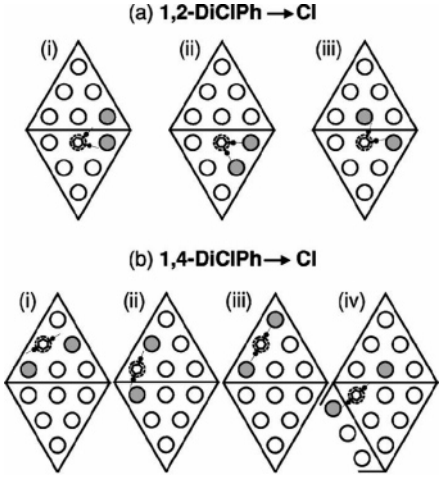

Figure 36. Most probable configurations of the Cl−Si pairs that were observed after 193 nm laser irradiation of the surfaces for (a) 1,2-diClPh and (b) 1,4- diClPh. Within each diamond-shaped 7×7 unit cell the open circles are the bare Si adatoms and the shaded circles are Cl−Si. The broken circles suggest locations for the parent molecule for (a) 1,2-diClPh and (b) 1,4-diClPh. The parent molecules are drawn to scale to show how each could result in the observed Cl−Si imprint by an approximately linear extension of the C−Cl bonds. (a) Separations between Cl−Si are (i) 6.7, (ii) 7.7, and (iii) 10.2 Å. (b) Separations are (i) 13.3, (ii) 13.9, (iii) 15.4, and (iv) 16.8 Å. (Placement of aromatic rings directly above adatoms is an approximation.) Reprinted with permission from ref 23. Copyright 2000 American Institute of Physics.

of separation about the mean is broad, the mean separation has increased by approximately a factor of 2 , from 8 ± 3 to 14 ± 3 Å. A change in the 193 nm UV photolysis intensity by a factor of 3 left the photolytic cross-section (and pair distribution, see Figure 35, top) unaltered, indicating that the C−Cl bond was ruptured in a single-photon process. Since the alteration in Cl−Si nearest-neighbor distance in going from 1,2-diClPh to 1,4-diClh is not present in the nearest-neighbor distance of the parent molecules at the surface, it can be ascribed to the effect on the pattern of chemical reaction of differing geometries of the chlorine atoms within the two adsorbates.

Figure 36 suggests a crude geometric explanation of the observed alteration in the pattern of reaction. The parent molecules 1,2-dichlorobenzene (Figure 36a) and 1,4-dichlorobenzene (Figure 36b) are drawn to scale with the appropriate substituent geometry to indicate how each could result in the observed Cl−Si imprints (including separations from approximately 7−10 Å in the first case and 13−17 Å in the second) by linear extension of the C−Cl bonds and reaction at the first Si−adatom encountered. Photoreaction, it would appear, is mainly localized to a site adjacent to the parent molecule despite the excess energy in the 193 nm photons.

The major source of the observed distribution of Cl−Si separations stemming from photodissociation of single dihalide molecules would appear to be the variation in the parent-molecule geometry between the isomers, i.e., alteration in the Cl···Cl separation in going from 1,2- to 1,4-diClPh. To this must be added the variation in alignment of the molecules on the Si(111)-7×7 surface (Figure 36). The latter effect being only a perturbation on the former, the Cl−Si pair distribution at the surface bears a simple relation to that in the parent molecule.

3.7.2. Si(111)-7×7/$C_6H_4Br_2$

Supporting evidence for this crude linear-bond-extension model of surface halogenation at Si(111)-7×7 is to be found in a similar single-molecule STM study of the thermal reaction of three isomers of dibromobenzene (diBrPh). The three parent molecules in this case were 1,2-, 1,3-, and 1,4-diBrPh.[129] The Br−Si to Br−Si pair separation at the surface was found to depend systematically on the parent molecule, as shown in the three histograms of Figure 37; the mean separation of the imprints at the surface increased from 7.6 to 10.3 to 11.3 Å down the series. These separations are in every case about 4 Å greater than that of the Br atoms in the intact parent molecule, also shown in the figure. (This increase of interhalogen separation upon surface halogenation is illuminated by a simple model discussed below.) If reaction is localized to the neighborhood of the parent halogen atom, correlation of interhalogen separation between parent and daughter is to be expected.

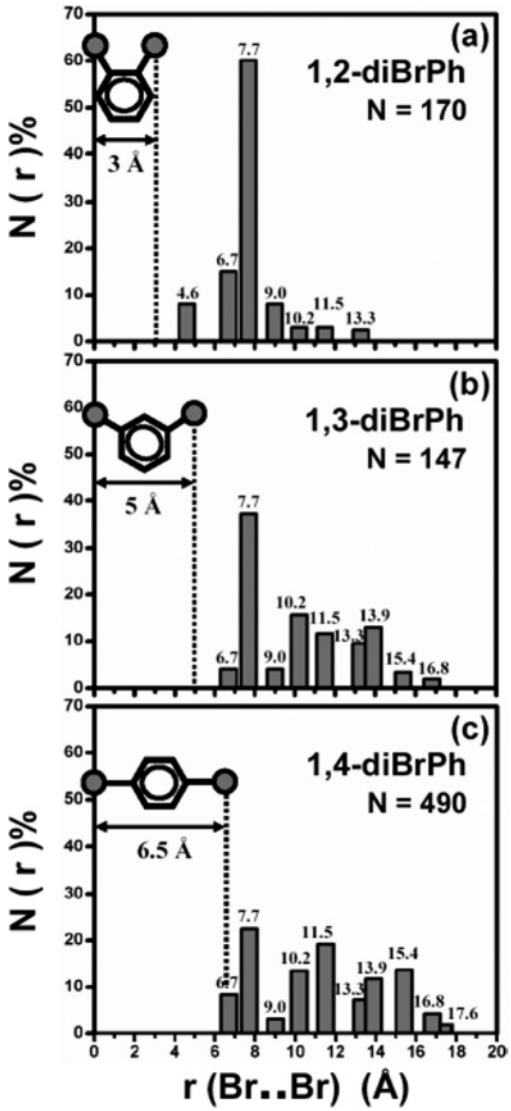

Figure 37. Distribution of Br-atom pair separations (present as Br−Si) for (a) 1,2-diBrPh, (b) 1,3-diBrPh, and (c) 1,4-diBrPh. The magnitude of the pair separations is given, in Angstroms, above each histogram bar. The total number of Br-atom pairs (N) is indicated for each histogram. The separation between the Br atoms in the intact molecule is indicated in each case. Reprinted with permission from ref 129. Copyright 2004 Elsevier.

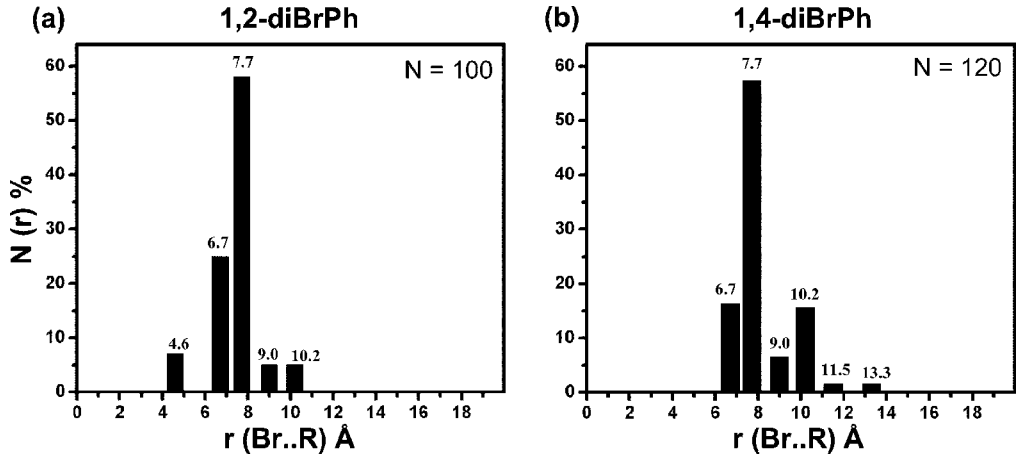

Figure 38. Distribution of separations between the parent molecule (as indicated by its organic residue, R) and the daughter Br atoms (present as Br−Si) for (a) 1,2-diBrPh and (b) 1,4-diBrPh. The magnitude of the parent−daughter separations is given, in Angstroms, above each histogram bar. The total number of parent−daughter pairs (N) is indicated for each histogram. Reprinted with permission from ref 129. Copyright 2004 Elsevier.

Further experimental evidence of the localized nature of the reaction comes from an investigation of the pair separation between the organic residue R−Si and the daughter Br−Si, i.e., parent−daughter separation (rather than daughter−daughter as in the previous studies of halogen-to-halogen separation). (In this instance no distinction was made between bromination of the surface by one or two Br atoms for a given parent molecule.) For both parent molecules 1,2-diBrPh and 1,4-diBrPh (Figure 38a and b) the Br−Si imprint at the surface was formed preferentially at the dangling bond of a Si−adatom adjacent to the organic residue, R−Si, of the parent molecule, the mean separation between dangling bonds at Si(111)-7×7 being 7.7 Å.

Interesting small differences were, nonetheless, evident in the reaction dynamics for these two parents. The close separation of 4.6 Å between R−Si and Br−Si reaction products, for example, was found only for the 1,2-diBrPh parent, indicating that this molecule alone, with its closely spaced Br substituents, permits reaction of R with an adatom and concurrently a second Br with an adjacent rest atom within the same half of the unit cell. Recently, Dobrin made a calculation of the atomic reactions of 1,2-dibromobenzene on Si(111)-7×7 using DFT and a small 12-atom silicon cluster to represent the surface.[159] As theory develops it will be interesting to see why 1,4-diBrPh, with its more widely spaced Br substituents, is precluded from reacting at these closely adjacent silicon-atom sites.

A further significant clue to the reaction dynamics yielded by STM is the observation of a significant decrease in the percentage of R−Si accompanying formation of Br−Si in going down the series of isomeric reagents. For 1,2-diBrPh 70% of Br−Si was accompanied by R−Si, whereas for 1,4-diBrPh this fell to only 20%. This diminished yield of R−Si was interpreted as being due to a decrease in the percentage of what was termed benzene-mediated reaction, or more generally parent-mediated reaction, in which the intact RBr first adsorbs at the surface, later reacting to yield the observed products R−Si plus Br−Si.

The reaction pathway that failed to leave organic residue, R−Si, at the surface was interpreted as bromine mediated or more generally daughter mediated (Figure 39). In daughter-mediated reaction the reactive substituent (Br) was thought to be transferred directly to the silicon in an encounter of the halogenated end of the molecule with the surface. Further evidence for alternative reaction pathways came from STM observation of the relative yields of R−Si to Br−Si for reaction at a slightly elevated surface temperature. At T_s = 45 °C, bromination of the surface was observed in the presence of little R−Si. This suggested a shift in the reaction dynamics away from parent-mediated in favor of the more direct daughter-mediated atom transfer.

The observed Br pair separation at the surface for the parent-mediated pathway with 1,2- and 1,4-diBrPh parent molecules can be understood once again in terms of nearest-neighbor reaction, as pictured in Figure 40 (top) for approximately linear bond extension. For the daughter-mediated pathway, i.e., without accompanying R−Si, the pair of Br atoms exhibited interatomic separations that can be pictured (in part) as due to the 'stamping' of the Br substituents at the surface (without attachment of the parent molecule), as illustrated for 1,2- and 1,4-diBrPh (Figure 40a and b, bottom). Wider Br−Br separations stemming from daughter-mediated reaction are pictured in the referenced paper[124] as being due to sequential approach of the two Br substituents to the surface, i.e., due to a 'rocking' motion of the adsorbate with its Br's pointing down without attachment of the organic residue R.

Recent STM studies of the very different reaction of long-chain 12-carbon 1-haloalkanes at Si(111)-7×7, over a range of temperatures, have once again given evidence of two reaction pathways: parent mediated[126] and daughter mediated.[160] In the first case the halohydrocarbon is visible lying down on the surface prior to the surface-halogenation reaction and also after the reaction. In the second case (on the time scale of STM) halogenation occurs without measurable time delay and without prior or subsequent formation of R−Si (R in this instance being the C_{12} alkane-chain residue).

It appears that these alternative pathways, parent and daughter mediated, could be of importance in a considerable variety of reactions involving transfer of an atom or group, B, from an adsorbate, RB, to a surface. This generality is due to the fact that there will exist the possibility that reagent RB attaches by way of the R group, later transferring B to the surface, or, alternatively, that B encounters the surface first and undergoes direct transfer. The case where reaction involves initially B−R−Surf formation followed by R−Surf

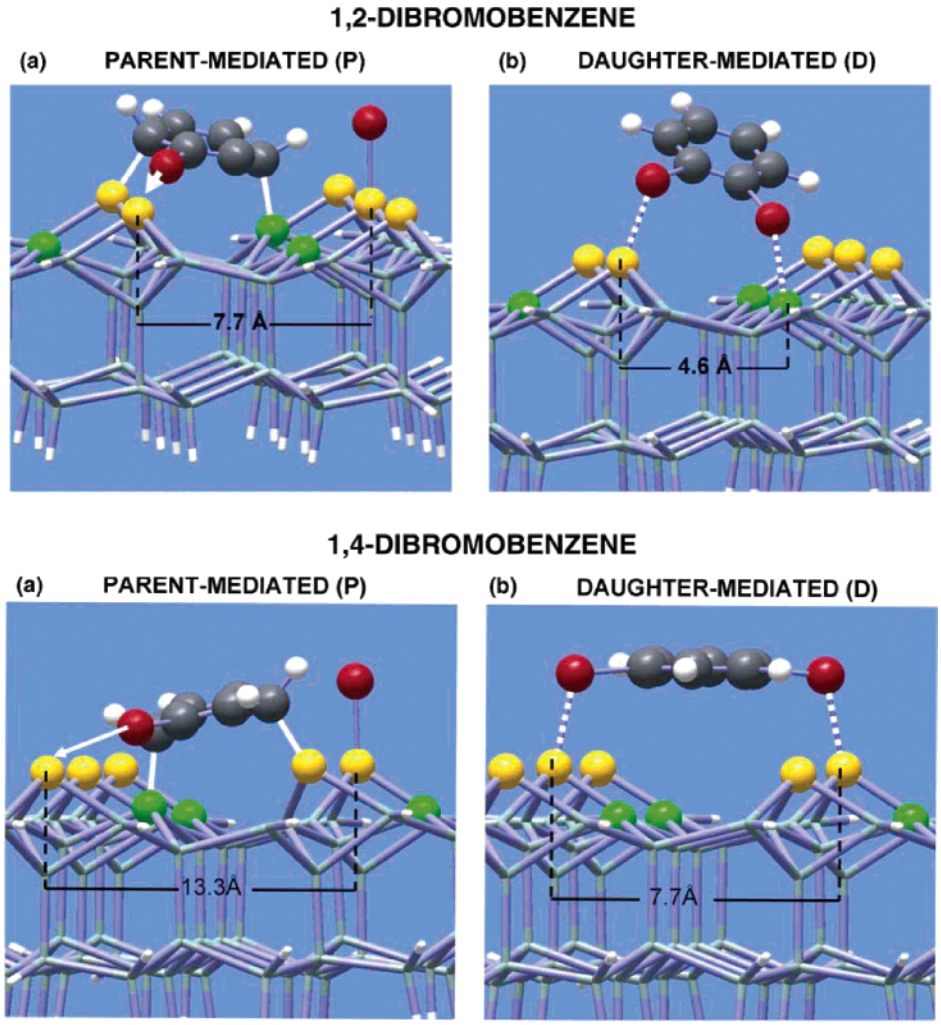

Figure 39. (a) P- and (b) D-mediated intermediate structures of 1,2-dibromobenzene, above, and 1,4-dibromobenzene, below, on Si(111)-7×7 indicating in a the origin of the pair distances with adjacent dark feature and b the origin of the pair distances without dark feature, i.e., the organic residue may remain at the surface or desorb. Red spheres in each picture represent Br atoms, dark gray spheres are carbon atoms of the benzene ring or silicon rest atoms (green), yellow spheres are silicon adatoms, white spheres are benzene hydrogen atoms, blue sticks bond Si atoms of lower layers, and white tips are hydrogen atoms terminating the crystal at sides and bottom. Reprinted with permission from ref 124. Copyright 2004 Elsevier.

+ B−Surf formation is parent mediated, whereas the more direct reaction in the arrangement R−B−Surf → R+B−Surf is daughter mediated.

A simple model, the ordered dangling bond (ODB), was used to gain insight into the reaction of a dihalogenated aromatic molecule to yield an adjacent pair of halogen atoms imprinted at silicon. Thermal dihalogenation by a dihalide Br−R−Br, with R = benzene or biphenyl, was modeled using a pair of silyl radicals placed a distance *d* apart. These represented adatom dangling bonds at the surface of Si(111)-7×7 (Figure 41). The objective of the study was to determine, for different aromatics R, the separation of dangling bonds most favorable to reaction (since R is not allowed to attach to the surface the reaction is daughter mediated, but the importance of dangling-bond separation, *d*, to the activation energy for the reaction can be expected to apply in either case). In the model, Figure 41,[122] the separation *d* could be treated as continuously variable, even though at Si(111)-7×7 it has only a discrete range of values indicated by the points (circles or squares) in the plot of E_b (energy barrier for dibromination) versus *d* (dangling-bond separation) at the bottom of Figure 41.

The question being addressed by means of the ODB approach was, for a given separation of halogen atoms in the parent molecule, what would be the preferred halogen-atom pair separation, *d**, at the ODB surface. The initial separation of the Br atoms in 1,4-dibromobenzene (experimentally and in the model) was *r*(Br, Br) = 6.6 Å. The interhalogen separations in the larger reagent, 4,4′-dibromophenyl, was *r*(Br,Br) = 10.9 Å. DFT was used to obtain the energy barrier for dihalogenation of the pair of silyls representing the ODB surface, a fixed distance, *d*, apart (Figure 41, top, showing only the 1,4-dichlorobenzene reagent). The adsorbate molecule was held parallel to the ODB surface at decreasing perpendicular distances, r_1, from the surface. At each stage as r_1 decreased, the bonds to be broken were extended symmetrically to an optimal C−Br separation r_2. The lowest energy reaction path and hence the activation energy for the fixed dangling-bond separation *d* are illustrated in the potential-energy surface of the Figure 41 (middle). The activation energies (more correctly barrier heights *E*) for differing dangling-bond separations, *d*, are collected in the subsequent illustration (Figure 41, bottom)

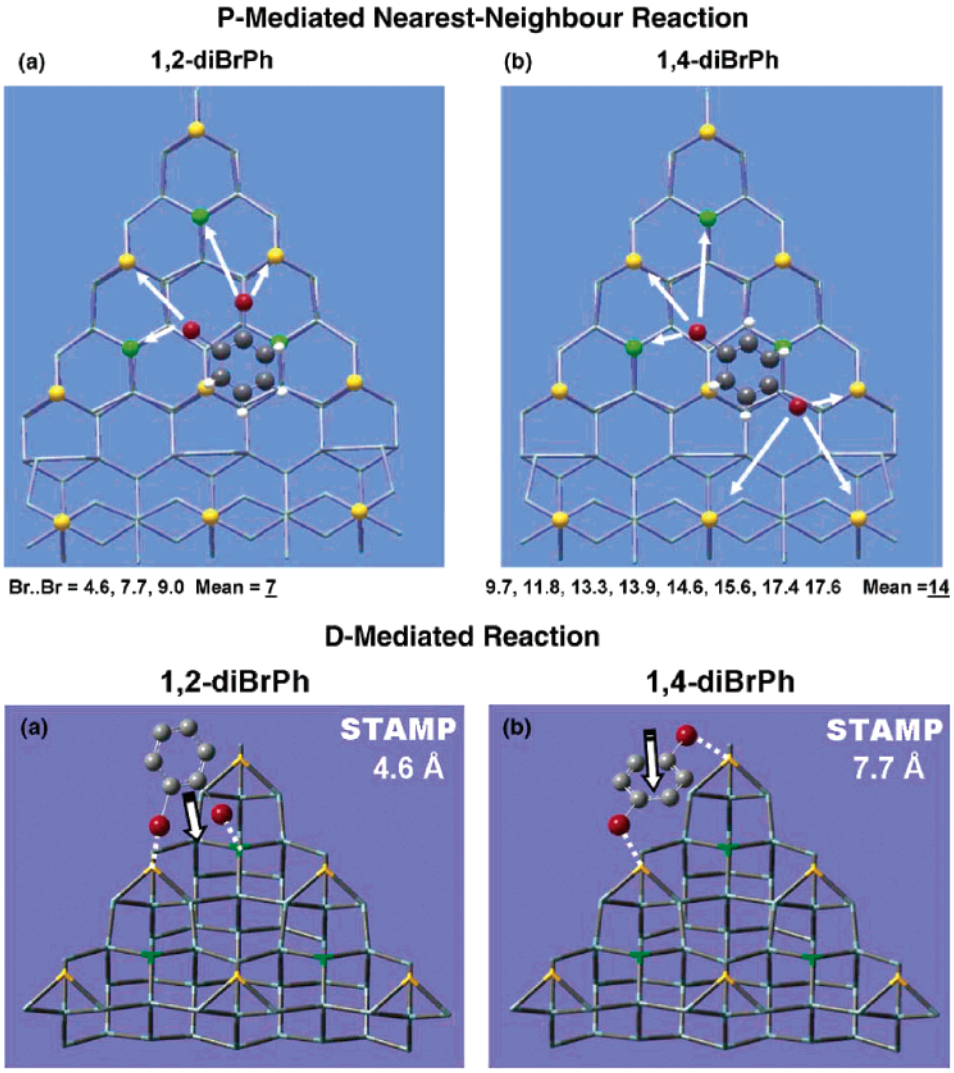

Figure 40. (Top) Parent-mediated (P) nearest-neighbor model for (a) 1,2-dibromobenzene and (b) 1,4-dibromobenzene reactions. Top view of the faulted half unit cell; color code as in Figure 39. Arrows indicate the target dangling bonds (Si adatoms and Si rest atoms) accessible by approximately linear stretching of the C−Br bonds along the direction of C−Br ± 45°. Mean Br−Br distance of 7 Å results from 1,2-dibromobenzene and a mean of 14 Å from 1,4-dibromobenzene with a broader range of separations in the latter case. (Bottom) Daughter-mediated (D) nearest-neighbor reaction model for (a and c) 1,2-dibromobenzene and (b and d) 1,4-dibromobenzene. Tilted top view of unfaulted half unit cell; color code as for Figure 39. (a and b) "Stamping" of Br pairs onto the surface for each adsorbate. Reprinted with permission from ref 124. Copyright 2004 Elsevier.

for both 1,4-dibromobenzene and 4,4′-dibromobiphenyl as reagents.

A number of noteworthy conclusions can be drawn from this ODB rendition of dihalobenzene reaction at silicon: (i) The activation barrier is sensitively dependent on the separation between the dangling bonds, (ii) the activation barrier is reduced by concerted reaction in which the old and new chemical bonds coexist in the transition state configuration (labeled ‡ on the potential-energy surface, Figure 41, middle), (iii) the optimal dangling-bond separation, *d**, and hence the predicted Br···Br imprint separation at the surface slightly exceeds (by 3.5 Å, similar to the observed extension of 4 Å) the prior separation in the parent molecule, (iv) the fact that the separation of the halogen atoms at the surface for the lowest activation-barrier reaction exceeded by 3−4 Å their previous internuclear separation in the reagent molecule is understandable in light of the fact that the electron charge clouds in the adsorbate molecule must overlap with those of the dangling bonds if surface reaction is to occur; these charge clouds are larger than the halogen−halogen internuclear separation in the adsorbate (see Figure 42), (v) the larger parent adsorbate molecule (biphenyl rather than phenyl) imprints a correspondingly larger pair separation at the surface, (vi) the marked lowering of the barrier to reaction for the optimal dangling-bond separation, *d** (Figure 41, middle), despite substantial dangling-bond separations of ∼10 Å for dibromobenzene and ∼14 Å for dibromobiphenyl provides the rationale for the localized reaction, i.e., the observed pattern of halogen-atom imprinting, (vii) given sufficient reagent energy there will be a distribution of Br···Br pair separations at the surface due to concerted reaction (see ii above) through different transition-state geometries (rather than subsequent diffusion of Br across the surface).

For the optimal dangling-bond separation at the surface, *d**, the charge-cloud overlap with the substituents in the adsorbate is *maximized* (cf. points i−iv above and Figure 42) so that the reactive transition state is stabilized by coexistence of the old and new chemical bonds: the most favorable concerted reaction. This is in accord with the

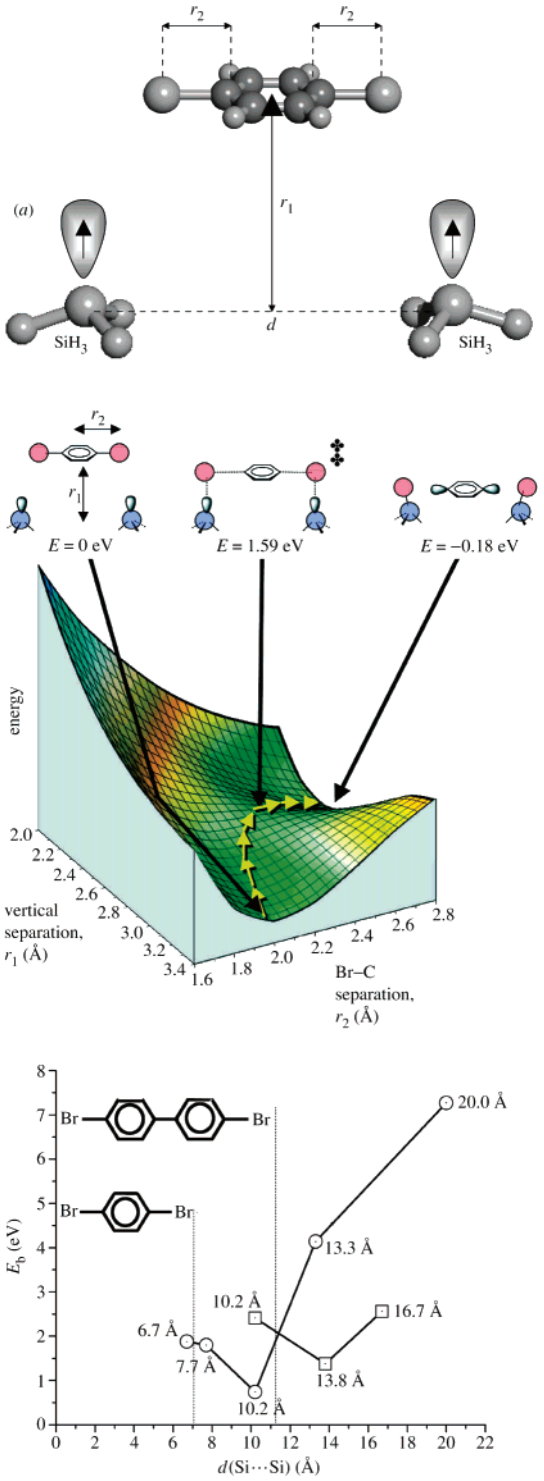

Figure 41. (Top) Ordered dangling bond (ODB) model for a fixed Si−Si separation, *d*, with a 1,4-dibromobenzene molecule approaching along the r_1 coordinate while the Br atoms separate from the molecule symmetrically along r_2. The model is in a triplet state, as indicated by the arrows on the dangling bonds. (Middle) Example of a PES obtained in this study for a fixed Si···Si separation. The potential energy is plotted against r_1 and r_2 defined in the top figure. Initial, transition, and final states are illustrated above and indicated on the PES. The PES is plotted for a *symmetric* stretch of the Br−C bonds. (Bottom) Barrier heights for differing dangling-bond separations, *d*, selected to correspond to the adatom−adatom separations on the Si(111)-7×7 surface. Circles refer to 1,4-dibromobenzene and squares to 4,4-dibromobiphenyl as reagent. Dotted lines indicate the approximate Br···Br internuclear separations in these two molecules. Reprinted with permission from ref 122. Copyright 2004 Royal Society of London.

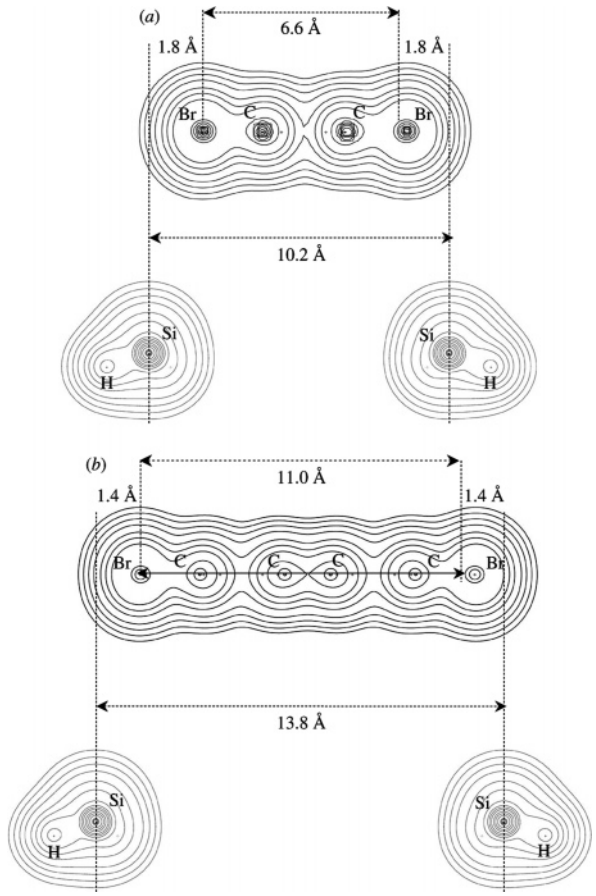

Figure 42. Electron density contour map for (a) 1,4-dibromobenzene and (b) 4,4-dibromobiphenyl, shown above the electron density for a disilyl model. The density increases from the outermost 0.001 au (ca. 0.0068 e $Å^{-3}$) isodensity contour in steps of 2×10^n, 4×10^n, and 8×10^n au with *n* starting at −3 and increasing in steps of unity. The outer contour represents the envelope which contains more than 99% of the electron population, commonly identified with the van der Waals size. The plane of the figure is the mirror plane bisecting the system through the bromine atoms and their attached para carbon atoms. The positions of the nuclei of the atoms which are located above or below this plane are denoted by small crosses. The Si−Si separation is the one corresponding to the lowest barrier on the symmetric stretch PES, the separation being (a) 10.2 and (b) 13.8 Å for 1,4-dibromobenzene and 4,4-dibromobiphenyl, respectively. (The irregular core contours are an artifact of the plotting grid size.) Reprinted with permission from ref 122. Copyright 2004 Royal Society of London.

explanation of localized reaction given on the basis of the DFT calculation for the halogenation of Si(111)-7×7 by chlorobenzene, described above (Figure 42).

The major theme of this review is the revolution in the field of molecular reaction dynamics to be expected as a result of the application of STM to the tracking of atomic and molecular motions in the course of the elementary steps of surface reaction. This is particularly true of parent-mediated reaction, as defined above, since the location at the surface of the parent molecule, RX or RX X′ and of its daughter molecules, R, X, and X′, can be evidenced in the STM image.

The STM images reproduced in Figures 1 and 2 of ref 129 exhibited differing reaction dynamics for 1,2-diBrPh and 1,4-diBrPh. In the former reaction the daughter pair of Br atoms (bright features) were both to one side of R (dark feature). In this they mirrored the structure of the parent molecule with its Br substituents to one side of the benzene

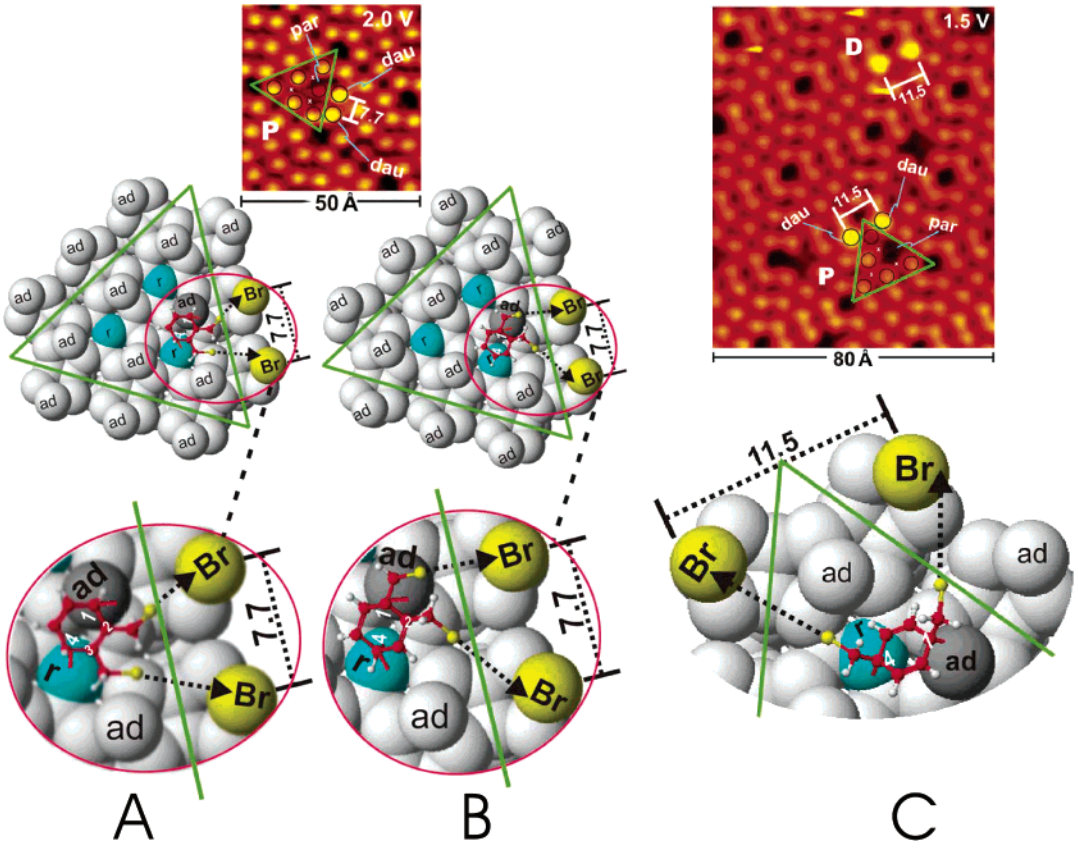

Figure 43. (A and B) STM image (2.0 Vs, 0.2 nA) of the Si(111)-7×7 surface after thermal reaction with 1,2-diBrXy at room temperature. The triangle indicates a half unit cell with adsorbed reaction products. Two adsorbed Br atoms, labeled dau for daughter, appear as bright spots with separation of 7.7 Å; the adjacent organic residue, labeled par for parent (dark feature), is located on a middle adatom. Molecular dynamics for this parent-mediated reaction (P) are shown in A and B. The circled areas of A and B are magnified below. Carbon atoms 1 and 4 of the parent molecule are attached to the middle Si adatom (dark gray) and the rest atom (labeled r). The two CH_2Br groups of the parent molecule are attached to carbon atoms 2 and 3 in A and to carbons 1 and 2 in the alternative interpretation B. In both cases the C−Br bond axes of the parent molecule are approximately collinear with the C−Si axis. (C) STM image (1.5 Vs,[164] 0.2 nA) of the Si-(111)-7×7 surface after spontaneous reaction with 1,4-diBrXy molecule at room temperature. The triangle indicates a half unit cell embodying the adsorbed reaction products. Two pairs of adsorbed Br atoms with separation of 11.5 Å are present. One pair is labeled D, originating from the daughter-mediated reaction, and another P due to parent-mediated reaction. Reaction products are labeled dau (Br atom) and par (organic residue, hence parent location). Dynamics are illustrated in the schematic in which the upper part of the indicated half unit cell is magnified. Carbon-atom 1 of the parent molecule is attached the middle silicon adatom and carbon 4 to the rest atom. CH_2Br groups of the parent molecule are attached to carbon atoms 1 and 4. They have cis-oriented Br atoms. The C−Br bond axes of the parent are approximately collinear with C−Br axes. Reprinted with permission from ref 125. Copyright 2005 Elsevier.

ring. In the latter case, 1,4-diBrPh, the STM image gave, in contrast to the case of 1,2-diBrPh, for the first time numerous cases in which the bright Br daughter atoms at the surface had the dark R residue midway between the two Br imprints (i.e., they exhibited a bright−dark−bright pattern of reaction products). Here again the reagent geometry, with Br substituents at either end of the aromatic ring, coupled with the simple picture of linear bond extension in the course of reaction led to the expectation that for this reagent a Br + R + Br (bright−dark−bright) product imprint would be seen at the surface with the halogens, Br−Si, to either side of the central R−Si residue of the aromatic ring.

Since newly formed Br−Si is not invariably at the nearest adjacent site to its parent RBr (see, for example, the ODB model, above), the sequence Br···R···Br was not the only one observed but constituted a probable outcome when 1,4-diBrPh was the parent molecule and an extremely rare outcome with 1,2-diBrPh as reagent. This observation represented therefore a marked and comprehensible alteration in the dynamics of the surface reaction directly visible in the STM images.

3.7.3. Si(111)-7×7/$(BrCH_2)_2C_6H_4$

In closing, we report the recent case of the thermal reactions of 1,2- and 1,4-dibromoxylene at Si(111)-7×7[125] recently studied. Reaction to form single Br atoms at the silicon surface was approximately three times more likely than formation of Br pairs. As observed generally for halogen pair formation at the silicon (111) surface, the mean separation between the members of a pair imprinted on the surface exceeded by a few angstroms the separation between the Br atoms in the parent adsorbate molecule.

Of particular interest was the fact that STM observation of the parent-mediated surface dibromination permitted detailed characterization of the 'vectorial' molecular dynamics for the individual reactive events. This assumed, as is plausible in view of the patterns of halogenation by organic halides described above, that these concerted reactions, with the new bond forming nearby as the old one dissolved, involved predominantly linear transfer of the halogen atoms (extension of C−X to form adjacent X−Si). Attachment of the aromatic ring of the parent molecule to the underlying Si was taken to, by the well-established mechanism of bond

opening, convert the aromatic triene into the corresponding hexadiene.[161−163] This same mechanism was thought to be operative in all the parent-mediated reactions of aromatics described above.

This mode of attachment in parent-mediated reaction raises, at a detailed level, the question as to whether the reactive substituents are attached at the carbons that bind the aromatic hexadiene ring by σ bonds to the surface or adjacent to this. The question is significant since in the former case the substituent is linked to an sp^3-hybridized carbon and in the latter is attached to a very different sp^2 carbon, affecting both its bond energy and angle relative to the benzene ring. The question cannot be answered, as yet, a priori. It can, however, be addressed, as will be shown, by examining the pattern of reaction as revealed by STM, a further example of the power of this approach as a means to reveal reaction dynamics.

Figure 43 (A and B) shows the vectorial dynamics, i.e., the directions of the approximately linear C−Br bond extension, relative to the alignment of the hexadiene adsorbate molecule at the surface that conforms to the pattern of reaction observed for approximately 50% of the parent-mediated dibromination events involving 1,2-diBrXy. The di-σ-bound parent molecule[161−163] binds to an adatom and a rest atom at the surface. Assuming, as is reasonable, that the reaction leaves the doubly bound R in place while the C−Br bonds extend approximately linearly, one can explain the observed pattern of one dark (R−Si) and two adjacent bright (Br−Si) features in the STM images by the patterns of reaction shown in Figure 43 (A and B). Two alternative dynamical schemes which can result in the particular pair of Br−Si, 7.7 Å apart to one side of the R−Si residue, are shown. The salient features of the reactive events are as follows: (i) the parent aromatic dihalide is attached to the middle adatom and the rest atom indicated in the figure, (ii) the CH_2Br substituents are bound to carbon atoms C1 and C2, or alternatively C2 and C3, of the benzene ring, (iii) the Br atoms of the reagent are in the cis configuration relative to one another.

An example of parent- and daughter-mediated (P- and D-mediated, respectively) reaction of 1,4-diBrXy is to be found in Figure 43C. The pattern of P reaction shown was common to approximately 75% of the dihalogenation observed for that molecule. Since the dark feature R is attached to an adatom (labeled ad here) and a rest atom (labeled r) and the C−Br bonds can be regarded as extending approximately linearly to yield Br−Si at the observed neighboring pair of adatoms (11.5 Å apart), the parent-mediated reaction can be inferred to have the (unique) dynamics illustrated: (i) the parent molecule is attached to the middle and rest adatoms indicated, (ii) the CH_2Br substituents are bound to carbon atoms C_1 and C_4 (the sp^3 carbons), and (iii) the Br atoms are in the cis configuration to one another. Two further (alternative) characteristic reactive molecular dynamics were also found, covering the remaining 25% of cases (see ref 125, Figure 5).

The significance of these findings is that STM is presently opening the way to full characterization of the molecular dynamics of surface reactions by permitting a record to be made of the relative positions of reactants and products for all reactive events before and after the reactive encounters. This is a level of information, and eventual understanding, undreamed of even in the halcyon days of crossed molecular-beam chemistry.

4. Conclusion

The chemical reactions reviewed here are those that involve the breaking or formation of new chemical bonds in adsorbates. The study of the patterned imprinting of reaction products at surfaces by STM is presently inaugurating a new chapter in the study of reaction dynamics—elucidation of the motions of atoms and molecules engaged in chemical reaction.

In a simple case a diatomic molecule, AB, impinging on a surface with sufficient collision energy reacts to form two new bonds: A−Su and B−Su (where Su symbolizes the surface), a type of reaction termed dissociative chemisorption. In a number of cases this dissociative pathway is replaced at low collision energy by a reaction that forms only a single new bond to the surface

$$AB(g) + Su \rightarrow A(ad)/Su + B(g)$$

termed abstractive chemisorption.

It was thought at first that the higher collision-energy process of dissociation at a smooth surface gave rise to widely separated fragments, A−Su and B−Su, by way of 'ballistic recoil'. The prevailing view today, however, is that the products give predominantly closely spaced pairs, A−Su and B−Su.

Parallel work on the surface reactions of larger molecules, particularly organic halides, RX or RXX′, at silicon has yielded a picture of preference for localized reaction. The organic residue, R, and one or two halogen atoms, X and X′, can be transferred to the surface in the reaction. In a favorable case the location of R as well as that of the halogen atoms X is evident from the STM image. Both the R-to-X separation at the surface (identified as parent-to-daughter) and the X-to-X′ (daughter-to-daughter) separation peak at near-neighbor distances. The finding appears qualitatively unchanged by moderate excitation of the reagent molecule using heat, light, or electron impact. This type of dynamics, termed localized reaction, is favored, as theory shows, since it permits concerted reaction, i.e., coexistence of old and new chemical bonds in the course of reaction, thereby stabilizing the transition state. Concerted reaction can occur through more than one transition state, leading to some broadening of the product distribution. Ballistic recoil appears to be most often damped by efficient energy dissipation.

Employment of STM as a diagnostic tool makes it possible to distinguish two broad categories of molecular dynamics for the surface reactions of RX, termed parent mediated and daughter mediated. In the former case RX(ad) is adsorbed in defined configurations with R attached to the surface prior to the reaction. In the latter case the initial point of attachment of the molecule to the surface is the X end of RX, X being directly transferred to the surface to give X−Su in the initial encounter (Su being the surface). Parent-mediated reaction is generally characterized by R−Su residue following reaction, whereas in daughter-mediated reaction the R not having attached to the surface can escape. Both pathways evidence, preferentially, localized reaction.

Of particular note is the fact that STM, in favorable cases, permits characterization of the geometry of the reactants and products prior to and directly following surface reaction. The technique opens the way, therefore, to revealing the molecular motions in such reactions at an unprecedented level of detail. From a practical standpoint, understanding the motions of atoms and molecules binding to surfaces by chemical

reaction is crucial to the development of molecular printing presses in which labile self-assembled patterns are converted by heat, light, or electrons into the durable bound nanopatterns that will be needed for engineering on the nanoscale.

5. Acknowledgments

The authors are indebted to the Natural Sciences and Engineering Research Council of Canada (NSERC), Photonics Research Ontario (PRO) an Ontario Centre of Excellence, the Canadian Institute for Photonic Innovation (CIPI), and the Canadian Institute for Advanced Research (CIAR) for their support of the work of this laboratory reported here.

6. References

(1) Polanyi, J. C.; Rieley, H. Photochemistry in The Adsorbed State. In *Dynamics of Gas−Surface Interactions*; Rettner, C., Ashfold, M. N. R., Eds.; Royal Society of Chemistry: London, 1991; p 329.
(2) Polanyi, J. C.; Zeiri, Y. Dynamics of Adsorbate Chemistry. In *Laser Spectroscopy and Photochemistry on Metal Surface, Part II*; Dai, H.-L., Ho, W., Eds.; World Scientific: Singapore, 1995; p 1241.
(3) Polanyi, J. C.; Zewail, A. H. *Acc. Chem. Res.* **1995**, *28*, 119.
(4) Tripa, C. E.; Yates, J. T., Jr. *Chem. Phys.* **2000**, *112*, 2463.
(5) Avouris, Ph. *J. Phys. Chem.* **1990**, *94*, 2246.
(6) Wolkow, R. A. *Annu. Rev. Phys. Chem.* **1999**, *50*, 413.
(7) Hamers, R. J.; Coulter, S. K.; Ellison M. D.; Hovis, J. S.; Padowitz, D. F.; Schwartz, M. P.; Greenlief, C. M.; Russel J. N. *Acc. Chem. Res.* **2000**, *33*, 617.
(8) Rosei, F.; Schunack, M.; Naitoh, Y.; Jiang, P.; Gourdon, A.; Laegsgaard, E.; Stensgaard, I.; Joachim, C.; Besenbacher, F. *Prog. Surf. Sci.* **2003**, *71*, 95 and references therein.
(9) Avouris, Ph. *Acc. Chem. Res.* **1995**, *28*, 95.
(10) Hamers, R. J.; Chen, X.; Frank, E. R.; Higgins, S. R.; Shan, J.; Wang, Y. *Isr. J. Chem.* **1996**, *36*, 11.
(11) See, for example: Wiesendanger, R. *Scanning Probe Microscopy and Spectroscopy−Methods and Applications*; Cambridge University Press: Cambridge, 1998 and references therein.
(12) Eigler, D. M.; Schweizer, E. K. *Nature* **1990**, *344*, 524.
(13) Nyffenegger, R. M.; Penner, R. M., *Chem. Rev.* **1997**, *97*, 1195.
(14) Dujardin, G.; Walkup, R. E.; Avouris, Ph. *Science* **1992**, *255*, 1232.
(15) Bernstein, J.; Davis, R. E.; Shimoni, L.; Chang, N.-L. *Angew. Chem., Int. Ed. Engl.* **1995**, *34*, 1555.
(16) Philp, D.; Stoddart, J. F. *Angew. Chem., Int. Ed. Engl.* **1996**, *35*, 1154.
(17) Burrows, A. D. *Struct. Bond.* **2004**, *108*, 55.
(18) Prints, L. J.; Timmerman, P.; Reinhoudt, D. N. *Pure Appl. Chem.* **1998**, *70*, 1459.
(19) Clair, S.; Pons, S.; Brune, H.; Kern, K.; Barth, J. V. *Angew. Chem., Int. Ed.* **2005**, *44*, 7294 and references therein.
(20) De Feyter, S.; De Schryver, F. C. *Chem. Soc. Rev.* **2003**, *32*, 139 and references therein.
(21) Smith, R. K.; Lewis, P. A.; Weiss, P. S. *Prog. Surf. Sci.* **2004**, *75*, 1 and references therein.
(22) Li, X.-M.; Huskens, J.; Reinhoudt, D. N. *J. Mater. Chem.* **2004**, *14*, 2954.
(23) Lu, P. H.; Polanyi, J. C.; Rogers, D. *J. Chem. Phys.* **2000**, *112*, 11005.
(24) Brune, H.; Wintterlin, J.; Behn, R. J.; Ertl, G. *Phys. Rev. Lett.* **1992** *68*, 624.
(25) Brune, H.; Wintterlin, J.; Trost, J.; Ertl, G.; Wiechers, J.; Behm, R. J. *J. Chem. Phys.* **1993**, *99*, 2128.
(26) Diebold, U.; Hebenstreit, W.; Leonardelli, G.; Schmid, M.; Varga, P. *Phys. Rev. Lett.* **1998**, *81*, 405.
(27) Rezai, M. A.; Stipe, B. C.; Ho, W. *J. Chem. Phys.* **1998**, *109*, 6075 and references therein.
(28) Lauhon, L. J.; Ho, W. *J. Chem. Phys.* **1999**, *111*, 5633.
(29) (1) Schunack, M.; Lindertoth, T. R.; Rosei, F.; Laegsgaard, E.; Stensgaard, I.; Besenbacher, F. *Phys Rev. Lett.* **2002**, *88*, 156102.
(30) Tanaka, K.; Matsumoto, Y.; Fujita, T.; Okawa, Y. *Appl. Surf. Sci.* **1998**, *130−132*, 475.
(31) Besenbacher, F. *Rep. Prog. Phys.* **1996**, *59*, 1737 and references therein.
(32) Chiang, S. *Chem. Rev.* **1997**, *97*, 1083.
(33) Herzberg, G. *Molecular spectra and molecular structure*; Krieger: Malabar, FL, 1989; Vol. 1 (spectra of diatomic molecules) and references therein.
(34) Engdahl, C.; Wahnströmm, G. *Surf. Sci.* **1994** *312*, 429.
(35) Wahnström, G.; Lee, A. B.; Strömquist, J. *J. Chem. Phys.* **1996**, *105*, 326.
(36) Strömquist, J.; Hellbert, L.; Kasemo, B.; Lundqvsit, B. I. *Surf. Sci.* **1996**, *352−354*, 435.
(37) Österlund, L.; Zoric, I.; Kasemo, B. *Phys. Rev.* **1997**, *55*, 15452.
(38) Binetti, M.; Weisse, O.; Hasselbrink, E.; Komrowski, A. J.; Kummel A. C. *Faraday Discuss.* **2000**, *117*, 313.
(39) Komrowski, A. J.; Sexton, J. Z.; Kummel, A. C.; Binetti, M.; Weisse, O.; Hasselbrink, E. *Phys. Rev. Lett.* **2001**, *87*, 246103.
(40) Ciacci, L. C.; Payne, M. C. *Phys. Rev. Lett.* **2004**, *92*, 176104.
(41) Wintterlin, J.; Schuster R.; Ertl, G. *Phys Rev. Lett.* **1996** *77*, 123.
(42) Stipe, B. M.; Rzaei, M. A.; Ho, W.; Gao, S.; Persson, M.; Lundquist, B. I. *Phys. Rev. Lett*. **1997**, *78*, 4410.
(43) Stipe, B. M.; Rzaei, M. A.; Ho, W. *J. Chem. Phys*. **1997**, *107*, 6443−6447.
(44) Ho, W. *Acc. Chem. Res.* **1997**, *31*, 5567.
(45) Hahn, J. R.; Lee, H. J.; Ho, W. *Phys. Rev. Lett.* **2000**, *85*, 1914.
(46) Hahn, J. R.; Ho, W. *J. Chem. Phys.* **2005**, *122*, 244704.
(47) Zambelli, T.; Barth, J. V.; Wintterlin, J. *J. Phys.: Condens. Mater*. **2002**, *14*, 4241.
(48) Olsson, F. E.; Lorente, N.; Persson, N. *Surf. Sci.* **2003**, *522*, L27.
(49) Briner, B. G.; Doering, M.; Rust, H.-P.; Bradshaw, A. M. *Phys. Rev. Lett.* **1997**, *78*, 1516.
(50) Rose, M. K.; Borg, A.; Dunphy, J. C.; Mitsui, T.; Ogletree, D. F.; Salmeron, M. *Surf. Sci.* **2003** *547*, 162.
(51) Xu, H.; Yuro, R.; Harrison, I. *Surf. Sci.* **1998**, *411*, 303.
(52) Xu, H.; Harrison, I. *J. Phys. Chem. B.* **1999**, *103*, 11233.
(53) Lee, H. J.; Ho, W. *Science* **1999**, *286*, 1719.
(54) Hla, S.-W.; Bartels, L.; Meyer, G.; Rieder, K.-H. *Phys. Rev. Lett*. **2000**, *85*, 2777.
(55) Hla, S.-W.; Rieder, K.-H. *Annu. Rev. Phys. Chem*. **2003**, *54*, 307.
(56) Stipe, B. C.; Rezaei, M. A.; Ho, W. *Science* **1998**, *280*, 1732.
(57) Lauhon, L. J.; Ho, W. *Surf. Sci*. **2000**, *451*, 219.
(58) Lauhon, L. J.; Ho, W. *J. Phys. Chem. A* **2000**, *104*, 2463.
(59) Komeda, T.; Kim, Y.; Fujita, Y.; Sainoo, Y.; Kawai, M. *J. Chem. Phys.* **2004**, *120*, 5347.
(60) Gaudioso, J.; Lee, H. J.; Ho, W. *J. Am. Chem. Soc*. **1999**, *121*, 8479.
(61) Stroscio, J. A.; Bare, S. R.; Ho, W. *Surf. Sci* **1984**, *138*, 499.
(62) Kim, Y.; Komeda, T.; Kawai, M. *Phys. Rev. Lett.* **2002**, *89*, 126104.
(63) Kim, Y.; Komeda, T.; Kawai, M. *Surf. Sci.* **2002**, *502−503*, 7.
(64) See, for example: Oura, K.; Lifshits, V. G.; Saranin, A. A.; Zotov, A. V.; Katayama, M. *Surface science−an introduction*; Springer: Berlin, 2003; p 181 and references therein.
(65) Takayanagi, K.; Tanishiro, Y.; Takahashi, M.; Motoyoshi, H.; Yagi, K. *J. Vac. Sci. Technol. A* **1985**, *3*, 1502.
(66) Himpsel, F. J. *Surf. Sci. Rep.* **1990**, *12*, 3.
(67) Wolkow, R.; Avouris, Ph. *Phys. Rev. Lett.* **1988**, *60*, 1049.
(68) Avouris, Ph; Wolkow, R. *Phys. Rev. B* **1989**, *39*, 5091.
(69) Stauffer, L.; Van, S.; Bolmont, D.; Koulmann, J. J.; Minot, C. *Solid State Commun.* **1993**, *85*, 935.
(70) Brommer, K. D.; Galvan, M.; Pino, A. D., Jr.; Joannopoulos, J. D. *Surf. Sci*. **1994**, *314*, 57.
(71) Wang, Y. L.; Gao, H.-J.; Guo, H. M.; Liu, H. W.; Batyrev, I. G.; McMahpon, W. E.; Zhang, S. B. *Phys. Rev. B* **2004**, *70*, 073312.
(72) Bulavenko, S. Yu.; Melnik, P. V.; Nakhodin, M. G. *Surf. Sci.* **2000**, *469*, 127.
(73) Gomez-Rodriguez, J. M.; Saenz, J. J.; Baro, A. M.; Veuillen, J. Y.; Cinti, R. C. *Phys. Rev. Lett.* **1996**, *76*, 799.
(74) Veuillen, J. Y.; Gomez-Rodriguez, J. M.; Baro, A. M.; Cinti, R. C. *Surf. Sci.* **1997**, *377*, 847.
(75) Ganz, E.; Xiong, F.; Hwang, I.-S.; Golovchenko, J. *Phys. Rev. B* **1991**, *43*, 7316.
(76) Ganz, E.; Hwang, I.-S.; Xiong, F.; Theiss, S. K.; Golovchenko, J. *Surf. Sci.* **1991**, *257*, 259.
(77) Tang, D.; Elsayed-Ali, H.-E. *Phys. Rev. B* **1995**, *52*, 1481.
(78) Vitali, L.; Ramsey, M. G.; Netzer, F. P. *Phys. Rev. Lett.* **1999**, *83*, 316.
(79) Tosch, St.; Neddermeyer, H. *Phys. Rev. Lett.* **1988**, *61*, 349.
(80) Myslivecek, J.; Sobotik, P.; Ostadal, I.; Jarolimek, T. *Phys. Rev. B* **2001**, *63*, 045403.
(81) Li, J.-L.; Jia, J.-F.; Liang, X.-J.; Liu, X.; Wang, J.-Z.; Xue, Q.-K.; Li, Z.-Q.; Tse, J. S.; Zhang, Z.; Zhang, S. B. *Phys. Rev. Lett.* **2002**, *88*, 066101.
(82) Kohler, U. K.; Demuth, J. E.; Hamers, R. J. *Phys. Rev. Lett.* **1988**, *60*, 2499.
(83) Zhang, Y. P.; Yan, L.; Xie, S. S.; Pang, S. J.; Gao, H.-J. *Appl. Phys. Lett.* **2001**, *79*, 3317.
(84) Lin, X. F.; Chizhov, I.; Mai, H. A.; Willis, R. F. *Surf. Sci.* **1996**, *366*, 51.
(85) Yoon, M.; Lin, X. F.; Chizhov, I.; Mai, H.; Willis, R. F. *Phys. Rev. B.* **2001**, *64*, 085321.
(86) Lai, M. Y.; Wang, Y. L. *Phys. Rev. B* **2001**, *64*, 241404.
(87) Jia, J.; Wang, J.-Z.; Liu, X.; Xue, Q.-K.; Li, Z.-Q.; Kawazoe, Y.; Zhang, S. B. *Appl. Phys. Lett.* **2002**, *80*, 3186.

(88) Zhang, Y. P.; Yang, L.; Lai, Y. H.; Xu, G. Q.; Want, X. S. *Surf. Sci* **2003**, *531*, L378.
(89) Hashizume, T.; Motai, K.; Hasegawa, Y.; Sumita, I.; Tanaka, H.; Amano, S.; Hyodo, S.; Sakurai, T. *J. Vac. Sci. Technol. B* **1991**, *9*, 745.
(90) Watanabe, A.; Naitoh, M.; Nishigaki, S. *Jpn. J. Appl. Phys.* **1988**, *37*, 3778.
(91) Mayne, A. J.; Rose, F.; Comtet, G.; Hellner, L.; Dujardin, G. *Surf. Sci* **2003**, *528*, 132 and references therein.
(92) Yan, C.; Jensen, J. A.; Kummel, A. C. *Phys. Rev. Lett.* **1994**, *72*, 4017.
(93) Yan, C.; Jensen, J. A.; Kummel, A. C. *J. Chem. Phys.* **1995**, *102*, 3381.
(94) Yan, C.; Jensen, J. A.; Kummel, A. C. *J. Phys. Chem.* **1995**, *99*, 6084.
(95) Jensen, J. A.; Yan, C.; Kummel, A. C. *Science* **1995**, *267*, 493.
(96) Jensen, J. A.; Yan, C.; Kummel, A. C. *Phys. Rev. Lett.* **1996**, *76*, 1388.
(97) Liu, Y.; Masson, D. P.; Kummel, A. C. *Science* **1997**, *276*, 1681.
(98) Liu, Y.; Komrowski, A. J.; Taylor, P. R.; Kummel, A. C. *J. Chem. Phys.* **1998**, *109*, 2467.
(99) Lyubinetsky, I.; Dohnalek, Z.; Choyke, W. J.; Yates, J. T., Jr. *Phys. Rev.* B **1998**, *58*, 7950 and references therein.
(100) Rezai, M. A.; Stipe, B. C.; Ho, W. *J. Chem. Phys.* **1999**, *110*, 3548 and references therein.
(101) Rezai, M. A.; Stipe, B. C.; Ho, W. *J. Phys. Chem. B* **1998**, *102*, 10941.
(102) Avouris, Ph.; Lyo, I.-W. *Surf. Sci.* **1991**, *242*, 1.
(103) Lo, R.-L.; Hwang, I.-S.; Tsong, T. T. *Surf. Sci.* **2003**, *530*, L302.
(104) Hamers, R. J.; Avouris, Ph.; Bozso, F. *Phys. Rev. Lett.* **1987**, *59*, 2071.
(105) Avouris, Ph.; Bozso, F.; Hamers, R. J. *J. Vac. Sci. Technol. B* **1987**, *5*, 1387.
(106) Hamers, R. J.; Avouris, Ph.; Bozso, F. *J. Vac. Sci. Technol. A* **1988**, *6*, 508.
(107) Bozso, F.; Avouris, Ph. *Phys. Rev. Lett.* **1986**, *57*, 1185.
(108) Kang, M. Y. *Phys. Rev. B.* **2003**, *68*, 205307.
(109) Rauscher, H. *Surf. Sci. Rep.* **2001**, *42*, 207.
(110) Wang, Y.; Bronikowski, M. J.; Hamers, R. J. *Surf. Sci.* **1994**, *311*, 64.
(111) Memmert, U.; Berko, A.; Behm, R. J. *Surf. Sci.* **1995**, *325*, L441.
(112) Lim, H.; Cho, K.; Park, I.; Joannopoulos, J. D.; Kzxiras, E. *Phys. Rev. B* **1995**, *52*, 17231.
(113) Komura, T.; Okano, S.; Morikawa, K.; Hanada, T.; Yoshimura, M.; Yao, T. *Appl. Surf. Sci.* **1998**, *130*, 23.
(114) Miyake, K.; Ishida, M.; Shigekawa, H. *Appl. Surf. Sci.* **1998**, *130*, 78.
(115) Miyake, K.; Kaikoh, T.; Jata, K.; Morita, R.; Yamashita, M.; Shigekawa, H. *J. Vac. Sci. Technol. A* **1999**, *17*, 1596.
(116) Kaikoh, T.; Miyake, K.; Li, Y. J.; Morita, R.; Yamashita, M.; Shigekawa, H. *J. Vac. Sci. Technol. A* **2000**, *18*, 1469.
(117) Bronikowski, M. J.; Hamers, R. J. *J. Vac. Sci. Technol. A* **1995**, *13*, 777.
(118) Woelke, A.; Imanaka, S.; Watanabe, S.; Goto, S.; Hashinokuchi, M.; Okada, M.; Kasai, T. *J. Electron Microsc.* **2005**, *54* (Suppl. 1), i21.
(119) Boland, J. *Science* **1993**, *262*, 1703.
(120) Jiang, G.; Polanyi, J. C.; Rogers, D. *Surf. Sci.* **2003**, *544*, 147.
(121) Dobrin, S.; Lu, X.; Naumkin, F. Y.; Polanyi, J. C.; Yang, J. (S. Y.) *Surf. Sci. Lett.* **2004**, *573*, L363.
(122) Matta, C. F.; Polanyi, J. C. *Philos. Trans. R. Soc. London, Ser. A* **2004**, *362*, 1185.
(123) Dobrin, S.; Harikumar, K. R.; Polanyi, J. C. *Surf. Sci.* **2004**, *561*, 11.
(124) Harikumar, K. R.; Petsalakis, I. D.; Polanyi, J. C.; Theodorakopoulos, G. *Surf. Sci.* **2004**, *572*, 162.
(125) Dobrin, S.; Harikumar K. R.; Matta, C. F.; Polanyi, J. C. *Surf. Sci.* **2005**, *580*, 39.
(126) Dobrin, S.; Harikumar, K. R.; Polanyi, J. C. *J. Phys. Chem. B* **2006**, *110*, 8010.
(127) Lu, P. H.; Polanyi, J. C.; Rogers, D. *J. Chem. Phys.* **1999**, *111*, 9905.
(128) Giorgi, J. B.; Kuhnemuth, R.; Polanyi, J. C. *J. Chem. Phys.* **1999**, *110*, 598.
(129) Dobrin, S.; Harikumar, K. R.; Polanyi, J. C. *Surf. Sci.* **2004**, *561*, 11.
(130) Li, Y.-C.; Wang, W.-N.; Cao, Y.; Fan, K.-N. *Acta Chim. Sin.* **2002**, *60*, 653.
(131) Wang, Z. H.; Cao, Y.; Xu, G. Q. *Chem. Phys. Lett.* **2001**, *338*, 7.
(132) Palmer, R. E.; Sloan, P. A.; Xirouchaki, C. *Philos. Trans. R. Soc. London, Ser. A* **2004**, *362*, 1195.
(133) Sloan, P. A.; Palmer, R. E. *Nature* **2005**, *434*, 367.
(134) Petsalakis, I. D., Polanyi, J. C.; Theodorakopoulos, G. *Isr. J. Chem.* **2004**, *45*, 111.
(135) Wolkow, R. A.; Mofatt, D. J. *J. Chem. Phys.* **1995**, *103*, 10696.
(136) Cao, Y.; Wei, X. M.; Chin, W. S.; Lai, Y. H.; Deng, J. F.; Bernasen, S. L.; Xu, G. Q. *J. Phys. Chem. B* **1999**, *103*, 5698.
(137) Cao, Y.; Deng, J. F.; Xu, Q. *J. Chem. Phys.* **2000**, *112*, 4759.
(138) Petsalakis, I. D.; Polanyi, J. C.; Theodorakopoulos, G. *Surf. Sci.* **2003**, *544*, 162.
(139) Naumkin, F. Y.; Polanyi, J. C.; Rogers, D.; Fisher, A.; Hofer, W. *Surf. Sci.* **2003**, *547*, 324.
(140) Naumkin, F. Y.; Polanyi, J. C.; Rogers, D. *Surf. Sci.* **2003**, *547*, 335.
(141) Lopinski, G.; Wayner, D. D. M.; Wolkow, R. A. *Nature* **2000**, *406*, 48.
(142) Hofer, W. A.; Fisher, A. J.; Lopinski, G. P.; Wolkow, R. A. *Chem. Phys. Lett.* **2002**, *365*, 129.
(143) Piva, P. G.; DiLabio, G. A.; Pitters, J. L.; Zikovsky, J.; Rezeq, M.; Dogel, S.; Hofer, W. A.; Wolkow, R. A. *Nature* **2005**, *435*, *658*.
(144) Hossain, Md. Z.; Kato, H. S.; Kawai, M. *J. Am. Chem. Soc.* **2005**, *127*, 15030.
(145) Hossain, Md. Z.; Kato, H. S.; Kawai, M. *J. Phys. Chem. B* **2005**, *109*, 23129.
(146) Xie, Z.-X.; Uematsu, Y.; Lu, X.; Tanaka, K.-i. *Phys. Rev. B* **2002**, *66*, 125306.
(147) Tanaka, K.-i.; Xie, Z.-X. *J. Chem. Phys.* **2005**, *122*, 054706.
(148) Tanaka, K.-i.; Nomoto, Y.; Xie, Z.-X. *J. Chem. Phys.* **2004**, *120*, 4486.
(149) Alavi, S.; Rousseau, R.; Lopinski, R. P.; Wolkow, R. A.; Seideman, T. *Faraday Discuss.* **2000**, *117*, *213*.
(150) Brown, D. E.; Moffat, D. J.; Wolkow, R. A. *Science* **1998**, *279*, 542.
(151) Lu, X.; Polanyi, J. C.; Yang, J. (S. Y.) *Nano Lett.* **2006**, *6*, 809.
(152) Marsh, E. P.; Gilton, T. L.; Meier, W.; Schneider, M. R.; Cowin, J. P. *Phys. Rev. Lett.* **1998**, *61*, 2725.
(153) Zhou, X. L.; White, J. M. *Surf. Sci.* **1991**, *241*, 259.
(154) Dixon-Warren, St. J.; Jensen, E. T.; Polanyi, J. C. *J. Chem. Phys.* **1993**, *98*, 5938.
(155) Yang, Q. Y.; Schwarz, W. N.; Lasky, P. J.; Hood, S. C.; Loo, N. L.; Osgood, R. M., Jr. *Phys. Rev. Lett.* **1994**, *72*, 3068.
(156) Xu, H.; Yuro, R.; Harrison, I. *Surf. Sci.* **1998**, *411*, 303.
(157) Khan, K. A.; Camillone, N., III; Osgood, R. M., Jr. *J. Phys. Chem. B* **1999**, *103*, 5530.
(158) Totir, G. G.; Le, Y.; Osgood, R. M., Jr. *J. Phys. Chem. B* **2005**, *109*, 8452.
(159) Dobrin, S. *J. Phys. Chem. B* **2005**, *109*, 22976.
(160) Dobrin, S.; Harikumar K. R.; Jones, R. V.; McNab, I. R.; Polanyi, J. C.; Waqar, Z. *J. Chem. Phys.* **2006**, submitted for publication.
(161) Wolkow, R. A.; Mofatt, D. J. *J. Chem. Phys.* **1995**, *103*, 10696.
(162) Cao, Y.; Wei, X. M.; Chin, W. S.; Lai, Y. H.; Deng, J. F.; Bernasen, S. L.; Xu, G. Q. *J. Phys. Chem. B* **1999**, *103*, 5698.
(163) Cao, Y.; Deng, J. F.; Xu, Q. *J. Chem. Phys.* **2000**, *112*, 4759.

CR0501745